

FABRICATION AND CHARACTERIZATION OF FUNCTIONALLY GRADED Al/AIB₂ MATRIX COMPOSITES FOR HIGH WEAR AEROSPACE APPLICATIONS USING CENTRIFUGAL CASTING

By

Zenón Humberto Melgarejo Pinto

A thesis submitted in partial fulfillment of the requirements for the degree of

MASTER OF SCIENCE

in

MECHANICAL ENGINEERING

UNIVERSITY OF PUERTO RICO
MAYAGÜEZ CAMPUS
2006

Approved by:

Paul A. Sundaram, PhD
Member, Graduate Committee

Date

Néstor L. Pérez, PhD
Member, Graduate Committee

Date

Oscar Marcelo Suárez, PhD
President, Graduate Committee

Date

Jorge L. Ortiz, PhD
Representative of Graduate Studies

Date

Paul A. Sundaram, PhD
Chairperson of the Department

Date

ABSTRACT

Functionally graded advanced composite materials contain reinforcement particles whose volume fraction varies continuously thereby bearing a non-uniform microstructure with continuously changing properties. Aluminum-based functionally graded materials (FGMs) reinforced with AlB_2 particles were manufactured by centrifugal casting to obtain these graded properties, which can not be achievable in monolithic or homogeneous materials. Volume fraction of pores and reinforcements particles, superficial Rockwell hardness ($HR15_w$), Vickers microhardness (HV_{50}), and stereological parameters from the microstructure were measured on Al -2 wt.% Mg - 1, 2, 3 and 4 wt.% B centrifugally cast and gravity cast composites. These materials showed AlB_2 particles segregation toward the external zone of the cast piece, resulting in higher hardness and microhardness in this region. Wear behavior of the composites was studied by pin-on-disk wear test. This test was conducted on five zones (0, 5, 10, 15 and 20mm) sectioned along the length of the cylinder of the centrifugally cast aluminum matrix composites (AMC's) and on stationary (gravity) cast specimens. The results of this study showed the smallest wear volume on the external zone (20mm) of the FGMs. Morphological characterization of the wear tracks by scanning electron microscopy (*SEM*) helped corroborate the wear volume results.

RESUMEN

Materiales compuestos avanzados de gradiente funcional contienen partículas de refuerzo cuya fracción de volumen varia permitiendo la formación de microestructuras no-uniformes con propiedades que cambian continuamente. Materiales de gradiente funcional a base de aluminio (FGMs) reforzados con partículas de AlB_2 fueron fabricados mediante fundición centrífuga a fin de obtener propiedades las cuales no se pueden lograr en materiales homogéneos o monolíticos. Fracción de volumen de poros y partículas de refuerzo, dureza superficial Rockwell ($\text{HR}_{15\text{w}}$), microdureza Vickers (HV_{50}), tamaño de grano de la fase de matriz de aluminio y tamaño de las partículas de diboruro fueron medidos sobre compuestos de $\text{Al-2 wt.\%Mg - 1, 2, 3 y 4 wt.\% B}$, fundidos centrífugamente y por gravedad. Estos materiales mostraron segregación de partículas de AlB_2 hacia la región más externa de la pieza fundida, resultando en una mayor dureza y microdureza en ésta región. Se estudió el comportamiento al desgaste de éstos compuestos por medio del ensayo de desgaste pin-on-disk. Este ensayo se realizó en cinco zonas (0, 5, 10, 15 y 20 mm) seccionadas a lo largo de la longitud de los cilindros de los compuestos de matriz de aluminio fundidos centrífugamente y sobre muestras fundidas estacionariamente (por gravedad). Los resultados del estudio mostraron el menor volumen de desgaste sobre la zona externa (20 mm) de los materiales de gradiente funcional. La caracterización morfológica de las pistas de desgaste haciendo uso del microscopio electrónico de rastreo (MER) ayudó a corroborar los resultados de volumen de desgaste.

To the memory of my father, Efrain.

To the inspiration of my life, my mother, Leonilde, example of love and tenacity.

To Jenny my sincere love, source of affection and understanding.

To my family by its words of strength and permanent support.

ACKNOWLEDGMENTS

During the development of my graduate studies in the University of Puerto Rico several persons and institutions have collaborated directly and indirectly with my research. That is why I wish to dedicate this section to recognize their support.

I want to start expressing a sincere acknowledgement to my advisor, Dr. O. Marcelo Suárez because he gave me the opportunity to research under his guidance and supervision. I received motivation; encouragement and support for him during all my studies. Special thanks I owe Dr. Kumar Sridharan for the opportunity of researching under, his support and guidance. I would like to thank to Dr Paul Sundaram for his supervision and advices.

I also want to thank the unconditional and uninterested collaboration of Hermes Calderón graduate student of Civil Engineering Department, Glorimar Ramos and Manuel Morales undergraduate students of Mechanical Engineering Department, and José Almodovar of Biology Department

Puerto Rico EPSCoR and the National Science Foundation (NSF) under Grant No. 0351449 provided the funding and the resources for the development of this research.

Table of Contents

ABSTRACT	I
RESUMEN	III
ACKNOWLEDGMENTS	V
TABLE OF CONTENTS	VI
TABLE LIST	VIII
FIGURE LIST	IX
1. INTRODUCTION	1
1.1 MOTIVATION	2
1.2 LITERATURE REVIEW	4
1.3 OBJECTIVES	8
1.4 ORGANIZATION OF THIS THESIS	9
2. THEORETICAL BACKGROUND	11
2.1 FUNCTIONALLY GRADED MATERIALS (FGMs)	11
2.2 CAST METAL PROCESSING	13
2.2.1 <i>Centrifugal Casting</i>	13
2.2.2 <i>Investment Casting</i>	17
2.3 METAL MATRIX COMPOSITES (MMCs)	19
2.3.1 <i>General Consideration</i>	19
2.3.2 <i>Characteristics of MMCs</i>	20
2.4 ALUMINUM MATRIX COMPOSITES (AMCs)	22
2.4.1 <i>Al – Mg Binary Alloy</i>	24
2.4.2 <i>Aluminum Diboride (AlB₂)</i>	27
2.4.3 <i>Other Transitional Metal Diborides</i>	28
2.5 STEREOLOGICAL ANALYSIS	30
2.6 WEAR	32
2.6.1 <i>Introduction</i>	32
2.6.2 <i>Surface Damage and Wear</i>	33
2.6.3 <i>Types of Wear</i>	36
2.6.3 <i>Tribological Parameters</i>	38
2.6.4 <i>Wear of Metal Matrix Composites</i>	41
3. DEVELOPMENT OF PROCESSING AND CHARACTERIZATION METHODOLOGY FOR FGM - Al-B COMPOSITES	45
3.1 INVESTMENT CASTING	46
3.2 CENTRIFUGAL CASTING PROCESS	48
3.3 SAMPLE PREPARATION	50
3.4 CHARACTERIZATION	52

3.4.1 Microstructure	52
3.4.2 Analysis of the Volume Fraction of Reinforcement	53
3.4.3 Superficial Rockwell Hardness and Vickers Microhardness Testing.....	54
3.5 PIN - ON - DISK WEAR TESTING	57
3.5.1 Wear Volume and Wear Coefficient.....	59
4. PROCESSING AND CHARACTERIZATION OF FGM Al-B-Mg COMPOSITES	63
4.1 INVESTMENT CASTING.....	64
4.2 CENTRIFUGAL CASTING PROCESS	65
4.3 SAMPLE PREPARATION	65
4.4 CHARACTERIZATION	66
4.4.1 Microstructure	66
4.4.2 Volume Fraction of Reinforcement and Pores	67
4.4.3 Superficial Rockwell Hardness and Vickers Microhardness Testing.....	72
4.4.4 Reinforcement Particle Size and Matrix Grain Size	76
4.4.5 Possible Scenario of Liquid-Particle Flow and Microstructure Formation of Al-B-Mg Composites Centrifugally Cast.....	81
4.5 PIN - ON - DISK WEAR TESTING	85
4.5.1 Wear Volume and Wear Coefficient.....	85
4.5.2 Morphological Characterization of Worn Surface.....	88
5. CONCLUSIONS	93
6. RECOMMENDATIONS	95
7. REFERENCES	96
APPENDIX	102

Table List

Tables	Page
Table 2.1 Reported bulk densities and melting points of some transition metal diborides.	30
Table 3.1 Calculated wear coefficient for the various AMC samples.	61
Table 4.1 Calculated wear coefficient for the various AMC samples.	88

Figure List

Figures	Page
Figure 2.1 Approaches to FGMs. a) homogeneous composite. b) FGM. c) coated-or joined-type composite.	12
Figure 2.2 The Basics of the Investment Casting Process. a) Wax Injection. b) Assembly. c) Shell Building. d) Dewax. e) Conventional Casting. f) Knockout. g) Cut Off. h) Finished Castings.....	18
Figure 2.3 Al-Mg Binary Alloy Phase Diagram	26
Figure 2.4 Crystal Structure of AlB_2	29
Figure 2.5 Classification of surface damage. a) Structural changes. b) Plastic deformation. c) Surface cracking. d) Wear. e) Gain of material. f) Corrosion	34
Figure 2.6 Scratch test devices. a) Single pass. b) Reciprocating. c) Multiple pass. d) Modified charpy pendulum. e) Modified grinding machine.....	39
Figure 3.1 Diagram showing the experimental procedure sequence	46
Figure 3.2 Investment Casting Process. a) Model. b) Investment. c) Dewaxing. d) Mold.....	48
Figure 3.3 Centrifugal Casting Machine. a) Romanoff 79-049-T. b)Schematic drawing.	50
Figure 3.4 Centrifugally Cast Piece a) Final piece. b) Mapped longitudinal zones ..	51
Figure 3.5 Micrograph of the microstructure of a centrifugal cast Al-5%wt B composite. a) Longitudinal section. b) Cross section.....	52
Figure 3.6 Measured volume fraction of reinforcement particles in the AMC samples investigated in this study.....	54
Figure 3.7 Rockwell superficial hardness (HR 15W) measured in the AMC samples investigated in this study.....	55
Figure 3.8 Vickers microhardness (HV_{50}) values measured on the matrices of the different AMCs investigated in this study.	56
Figure 3.9 Pin-on-disk wear test system a) Unlubricated Pin-on disk tester. b) Schematic drawing	58
Figure 3.10 Images of wear tracks resulting from pin-on-disk wear tests a) Wear track of Al-4wt.%B-2wt.%Mg external zone of FGM b) Track width of Al-5wt.%B casting c) Track depth of Al-5wt%B internal zone of FGM.....	59
Figure 3.11 Wear volume for the various AMC samples after undergoing pin-on-disk wear tests under identical conditions.	60
Figure 4.1 Diagram showing the experimental procedure sequence to Al-B-Mg composite.	64
Figure 4.2 Centrifugally Cast Piece. a) Final piece. b) Mapped longitudinal zones .	66
Figure 4.3 Microstructure of a centrifugal cast Al-2wt%Mg-1wt%B composite.	67
Figure 4.4 Micrographs of Al-2wt%Mg-2wt%B FGM mapped longitudinal sections.	68
Figure 4.5 Measured volume fraction of reinforcement particles in the FGM samples as a function of distance.	68

Figure 4.6 Measured volume fraction of reinforcement particles in the gravity cast samples as a function of %wt.B.	70
Figure 4.7 Measured volume fraction of pores in the FGM samples as a function of distance.	70
Figure 4.8 Measured volume fraction of pores in the gravity casting samples as a function of %wt.B.	71
Figure 4.9 Rockwell superficial hardness (HR 15W) measured in the FGM samples as a function of distance.	73
Figure 4.10 Rockwell superficial hardness (HR 15W) measured in the gravity casting samples as a function of %wt.B.	74
Figure 4.11 Vickers microhardness (HV50) values measured on the matrices of the different FGMs as a function of distance.	75
Figure 4.12 Vickers microhardness (HV50) values measured on the matrices of the different gravity casting samples as a function of %wt.B.	76
Figure 4.13 Micrograph of the reinforcement particle size of a centrifugal cast Al-2wt%Mg-4wt%B composite.	77
Figure 4.14 Reinforcement particle size values measured on the FGM samples as a function of distance.	78
Figure 4.15 Reinforcement particle size values measured on the gravity casting samples as a function of %wt.B.	78
Figure 4.16 Micrograph of the matrix grain size of a gravity casting Al-2wt%Mg-4wt%B composite.	79
Figure 4.17 Matrix grain size values measured on the FGM samples as a function of distance.	80
Figure 4.18 Matrix grain size values measured on the gravity casting samples as a function of %wt.B.	80
Figure 4.19 Liquid-particle laminar flow filling the mold.	82
Figure 4.20 Schematic of microstructure zone formation in centrifugally cast piece. a) Equiaxed zone preferentially formed in the outer zone by effect of AlB ₂ particles. b) Growth of a dendrite. c) Resulting structure of crystal growth in equiaxial solidification.	84
Figure 4.21 AFM images of tracks depth resulting from pin-on-disk wear tests on Al-2wt%Mg-1wt%B FGM a) 0 mm zone. b) 10 mm zone. c) 20 mm zone.	86
Figure 4.22 Wear volume for the various FGMs-AMCs samples after pin-on-disk wear tests under identical conditions.	87
Figure 4.23 Wear volume for the various Gravity Casting - AMCs samples after pin-on-disk wear tests under identical conditions.	87
Figure 4.24 Wear Track backscatter electron image of Al- 2wt %Mg- 1wt.% B alloy. a) FGM 10mm zone. b) FGM 20mm zone. c) Gravity casting.	90

1. INTRODUCTION

Metal matrix composites (MMCs) reinforced with ceramic or metallic particles are widely used due to their high specific modulus, strength and wear resistance. Furthermore, MMCs have been considered as an alternative to monolithic metallic materials or conventional alloys in a number of specialized applications [1]. In particular, aluminum matrix composites (AMCs) have been reported to possess higher wear resistance and lower friction coefficient with increasing volume fraction of reinforcement particles, compared to aluminum alloys without reinforcement [2].

Functionally graded composite materials (FGMs) contain volume fraction distribution of reinforcement particles which varies continuously from the inner to the outer sections of the cast piece giving a controlled non-uniform microstructure with continuously changing properties [3]. Surface modification and coating methods provide this effect and are widely used to improve tribological properties of metallic materials, but the added surface treatment increases the manufacturing costs. On the other hand, centrifugal casting is appears to be an effective method to process FGMs. This type of pressure casting method involves pouring molten metal into a mold when the mold assembly is under the action of a centrifugal (inertial) force produced by a rotational or spinning motion.

This research reports the manufacturing, composition gradient determination, preliminary characterization of microstructural and mechanical properties, and wear response of FGM-AMCs reinforced with AlB_2 particles obtained by centrifugal casting. The original semisolid material consisted of a uniform dispersion of AlB_2 particles entrapped in molten aluminum. The resulting redistribution of volume fraction of reinforcement particles was controlled by the inertial forces toward the outer region of the cast component during centrifugal casting. This redistribution was assisted by the higher density of the AlB_2 particles compared to the molten aluminum. The forced segregation of hard borides towards the outer regions of the casting provided a unique approach to improve surface hardness [4] and wear resistance of the composite.

1.1 Motivation

Surface modification and coating methods are widely used to improve tribological properties of metallic materials for a wide range of applications. The corresponding techniques are very diverse; thermo-chemical diffusion, laser treatment and plasma, and physical and chemical vapor deposition. However, in all these methods the surface treatment is applied after the part has been fabricated, adding significantly to the overall costs.

FGMs are useful in applications where high wear resistance and high bulk toughness are a necessity. Therefore, special processing is required to produce

these materials in order to exhibit characteristics that are not achievable by monolithic or homogeneous materials [5].

FGMs - AMCs reinforced with diborides have not been studied extensively despite being strong and lightweight materials. AMCs combine the low density of the matrix with the high hardness of the reinforcers. For this reason extensive analysis and characterization of these AMCs are relevant if they are proposed as alternative materials for aerospace applications.

Cast FGMs - AMCs reinforced with diborides represent an effective, alternative in aerospace application where light weight, low-cost and wear resistance are a necessity. Furthermore, centrifugal casting is one of the most effective methods for processing this kind of AMCs because, under centrifugal forces, the heavier ceramic particles entrapped in the liquid metal are displaced toward the outer surface of the casting [6]. The principal advantage of centrifugal casting is to produce very good mold filling combined with good microstructural control, which usually results in improved mechanical properties. However, a complete understanding of the particle segregation and distribution phenomena has not been yet fully described. Nevertheless, it is still possible to formulate a composition gradient due to the difference in material density [7].

1.2 Literature Review

The tribological behavior of reinforced AMC's has been investigated by numerous researchers and there are many published works related to this subject. Most of them have demonstrated the enhanced tribological performance of the composites compared to unreinforced alloys [1]. However most of the literature on reinforced AMCs has been focused on homogeneous materials (uniform distribution of reinforcers).

Some previous work in the area of FGM aluminum matrix composites include the study of Kang and Rohatgi (1996) who performed a transient thermal analysis of solidification in a centrifugal casting for composite materials containing particle segregation [8]. In this research one-dimensional heat transfer analysis during centrifugal casting of aluminum alloy and copper-based MMCs containing Al_2O_3 , SiC_p , and graphite particles were studied. They proposed a numerical model of particle segregation during centrifugal casting of liquid metal containing suspended particles. In addition, they considered that liquid metal temperature is influenced by the speed of rotation, the variation of reinforcement and the constitution of the base alloy. Additionally, the initial mold temperature and its speed of rotation were found to be significantly affected by the solidification time due to particle segregation (measured as volume fraction).

Watanabe and Fukui (2000) carried out an analysis of microstructures and mechanical properties of FGMs fabricated by a centrifugal casting method [7]. The

particle distribution gradient of the dispersed compounds (Al/SiC; Al/Al₃Ti; Al/Al₃Ni) was established. The author reported the variation of matrix hardness with the composition gradient. Mechanical properties such as Young's modulus, internal friction, fatigue crack growth in an *in-situ* Al/Al₃Ni FGM were evaluated. Analysis of thermal residual stress was done on Al/SiC FGM and, wear behavior of Al/Al₃Ti FGM was determined. This study mainly showed that SiC particles move toward the casting outer parts under the action of centrifugal force (due to the denser particles). The same trend was found in Al₃Ti. Al/Al₃Ni FGM which is an application of the *in-situ* technique using the crystallization phenomena exposed a uniform volume fraction distribution of particles and decrease in particle diameter in the outer region of the casting. Analysis of matrix revealed a direct relation between hardness and volume fraction of particles. Internal friction and Young's modulus increased with increasing volume fraction of particles. Effect of graded composition on the fractography is not clear. However, since the graded composition affects the crack path, this may increase the toughness of material. The analysis on Al/SiC FGM showed that thermal residual stresses are greater for higher composition gradient. Finally, the wear volume of Al/Al₃Ti specimens were much lower than those of pure Al.

Gomes et al. (2003) performed a tribological characterization of homogeneous gravity cast aluminum-based matrix composites and aluminum composites with functionally graded properties, obtained by centrifugal casting and reinforced with SiC particles [9]. These composite materials were tested against

nodular cast iron in a pin-on-disc tribometer in order to evaluate their friction and wear properties. The worn surfaces as well as the wear debris were characterized by SEM/EDS and by atomic force microscope (AFM). The friction coefficient revealed a slight decrease when FGMs are involved in the contact instead of the homogeneous composite. Relatively low values of the wear coefficient were obtained for functionally graded aluminum matrix composites. Characterization of the worn surface indicated that the effect of reinforcing particles played a decisive role in the friction and wear properties of aluminum matrix composites.

In 2003 Velinho et al. presented the effect of particle size on reinforcement distribution [10]. In this work, different SiC particle sizes (reinforcing elements) were added to AMCs which were molten and centrifugally cast in order to produce the FGM composites. They found that larger sized particle reinforcement gives rise to higher hardness levels throughout the material. At the same time this originates steeper gradients than in those materials prepared with smaller reinforcements. In particular, if the particles are large enough, total or partial particle depletion occurs in some regions away from the FGM surface.

In 2004 Nai et al. analyzed the effects of different reinforcement particles such as SiC, Al₂O₃ and TiC on three aluminum based FGMs [5]. Further analysis of porosity level, microhardness, thermomechanical and wear on these AMCs were carried out. The results for Al/SiC and Al/Al₂O₃ revealed a general increase in the weight percentage of reinforcement along the direction of deposition, which results in

an increase in porosity and microhardness. On the other hand, the opposite trend was observed for Al/TiC, Thermomechanical analysis of the FGMs showed that the average coefficient of thermal expansion of the high reinforcement end was reduced, when compared to the aluminum-rich end. Sliding wear test results also revealed that the high reinforcement end was more wear resistant than the aluminum-rich end, except for the case of Al/Al₂O₃.

Although there are other publications on FGMs, most of them explain processing techniques and characterization methods very similar to the ones described previously. A common finding in this literature review has been the use of SiC as reinforcement particle inside the aluminum matrix. Other ceramic and intermetallic reinforcement particles have been used but to a lesser degree.

In a previous thesis completed at UPRM [11] the advantageous mechanical properties of the Al/AlB₂ composites were demonstrated. The present work will establish the specific properties of this composite as FGM.

A binary Al-B alloy rich in Al consists of an almost pure aluminum matrix containing small ceramic particles (AlB₂). In the equilibrium Al-B system, boron is practically insoluble. Currently, Al-rich alloys of this system are used as master alloys for grain refining of aluminum [12]. The aluminum diborides contained in those alloys are in reality catalytic substrates for the early crystallization of the aluminum phase [13]. There is an excellent wettability between the borides, acting as

reinforcing particles, and the aluminum melt without any deleterious chemical reaction. Other ceramic particles such as SiC react with the molten alloy to form reaction products that weaken the particle-matrix interface, which results in harmful effects on the composite.

1.3 Objectives

The main purpose of this research is to develop a technique to produce FGMs made of Al-B-Mg composites. Additionally, these FGMs will be characterized in order to identify their composition gradient and microstructural and tribological properties.

The specific objectives of this work are:

- Develop a process of centrifugal casting which allows producing functionally graded Al/AlB₂ composites.
- Obtain FGM-AMCs reinforced with AlB₂ particles from Al-B-Mg composites.
- Characterize and analyze volume fraction distribution of reinforcement particles (composition gradient) and pores of FGMs-AMCs.

- Determine microstructural and mechanical properties on FGMs-Al-B-Mg composites such as, matrix grain size, reinforcement particle size and superficial Rockwell hardness and Vickers microhardness.
- Conduct a preliminary tribological characterization of FGMs-AMCs through wear volume and wear coefficient measurements obtained from pin on disk wear tests.

1.4 Organization of this Thesis

In Chapter 2 the necessary theoretical background is developed. Chapter 3 treats the performance of the methodology to process the Al-B FGM composites from centrifugal casting. Characterization of the Al-B FGMs composites is done by determination of volume fraction distribution of reinforcement and pores, superficial Rockwell hardness and Vickers microhardness testing. Then, wear volume and wear coefficient of Al-B FGM composites are measured from wear tests in a pin-on-disk apparatus. The fourth chapter presents the processing and characterization of FGM-Al-B-Mg composites. Investment casting and centrifugal casting are used as processing methods. Volume fraction distribution of reinforcement and pores, superficial Rockwell hardness and Vickers microhardness testing, matrix grain size and reinforcement particle size are to be characterized in this Al-B-Mg FGM. Afterwards, the results of wear volume, wear coefficient and morphology of worn

surface were analyzed after the pin-on-disk wear tests. Conclusions are presented in Chapter 5 while Chapter 6 provides some recommendations for future research.

2. THEORETICAL BACKGROUND

2.1 Functionally Graded Materials (FGMs)

Functionally graded materials (FGMs) are new advanced multifunctional composites where the volume fractions of the reinforcements phase(s) (or dispersoids) vary smoothly. This is achieved by using reinforcements with different properties, sizes, and shapes, as well as by interchanging the functions of the reinforcement and matrix phases in a continuous manner. The result is a microstructure bearing continuous changes in thermal and mechanical properties at the macroscopic or continuum scale [14]. In other words FGM is usually a combination of two materials or phases that show a gradual transition of properties from one side of sample to the other. This gradual transition allows the creation of superior and multiple properties without any mechanically weak interface. Moreover, the gradual change of properties can be tailored to different applications and service environments.

In general, there are two approaches to fabricate FGMs, as shown in Fig 2.1. The first one is to eliminate the interface of coated – or joined-type composites (from c to b), eliminating discontinuities in the properties at the interface. The second one is to induce non-uniform distributions of reinforcement particles in an originally homogeneous composite (from a to b), creating multiple functions inside the material. Several FGM fabrication methods have been proposed. However, thus far,

it has been difficult to produce relatively large FGM components by most fabrication methods. In addition, those methods require relatively new techniques and expensive fabrication equipment [7].

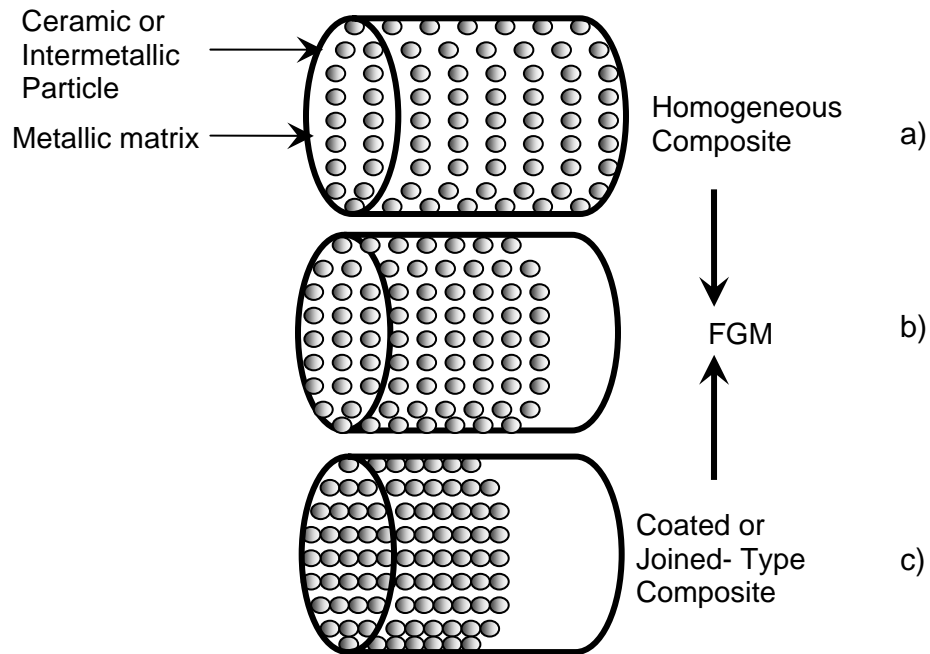


Figure 2.1 Approaches to FGMs, a) homogeneous composite, b) FGM, c) coated-or joined-type composite.

This new concept of materials engineering hinges on materials science and mechanics due to the integration of the material and structural considerations into the final design of structural components. Because of the many variables that control the design of functionally graded microstructures, full utilization of the FGMs potential requires the development of appropriate modeling strategies for their response to combined thermomechanical loads.

FGMs are ideal candidates for applications involving severe thermal gradients, varying from thermal structures in advanced aircraft and aerospace engines to computer circuit boards. These materials were introduced to take advantage of ideal behavior of its constituents, e.g. heat and corrosion resistance of ceramics together with mechanical strength and toughness of metals [15].

Many processing methods have been proposed to fabricate FGMs, such as chemical vapor deposition, the plasma spray technique and various powder metallurgy techniques. The centrifugal method was introduced recently and has attracted a lot of attention due to its unique merits [16]. In particular, Al based FGMs fabricated by the centrifugal method showed interesting properties that are not obtained in conventional monolithic materials, such as gradual changes in hardness, wear resistance, Young's modulus, etc [17].

2.2 Cast Metal Processing

2.2.1 Centrifugal Casting

One application of centrifugal casting is in FGM fabrication. In this method, a centrifugal force applied to a homogeneous semiliquid composite, (containing ceramics or intermetallic compound particles) drives the formation of the desired gradient (from a to b in Fig 2.1). The resulting composition gradient is produced by the difference in density between the molten metal and the particles under the same

centrifugal force. Compared to other techniques, the centrifugal method is potentially applicable to mass production of both small and large FGM components at a low cost. Mechanical properties of FGMs fabricated by this method have been investigated using relatively large samples [7].

The fabrication of ceramic or intermetallic compound-dispersed FGMs made by the centrifugal method can be classified into two categories according to the melting point of the ceramic or intermetallic compound. If the melting point is significantly higher than the processing temperature, the intermetallic compound remains solid in a liquid matrix. The FGMs obtained by this method are named as a *solid particle* technique. On the other hand, if the melting point of the intermetallic compound is lower than the processing temperature, centrifugal force can be applied during the solidification both to the intermetallic compound and to the matrix. This solidification is similar to the production of *in-situ* composites using the crystallization phenomena, and this method is, therefore, named as an *in-situ* technique [7].

Centrifugal casting is one of the most effective methods for processing metal matrix composites (MMCs). Nevertheless, understanding of the particle distribution mechanisms has not yet been fully achieved. Several parameters influence the characteristics of FGMs: atmosphere in the neighborhood of the melt, melt pouring temperature, mold temperature, thermal gradient across the molds, solidification rate, centrifugal force and pouring rate. These parameters affect several phenomena when the liquid metal containing solid particles solidifies in the mold such as:

interaction and/or chemical reactions between the solidification front and the moving particles; rate of variation of the melt viscosity during solidification; interaction between particles and liquid; or the initial position of the particles in the mould, before starting their movement in the liquid. The balance between these phenomena determines the effect in terms of particle distribution, overall microstructure and FGM properties [10].

Centrifugal casting method has been used to avoid interdendritic segregation of reinforcing particles, such as Al_2O_3 and SiC_p . In addition, some models have been developed for this procedure in order to predict mainly, composition gradient, temperature distribution and local solidification time. As an illustration, transient thermal analysis of solidification in AMCs centrifugally cast has been proposed to describe particle segregation [8]. Although the model developed has not been fully validated it provides an adequate one-dimensional heat-transfer analysis during centrifugal casting of AMCs containing Al_2O_3 , SiC_p and graphite particles. The model of particle segregation is calculated by varying the volume fraction during centrifugal casting, using the finite difference method. According to this research article, when the reinforcer density ρ_p is higher than that of the liquid matrix ρ_m , the particle volume fraction V_f at a distance r_i of the casting rotation axis after a time increment Δt can be linearized as indicated in equation 3.1.

$$V_f(t+\Delta t) = V_f(t) \cdot \frac{1-r_i(t+\Delta t)}{1-r_i(t)} + V_f(t) |_{t=0} \quad (3.1)$$

The actual nondimensional position of each individual particle r_i is obtained by ratio between the actual position x_i and the maximum radius of the casting X : $r_i = \frac{x_i}{X}$. If each particle is assumed to be spherical with radius R_p then, its position can be also estimated as a function of time and the rotation speed ω :

$$r_i(t) = r(0) \cdot \exp\left(\frac{2\omega^2(\rho_p - \rho_m) R_p^2 t}{9\eta}\right) \quad (3.2)$$

Where, $r(0)$ is the position of the particle at $t=0$ and η is the kinematic viscosity of the composite constituted by a liquid metallic matrix and solid particles. The thickness of the particle-rich region near the inner periphery, therefore, can be modeled by using equation 3.2. This allows for adjusting the mold rotation speed ω to produce a certain volume fraction of reinforcing particles V_f . The solidification time of the casting decreases with an increase of ω . The apparent viscosity η of the composite is estimated as a function of the liquid matrix viscosity η_L and the particle volume fraction V_f as indicated by equation 3.3 [18].

$$\eta = \eta_L \left(1 + \frac{5}{2} V_f + 7.6 V_f^2\right) \quad (3.3)$$

Until now, there has been no attempt to apply this model to functionally graded composites where, intentionally and carefully, reinforcing particles are pushed by centrifugal forces to the outer layers of a casting.

2.2.2 Investment Casting

Investment casting is also known as the lost wax process and is one of the oldest manufacturing processes. The name “Investment” was originated because the Egyptians approximately 5,000 years ago used this technique to make gold jewelry. Investment Casting is a simple technique that allows production of castings with complex shapes and high accuracy without the subsequent need to machining them. Also this technique can be used to make parts that cannot be produced by normal manufacturing techniques such as turbine blades that have complex shapes, or airplane parts that have to resist high temperatures.

The basic procedure of investment casting is illustrated in Fig. 2.2. The mold is made by making a pattern using wax or some other material that can be melted away. This wax pattern is immersed in refractory slurry, which coats the wax pattern and forms a skin. After drying (immersing in the slurry and drying), the process is repeated until a robust thickness is achieved. After this, the entire pattern is placed in an oven and the wax is melted away. This generates a mold that can be filled with the molten metal. Because the mold is formed around a one-piece pattern, very complex parts can be made. The wax pattern is made by duplicating using a stereo lithography or similar model-which has been fabricated using a computer solid model master.

The materials used for the slurry are a mixture of plaster, a binder and powdered silica, a refractory, for low temperature melts. For higher temperature melts, sillimanite, an alumina-silicate is used as a refractory, and silica is used as a

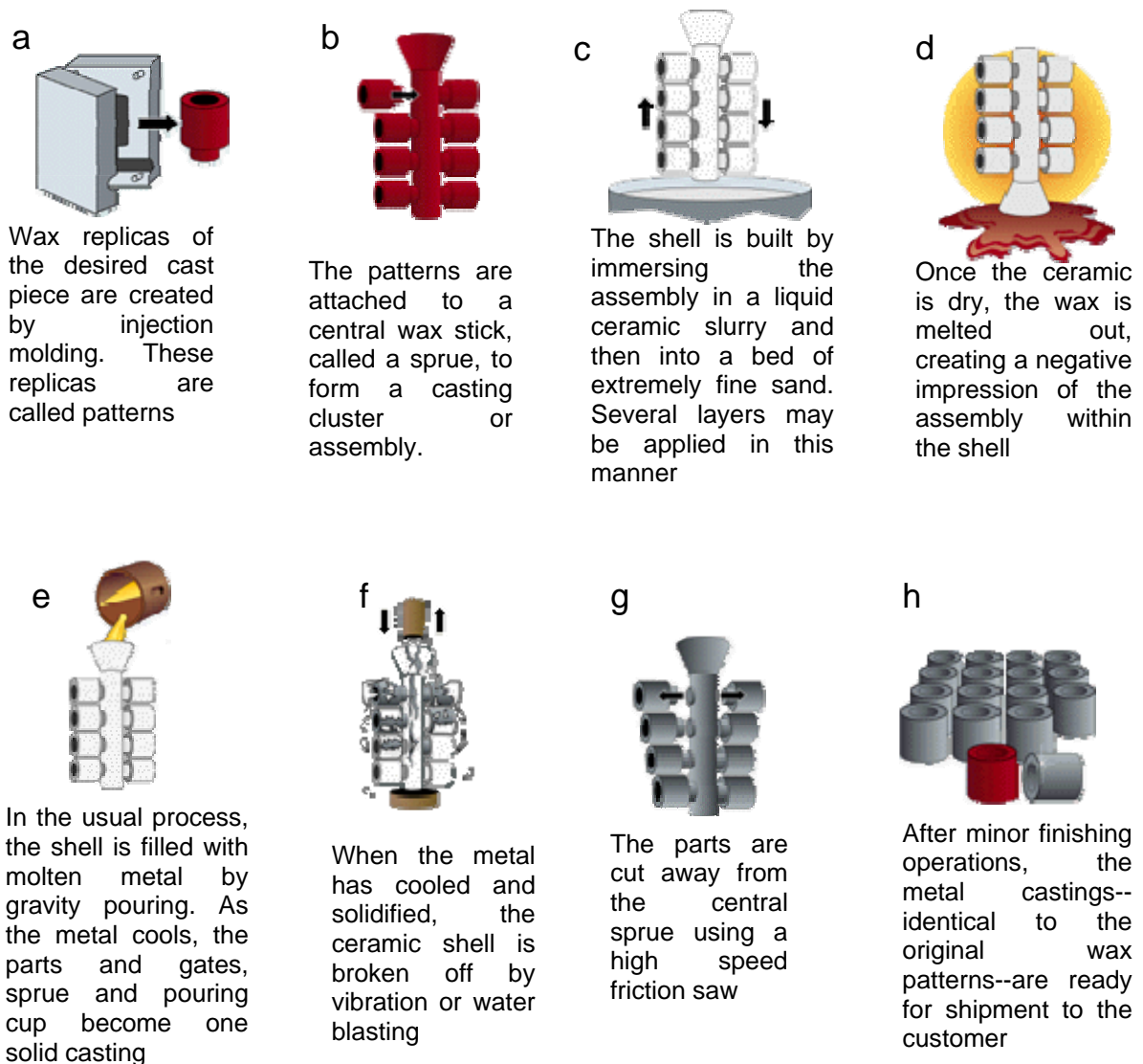


Figure 2.2 The Basics of the Investment Casting Process [19] **a)** Wax Injection **b)** Assembly **c)** Shell Building **d)** Dewax **e)** Conventional Casting **f)** Knockout **g)** Cut Off **h)** Finished Castings

binder. Depending on the fine quality of the finish desired additional coatings of sillimanite and ethyl silicate may be applied. The mold thus produced can be used directly for light castings, or be reinforced by placing it in a larger container and reinforcing it with more slurry or coarse sand. Just before the pour, the mold is pre-heated to about 1000 °C (1832 °F) to remove any residues of wax and harden the binder. The pour in the pre-heated mold also ensures that the mold will fill completely. Pouring can be done using gravity, pressure or vacuum conditions. Attention must be paid to mold permeability when using pressure, to allow trapped air to escape [20].

2.3 Metal Matrix Composites (MMCs)

Metal matrix composites are materials that have a metal or metal alloy as the matrix phase. The dispersed phase may be particulates, fibers, or whiskers that normally are stiffer, stronger, and/or harder than the matrix [21].

2.3.1 General Consideration

Three main types of MMCs can be classified according to these reinforcement; continuous-fiber, discontinuous-fiber, and particulate reinforced. Continuous-fiber reinforced MMCs, possess higher stiffness and strength because of continuous filaments. One of the first continuous-fiber to be developed MMC, was the aluminum alloy matrix-boron fiber reinforced system. Other continuous-fiber reinforcements that have been used in MMCs are silicon carbide, graphite, alumina,

and tungsten fibers. Many types of discontinuous and particulate reinforced MMCs have been produced. These materials have the engineering advantage of higher strength, greater stiffness, and better dimensional stability than the unreinforced metal alloys. Particulate reinforced MMCs commonly employ aluminum alloy MMCs made by using irregular-shaped particles of alumina and silicon carbide within 3 - 200 μm in diameter. The particulates, which sometimes were previously coated, can be mixed with the molten aluminum alloy and cast. Discontinuous-fiber reinforced MMCs are produced mainly by powder metallurgy and melt infiltration process. Whisker dispersion produces higher strength and stiffness than particulate ones. Nevertheless, the powder metallurgy processing and melt infiltration methods are more expensive [22].

2.3.2 Characteristics of MMCs

Metals are extremely versatile engineering materials. A metallic material can exhibit a wide range of easily controllable properties through appropriate selection of alloy composition and thermomechanical processing method. The broad use of metallic alloys in engineering shows not only their strength and toughness but also the relative simplicity and low cost of fabrication of engineering components by a wide range of manufacturing processes.

The necessity of achieving better properties than those obtained in monolithic metals has allowed the development of different kinds of MMCs. Therefore, new materials resulting from the addition of reinforcements to a metal may provide

enhanced specific stiffness coupled with improved fatigue and wear resistance, or perhaps increased specific strength coupled with desired thermal characteristics in the resulting MMC. However, the cost of achieving appropriate improvements remains a challenge in many potential MMC applications.

One of the main problems is focused on ensuring the optimum degree of chemical contact (or wetting) between the fibers or reinforcements and the matrix. In many systems, wetting is inhibited by oxide films or surface chemistry features of the reinforcing phase. Procedures to improve the interfacial characteristics often results in an undesirable degree of fibers/matrix interaction and damage. At elevated temperatures, inherent thermodynamic incompatibility was observed in the early MMCs. They are associated with wetting and stability problems [23].

Some differences among MMCs, polymer matrix composites (PMCs), and ceramic matrix composites (CMCs) are as follows. MMCs evidence higher ductility and toughness than CMCs, although they have lower ductility and toughness than their respective unreinforced metal matrix alloys. The role of the reinforcement in MMCs is to increase strength as is the case with PMCs. Reinforcement in CMCs is generally to provide improved damage tolerance; MMCs are temperature resistant, generally higher than polymers and PMCs but less than ceramics and CMCs.

The choice of a matrix alloy for an MMC is dictated by several considerations, the type of reinforcement is one of particular interest. In continuously reinforced

AMCs the use of fibers as reinforcements may result in transfer of most of the load to the reinforcing filaments and hence composite strength will be governed primarily by the fiber strength. For discontinuously reinforced MMCs, the matrix may govern composite strength in which case, the choice of matrix will be influenced by the required composite strength and matrix alloys [24].

2.4 Aluminum Matrix Composites (AMCs)

Particular interest has been paid on the use of aluminum and its alloys as matrix material in metal matrix composite owing to their low density. Al/SiC, Al/Graphite, Al/Boron, Al/Al₂O₃ are all well known aluminum matrix composites systems. In the manufacturing of these cast metal matrix composites a foremost topic is the appropriate incorporation of the reinforcements into the molten alloy, feature briefly mentioned earlier. It is a major issue that the melt should not only engulf but also “wet” the ceramic particles or reinforcement in order to prevent particle agglomeration, settling, and segregation, and to avoid discontinuities in the particle-matrix interface. Non-reactive, highly stable oxides, such as Al₂O₃ particles, are not wetted by molten aluminum, and these particles are pushed by the solidification front and segregate in the last metal to freeze. In many cases the reinforcers (e. g. SiC, graphite, etc.) react with the molten alloy to form reaction products that weaken the particle-matrix interface. As a consequence, deleterious reaction products can be formed in the composite (e.g. Al₄C₃ particles in AMC containing graphite or some carbide as reinforcements). In other words, chemical

reactivity between liquid Al matrix and ceramic particles must be considered in developing new Al matrix composites.

The lack of wetting and the potential reaction between Al and reinforcements can be overcome if the reinforcing particles are already present in the microstructure under thermodynamic equilibrium for the aluminum solidification temperature range. One system that results in an almost pure aluminum matrix containing small ceramic particles is Al-B. Currently, Al-rich alloys of this system are used as master alloys for grain refining of aluminum alloys [12]. The AlB_2 present in these alloys is basically a catalytic substrate for the early crystallization of the aluminum phase [13]. This is to say that there is an excellent wettability between the borides, acting as reinforcing particles, and the aluminum melt without any deleterious chemical reaction.

Several melt-processing techniques have been used in aluminum matrix composites (AMC) with different degrees of success to favor the incorporation of reinforcing particles. The high cost of production of AMCs can postpone additional applications of these profitable materials. For this reason, the design of new AMCs with a stable microstructure (in terms of matrix/reinforcer reactivity) is a requirement to keep the cost of production at low levels.

Mechanical properties of AMCs are significantly affected by the magnitude and the nature of residual stresses inherent in metal matrix composites. These stresses frequently are related with differences in thermal expansion coefficients

between matrix and reinforcements particles. Sometimes phase transformations can result in additional micro-residual stresses as well. Besides, small amounts of plastic deformation can significantly alter the state of residual stresses produced during fabrication [25]. As a final point, reinforcing aluminum alloys with ceramic particles produces high strength aluminum matrix composites. This property enables the applicability of AMC in the aerospace and defense industries, as well as in automotive disk brake rotors, pistons, upper control arms, etc.

2.4.1 Al – Mg Binary Alloy

The Al-Mg system, its thermodynamic and physical properties, phase equilibria, and diffusion data are important for the production of light, multicomponents alloys. For this reason thermodynamic studies of liquid Al-Mg alloys, and complementary studies of solid, and phase equilibria of Al-Mg alloys have been performed in order to calculate the phase diagram of the Al-Mg system [26].

Aluminum – Magnesium alloys are broadly classified as wrought (1 to 5 wt% Mg) and cast (5 to 10 wt% Mg) alloys. Above 7% Mg at room-temperature precipitation takes place and causes an increment in strengthening by work hardening in both types of Al-Mg alloys. On the other hand the mechanical properties are not affected by the aging treatment. This point of view is controversial, since the precipitation hardening treatment generally enhances the mechanical strength of aluminum alloys. Equilibrium precipitate $[Al_3Mg_2(\beta)]$, complex face-

centered cubic (fcc), $a = 28.2\text{\AA}$, 37.3 % Mg] has been observed to be preceded by nonequilibrium precipitates (e.g., Guinier–Preston (GP) zones, β'' [Al_3Mg with $L1_2$ structure] and β' [hexagonal phase with $a = 11.3\text{\AA}$ and $c = 17\text{\AA}$]). Recent calorimetric studies have indicated that the precipitation temperatures of β' and β are 100° and 250°C , respectively, and the dissolution temperature of $\beta' + \beta$ is 250°C to 420°C . The presence of trace amounts of heterogeneities facilitate formation of β' , and, the lack of heterogeneities/dislocations allows the formation of β . This phase has been reported to be susceptible to twinning, which can be avoided only by slow cooling from the melting temperature. The decline of mechanical properties during long-term (natural aging) is usually attributed to the formation of GP zones. This phenomenon is widely studied and compared with the formation of β'/β precipitates at relatively high temperatures [27].

Mg forms a complicated system with Al, as is shown in Fig 2.3. Mg decreases the density of Al; density decreases linearly by approximately 0.5% for every 1%wt% Mg in solid solution [25].

Magnesium has a very high solid solubility in solid aluminum (up to 14.9 wt% at 450°C); this solubility decreases to approximately 1.7 wt% at room temperature, but the rate of decomposition of the supersaturated solid solution is very low [25]. In addition, Mg provides to molten aluminum alloy at 880°C better fluidity at 15wt% for each 1 wt% of Mg with respect to an unmodified alloy [28]. Nucleation and growth of the β phases on the grain boundaries in certain Al-Mg (>3wt%Mg) alloys at room

temperatures reduce ductility and resistance to stress-corrosion cracking. Both yield strength and ultimate tensile strength increase with increasing Mg content while elongation drops sharply with even small Mg additions. Similar behavior with increasing Mg content is observed in tensile properties of commercial alloys. On an atomic basis, Mg is more efficient in strengthening in concentrations less than 1 at% than in more concentrated alloys [25].

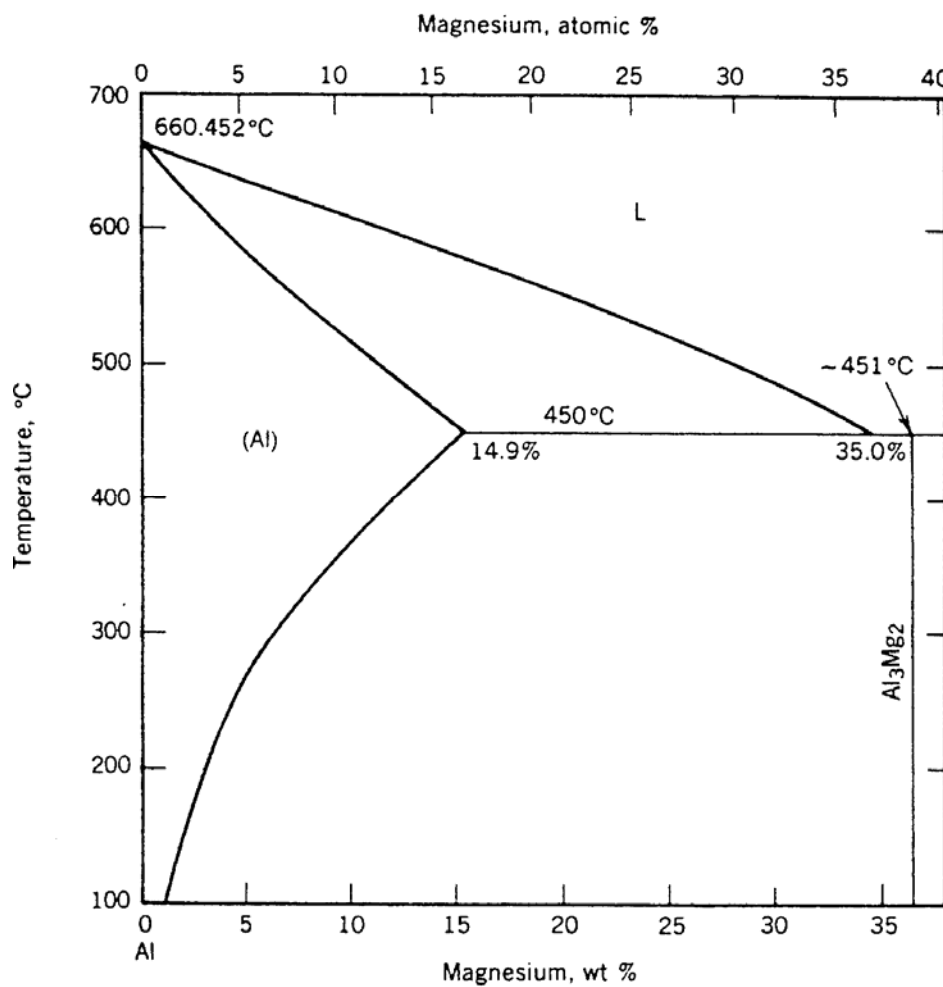


Figure 2.3 Al-Mg Binary Alloy Phase Diagram [25]

It is known that the addition of Mg influences the stacking-fault energy and thus, the strength, the recovery and the recrystallization characteristics of Al. Furthermore, the presence of Mg solute atoms may lead to the appearance of plastic instabilities resulting in the well known serrated yielding or Portevin-Le Châtelier (PLC) effect [29].

2.4.2 Aluminum Diboride (AlB_2)

Equilibrium phases in the Al-B system have been the object of extensive studies [30]. Experiments studying thermal behavior in all composition ranges in the binary Al-B system revealed at least seven invariant temperatures [30]. Early investigations of the constitution of the system Al-B claim the existence of a eutectic reaction $L \leftrightarrow Al + AlB_2$ at $560^\circ C$ at 30 to 35at.%B. AlB_2 forms peritectally from Al(L) and AlB_{12} at $1100^\circ C$ [30]. All things considered, it can be concluded that the stable solid phases in the Al-B stable system are βB , αAlB_{12} , βAlB_{12} , AlB_{10} , AlB_2 and Al. Despite the continuing controversy on the existence of βAlB_{12} and AlB_{10} , all the experimental evidence leads to the conclusion that these phases are impurity (carbon) stabilized and that AlB_2 and AlB_{12} are the only true binary aluminum boride compounds [31]. It is also shown that a carbon impurity has a tendency to shift the peritectic temperature to higher temperatures. Thus experimental viewpoint indicates that the Al-B system seems susceptible to impurities and the use of the crucible. It is apparent that the use of graphite crucible alters the occurrence of phases when B concentration is high enough.

2.4.3 Other Transitional Metal Diborides

The AlB_2 type structures (hp_3) types are among the most commonly found in intermetallic binary and ternary compounds. The boron atoms form honeycomb layers, while Al atoms are located at the centers of hexagonal prisms that are formed by the B sheets. Transition metal diborides, belonging to this family, are being studied in some detail because of their potential application in electronic devices to overcome current problems of electromigration, corrosion, and diffusion into the semiconductor substrate. The largest interest has undoubtedly been the discovery of superconducting properties in MgB_2 which also crystallizes in the simple AlB_2 as is shown in Fig. 2.4 [32].

In January 2001 the superconducting properties of MgB_2 were discovered with a $T_c = 39K$, which was followed by a flurry of studies seeking to increase T_c , by uncovering the basic physics. MgB_2 is analogous to other intermetallics compounds with high T_c coming from the exceptionally high vibrational energies in the graphite-like boron planes (honeycombed layers). MgB_2 has AlB_2 -like $hP3$ tetragonal crystal structure, as does TiB_2 , and the c/a ratios are similar for 1.082 and 1.142, respectively for AlB_2 and MgB_2 [33]. In a preliminary investigation, powder mixtures containing MgB_2 and high purity Al were compacted and sintered. The compact was later treated at $750^\circ C$ or arc-melted to investigate the stability of MgB_2 in the presence of molten Al. According to x-ray microanalysis the thin boride plates contain Al and Mg with a likely formula $Al_{1-x}Mg_xB_2$. This solubility is not entirely surprising due to the aforementioned affinity between AlB_2 and MgB_2 . Additionally,

due to the low atomic numbers of Mg and Al, both compounds have mostly metallic bonds, which differentiate them from other transition metal diborides, e.g. ZrB_2 , NbB_2 and HfB_2 , which have a strong covalent contribution to the atomic bonding, which results in higher melting points [34].

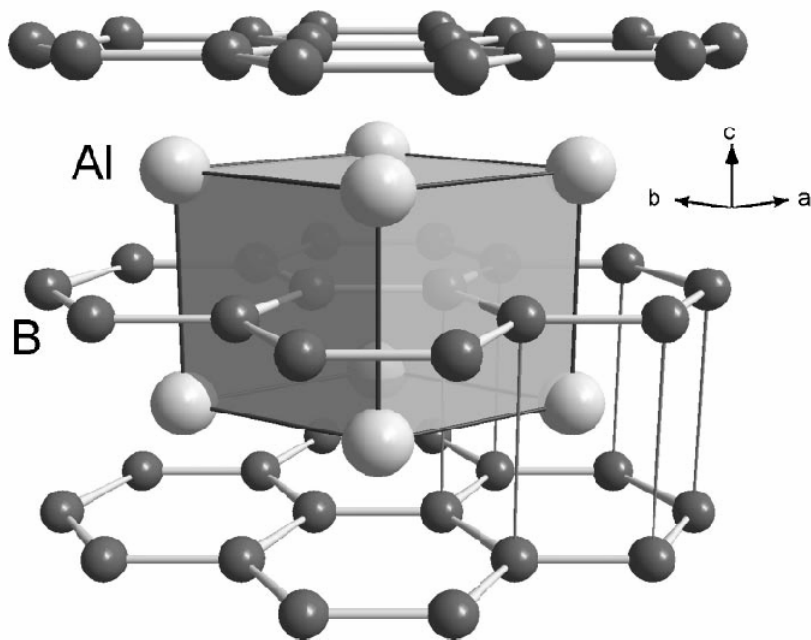


Figure 2.4 Crystal Structure of AlB_2 [32]

However, what makes all these diborides particularly interesting for the present research is their hardness [35] and small sizes, which translates into effective obstacles for dislocation glide on the $\{111\}$ Al planes, i.e. an aluminum matrix composite reinforced with diborides. Furthermore, the transition metal diborides also possess a higher density than aluminum, which is a major advantage.

Table 2.1 displays literature data on density and melting points of pertinent diborides.

Diboride	Bulk Density at Room Temperature (g/cm ³)	Melting Point (°C)
AlB ₂	3.09	1,655
CrB ₂	5.20	2,200
HfB ₂	11.20	~3,380
NbB ₂	6.60	3,036
TiB ₂	4.38	3,225
ZrB ₂	6.17	3,245

Table 2. 1 Reported bulk densities and melting points of some transition metal diborides [30, 36-38].

2.5 Stereological Analysis

Effective microstructural characterization has motivated the development of practical image analysis to measure particle count, phase volume fraction and size for various materials. Along the years the science of stereology was consolidated, based upon a mathematical framework that allowed systematic, manual and automatic measurements using various overlay grids for accurate and efficient measures of two- dimensional images which allowed three-dimensional information about the microstructure [39]. Stereology is the science of the geometrical relationships between a structure that exists in three dimensions and the images of

that structure that are fundamentally two-dimensional (2D) [40]. Although these images may be obtained by various means, they usually fall into two basic categories: images of sections through the structure and projection images viewed through structure. The most intensive use of stereology has been in combination with microscope images, which includes light microscopes (conventional and confocal), electron microscopes and other types.

Image analysis is based on processes which allow obtaining various measurements from images. There are many measurements that can be made, such as size, shape, position and brightness of all features present on a given image as well as the total area covered by each phase. Most of these values are not very directly related to the three-dimensional (3D) sample that is presented and represented in the image. Stereological relationships provide a group of geometrical tools that can relate some of the measurements on the images to important parameters of the actual 3D structure. Only those parameters that can be calculated from the stereological relationships truly characterize the 3D structure. Among objects that can occupy three dimensional space we can mention essentially: objects that have a volume, such as particles, grains, cells, pores or voids, and fibers; two dimensional surfaces, which include the surface of the 3D objects, the interfaces and boundaries between them, and objects such as membranes; one dimensional feature, which include curves in space formed by the intersection of surfaces; zero dimensional features, which are basically points in space. By comparison, image analyzers are quite good at counting but not as competent at

recognizing features of interest. Fortunately, there has been tremendous progress in the development of powerful, user friendly computerized image analyzers.

The introduction and the now widespread application of digital image processing system has allowed measuring the geometry of such two-dimensional structures more rapidly, more precisely and more comprehensively than ever before. Digital images analysis from a range of microscopic techniques can aid in the investigation of microstructural components across meter scale down to point defects in the atomic domain. The stereological interpretation of the geometrical data extracted from planar images is essential for the establishment of correlations between processing parameters, and the material properties. This topic has been greatly advanced in recent years by developments in stochastic geometry [41].

2.6 Wear

2.6.1 Introduction

Wear is an important topic from an economical point of view because it represents one of a very limited number of ways in which material objects lose their usefulness. The response of a material to friction and wear is determined by a number of factors related to fundamental properties of the materials in contact. Unfortunately the inherent interdependence among those factors and properties encumber a straightforward analysis of this phenomenon. Historically, the study of

the wear process was initiated very late, so the explanation of the laws of wear is relatively recent. There was the attitude on the part of many engineers and scientists that wear was a phenomenon so complicated and erratic that a systematic investigation was considered to be a waste of time [42].

Perhaps the biggest challenge in solving wear problems is related with preventing the types of wear to which components will be subject. Material can be removed from a solid surface in only three ways: by melting, by chemical dissolution, or by the physical separation of atoms from the surface. The last method can be accomplished either by the one-time application of a high strain or by cyclic straining at lower magnitudes. Mechanical and chemical processes may operate separately or together, such as abrasion in a corrosive medium [43].

2.6.2 Surface Damage and Wear

Surface damage is defined as topographical or microstructural changes, or both, on a surface layer. Surface damage to a tribosystem is most often generated in many consecutive small steps by a number of different micromechanisms that are active in the tribosurface. The observed damage is thus the cumulative effect on a macroscale of these micromechanisms [43]. Ideal classification of surface damage based on the resulting surface is illustrated in Fig 2.5. In principle, a tribosurface may exhibit damage of a single type, but generally the pattern is a combination of two or more types. Examination and interpretation may be quite complex. All the types of damage shown in Fig 2.5 will in practice influence a surface layer. It can be

noted that using the present definition, topographical or structural changes of the surface layer damage is not necessarily harmful.

The surface damage without exchange of material can be classified as: *structural changes* such as aging, tempering, phase transformations, recrystallization, etc; and *plastic deformation* which is the damage characterized by residual deformation of the surface layer, either locally or extensively. The latter is often revealed as a change in shape; *surface cracking* is the damage caused by excessive local contact strains or cyclic variations of thermally or mechanically induced strains. The latter case can cause dense patterns of parallel cracks whereas thermal cycling lattice generates a network of cracks.

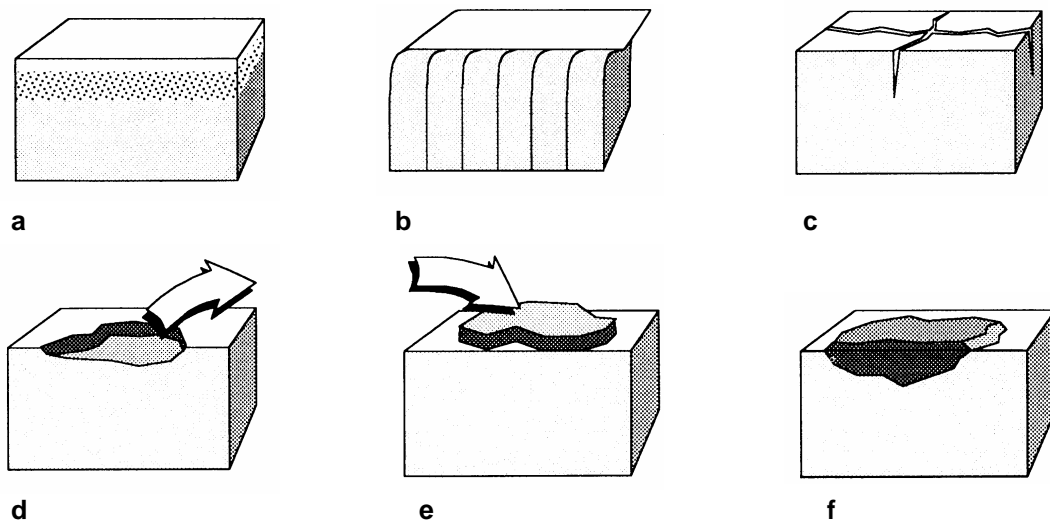


Figure 2.5 Classification of surface damage a) Structural changes b) Plastic deformation c) Surface cracking d) Wear e) Gain of material f) Corrosion [43].

Surface damage involving loss of material (*wear*) is based on the loss of material of the surface, which leaves behind wear scars of various shapes and sizes. Fundamental elements in the process of material removal can be shear fracture, extrusion, chip formation, tearing, brittle fracture, fatigue fracture, chemical dissolution, and diffusion. Finally surface damage involving *gain of material* explores, first, the phenomenon of picking up loose particles, transfer of material from the countersurface, etc, and the *corrosion* event consisting of material degradation by chemical reactions with ambient elements or elements from the countersurface.

The fact that the damage observed on a tribologically loaded surface normally is a combination of two or more of the types illustrated in Fig 2.5 indicates that several mechanisms have been operating simultaneously. The overlapping mechanisms generally do not operate independently, but interact to mutually increase the effects of one another. An example of such synergistic interactions is the simultaneous corrosion and wear involved in high temperature erosion. Occasionally, however, the combined effects can lead to a net reduction of the individual effects. One example of such a counteractive interaction is the inhibition of severe adhesive wear of metals in sliding contacts by the formation of an oxide layer [43].

Wear may be defined as the surface damage or removal of material from one or both of two solid surfaces in a sliding, rolling, or impact motion to one another as a result of mechanical action. It is characteristic that the amount of material removed

in the wear process is quite small [42]. Wear is generally based on loss of material, but it should be emphasized that damage due to material displacement on a given body, with no net change in weight or volume, also constitutes wear. In addition, wear as friction, is not a material property, it is a system response [44].

Finally we can say that wear is undesirable in almost all machine applications such as bearings, gears, and cams. Components may need replacement after a relatively small amount of material has been removed or if the surface is unduly roughened.

2.6.3 Types of Wear

Adhesive Wear. Adhesive wear occurs when two smooth bodies are in sliding contact, whether lubricated or not. Adhesion (or bonding) occurs at the asperity contacts at the interface and these contacts are sheared by sliding, which may result in detachment of a fragment from one surface and attachment to the other surface. Later these fragments may come off the surface on which they are formed and be transferred back to the original surface, or else form loose wear particles. Adhesive wear arises from the strong adhesive forces set up whenever atoms come into intimate contact [44].

In an early theory of sliding wear, it was suggested that shearing can occur at the original interface or in the weakest region in one of the two bodies. In most cases, interfacial adhesion strength is expected to be small as compared to the

breaking strength of surrounding local regions; thus, the break during shearing occurs at the interface in most of the contacts and no wear occurs in that sliding cycle. In a small fraction of contacts, break may occur in one of the two bodies and a small fragment may become attached to the other surface. In another mechanism, plastic shearing of successive layers of an asperity contact results in detachment of a wear fragment.

Abrasive Wear. Abrasive wear occurs when asperities of a rough, hard surface or hard particles slide on a softer surface and damage the interface by plastic deformation or fracture. In the case of ductile materials with high fracture toughness, hard asperities or hard particles result in the plastic flow of the softer material. Most metallic and ceramic surfaces during sliding show clear evidence of plastic flow, even some for brittle ceramic materials. Contacting asperities of metals deform plastically even at the lightest loads. In the case of brittle materials with low fracture toughness, wear occurs by brittle fracture. In these cases, the worn zone consists of significant cracking. There has sometimes been confusion between fine abrasive wear a form of relatively benign adhesive wear [44].

Corrosive Wear. Corrosive wear occurs when sliding takes place in a corrosive environments. In air, the most dominant corrosive medium is oxygen. Therefore chemical wear in air is generally called oxidative wear. In the absence of sliding, the products of corrosion will form a film on the surfaces. This film tends to delay or even detain the corrosion. However, the sliding action wears the film away,

so the corrosive attack continues. Thus chemical wear requires both chemical reaction (corrosion) and abrasion [44].

Surface Fatigue Wear. Surface fatigue wear is observed during repeated sliding or rolling over a track. The repeated loading and unloading cycles to which the materials are exposed may induce the formation of surface or subsurface cracks, which eventually will result in the break up of the surface with the formation of large fragments leaving large pits in the surface [44].

Studies of the wear process indicate that the adhesive wear is the most common and least avoidable form of wear. As far as is known, this form of wear is universal in all mechanical systems in which two solids slide in contact with each other. It cannot be eliminated but only reduced [42].

2.6.3 Tribological Parameters

Many investigators use standard test geometries for wear and friction test, such as pin-on-disk or four-ball tests. The amount and structures of damage to these components is of great interest in such tests. Parameters such as the volume of material removed by wear and the surface area of the wear scar (track) are commonly the items to be determined in these tests [43].

There are different types of scratch test devices which can be organized into three main categories (see Fig 2.6): *Type 1* corresponds to low-speed bench top

scratching machines, normally equipped with a stylus to produce a scratch on a flat with a single pass (Fig 2.6a), with a reciprocating movement (Fig 2.6b), or with a multiple pass (Fig 2.6c); *Type 2* are low-speed scratching devices that operate *in situ* in the beam path of a scanning electron microscope (SEM), intended for detailed mechanism studies; *Type 3* refers to high speed scratching machines, which include penduli (Fig 2.6d) and grinding wheels (Fig 2.6e); essentially used for single pass grooving.

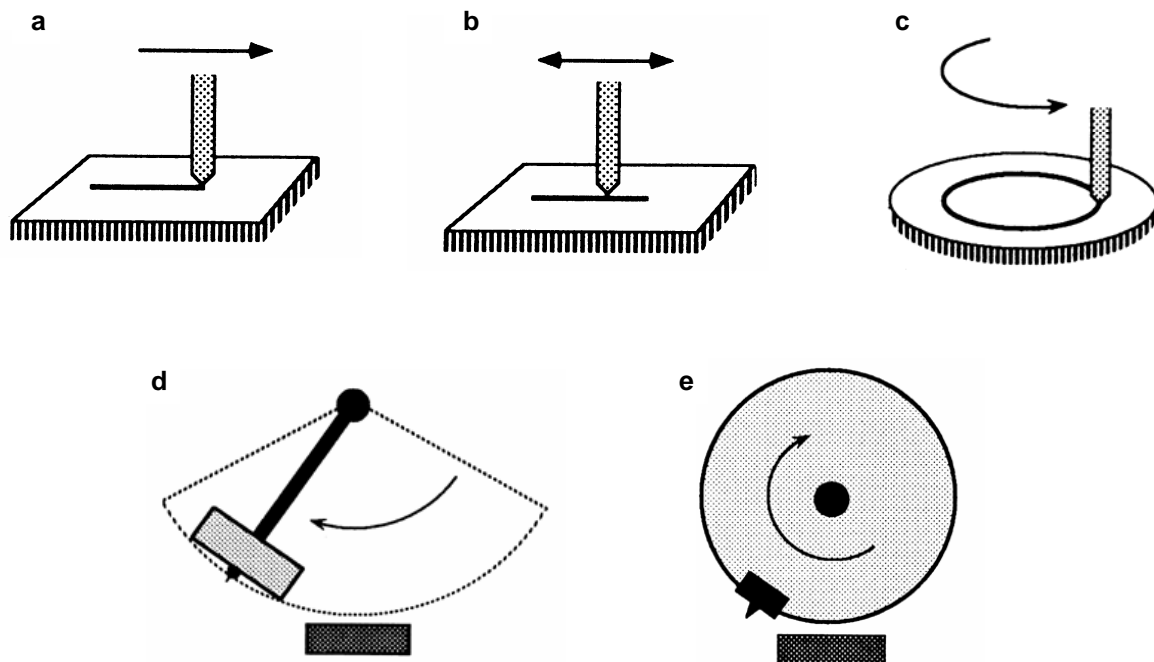


Figure 2.6 Scratch test devices a) Single pass b) Reciprocating c) Multiple pass d) Modified Charpy pendulum e) Modified grinding machine[43].

The analysis of wear data of such tribosystems or corresponding laboratory test configurations and test specimens requires special attention because numerous characteristics, parameters, and factors must be taken into consideration. In a wear

test the resistance against surface damage (wear) of a material pair (dry system) or a material/lubricant/material combination in a given environment is determined under the action of a certain type of motion, such as sliding or rolling. The resulting tribometric characteristics—in particular the wear data must be understood as characteristics of tribological systems associated with the structural, operational, and interaction parameters. The structural parameters are characterized by the component such as materials, lubricant and environment involved in the wear process and their physical, chemical, and technological properties. The operational parameters are mainly kinematic and temperature conditions and their functional duration. Interaction parameters characterize in particular the action of the operating parameters on the structural components of the tribological system and define its contact and lubrication modes.

The principal parameters that can be measured on the wear test are: *Length*, that is, one-dimensional changes in the geometry of the interacting triboelements perpendicular to their common contact area; *Area*, that is, two-dimensional changes of cross sections of interacting triboelements perpendicular to their common contact area; *Volume*, that is, three-dimensional changes of geometric regions of interacting triboelements adjacent to their common contact area. Wear volume is associated via density or specific gravity with wear masses or wear weights. In addition to these quantities, a wear-time ratio may be defined as wear velocity. Other common wear parameters are the wear rate, which is the wear volume per unit of sliding distance, and the wear coefficient, K , defined according to equation 3.4 [43].

$$K = \frac{W}{F_N \cdot s} \quad (3.4)$$

Where:

W = Wear volume (mm³)

F_N = Applied load (N)

s = sliding distance (m)

It should be emphasized that generally wear quantities must be determined for both components involved in a wear process.

The most common way of studying wear consists of pre and post examination of the sliding materials, with any differences in the materials attributed to wear. The detection of wear generally uses techniques of weighing, mechanical gaging, or optical examination of the surface features. The weighing method is usually the simplest way of detecting wear, since it at once gives the total amount of wear in the form of a single number. For this method it is necessary to remove from the sliding mechanism the component to be examined, to clean it carefully and then to carry out the weighing on a chemical balance. The limit of resolution of the weighing method is generally around 10⁻⁴ g [42].

2.6.4 Wear of Metal Matrix Composites

Metal matrix composites are attracting considerable interest because of their superior mechanical and tribological properties. As mentioned previously, these

materials have a metal matrix in which nonmetallic fibers, particles, or whiskers are dispersed. For use in tribological applications, metal-matrix composites must be able to support a load without excessive distortion, deformation, or fracture during performance and to maintain controlled friction and wear over long periods without breakdown under working conditions. The composites containing hard particles generally exhibit different friction and wear behavior than composites containing soft particles in alloys with the same matrix.

Particulate-reinforced composites are less expensive than fiber-reinforced composites, due to the lower cost of the particles providing their tribological applications. Furthermore, the mechanical and physical properties of particle composites are generally isotropic. In metal-matrix composites, mechanical properties depend on the amount, size, shape and distribution of the dispersed phase apart from the mechanical properties of the matrix material and on the nature of the interface.

The fracture toughness of particulate composites is low, and it decreases with volume fraction of a dispersed phase [43]. A weak interface leads to crack at low strain, and a low fracture toughness value indicates their easy propagation. In the context of the wear, these two properties are critical to the generation and propagation of cracks, resulting in wear debris. Pores in composite may act as preexisting crack nuclei in the system, and later become unstable at appropriate stress level. Porosity thus increases composite wear rate.

During tribological interaction between two surfaces, temperature rises significantly at and near the surface, and the mechanical properties of the composite at elevated temperature may be significant. The dispersed hard particles are helpful in retaining the high temperature strength of the matrix. Also, the loss of the strength due to dynamic recrystallization is supported by the presence of particles. Metal-matrix composites can thus have superior mechanical properties at elevated temperatures, even though their room temperature properties are not appropriate for certain systems.

Wear behavior of metal matrix composites depends on the nature of particle reinforcements in close relation to the matrix containing them. The particles can be softer or harder compared with the matrix. Ceramic particles generally used as reinforcements include carbon, silicon carbide, and alumina, which have low adhesion to a metallic counterface. The asperity of the counterface can easily break through softer particles such as carbon; it cannot do so through harder particles such as alumina or silicon carbide.

The abrasion resistance of a material generally is determined by two different types of test: low-stress tests, such as rubber wheel abrasion test and high-stress tests, such as pin-on-disk and pin-on-drum types of test. Tests employing high stress levels break the abrasive particles. The size and shape of the abrasive particles, as well as their relative hardness with respect to the composite being tested, are important parameters in determining the degree of wear. Under high-

stress conditions, the wear rate decreases almost linearly with the volume fraction of reinforcement particles in a composite.

Specific abrasive wear rates as a function of volume fraction for several hard particles dispersed in aluminum matrices showed that wear rates decrease with an increasing volume fraction of particles similarly to those observed in adhesive wear [43]. For a given volume fraction of particles, composites that contain harder particles exhibit a lower wear rate [43].

Under abrasive wear, the coefficient of friction in composites containing hard particles is also a function of the volume fraction of reinforcement particles. As the volume fraction of hard particles increases, the coefficient of friction decreases for both aluminum-based and copper-based composites. The increase in the volume fraction of hard particles in the matrix alloy reduces the area fraction of matrix, and thus there is enhanced ceramic-ceramic contact [43].

3. DEVELOPMENT OF PROCESSING AND CHARACTERIZATION METHODOLOGY FOR FGM - Al-B COMPOSITES

Through this chapter the reader will find the methodology used to manufacture aluminum-based FGMs reinforced with AlB_2 particles and their characterization procedure. To produce this FGM-AMC, centrifugal casting was considered the most appropriate technique for a commercial Al-5wt.% B alloy and an experimental Al- 4 wt.% B and 2 wt.% Mg alloy. The composite microstructure was characterized both qualitatively and quantitatively. Quantitative image analysis was used to evaluate the distribution of the reinforcement particles for Al-B and Al-Mg-B alloys in three conditions: as-received condition, gravity cast condition and internal and external zones of the centrifugally cast samples. These results were correlated to the values of superficial Rockwell hardness and Vickers microhardness measured on those composites. Unlubricated pin-on-disk configuration wear tests were conducted on the external and internal zones of the centrifugally cast AMC's and on stationary (gravity) cast specimens (disks). The Figure 3.1 illustrates a summary of methodology defined to processing and characterizing these material composites.

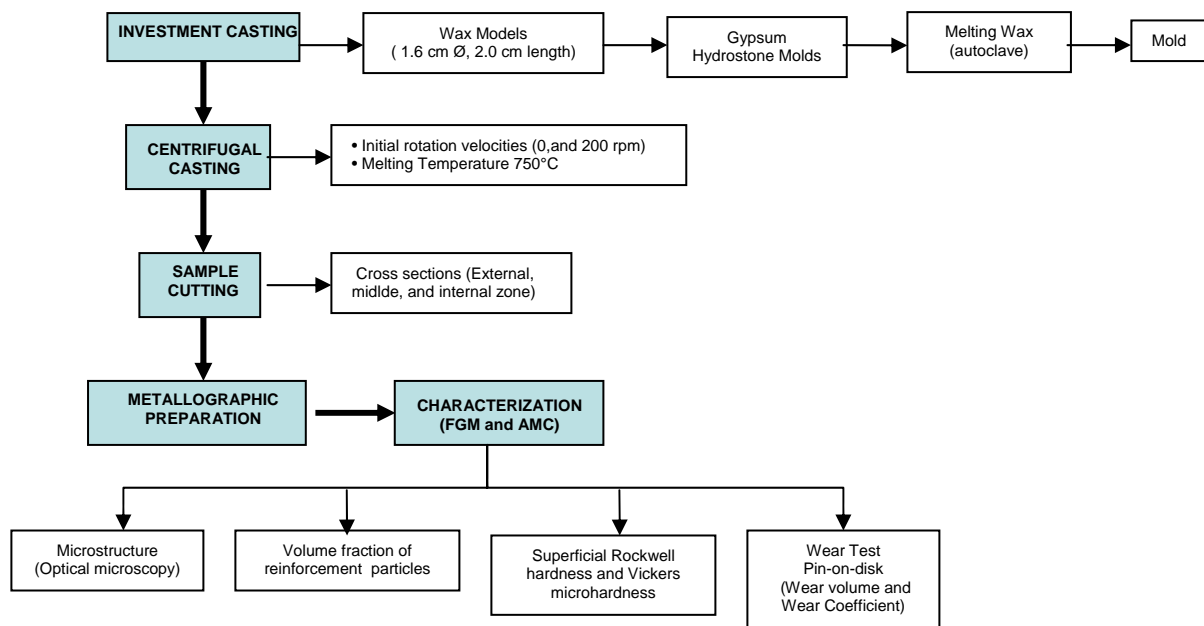


Figure 3.1 Diagram showing the experimental procedure sequence

3.1 Investment casting

The investment-casting process consists of three distinct steps: making an initial pattern (an exact replica of the article to be produced); building a refractory “shell” (mold) around the pattern and removing the original pattern, usually by heat and pouring molten alloy of the desired composition in to the shell. After the metal has solidified, other operations involve shell removal, finishing, and heat treating, but the general investment casting process is accomplished in these three steps.

In the present work, investment casting was limited to the first two steps: model-making and mold preparation. The metal pouring (third step) will be detailed in the centrifugal casting section. To fabricate the model, *FILE-ATM*- blue wax blocks were used. This wax is one of the most flexible carving waxes and excellent to

reproduce rounded parts and has a melting temperature of 105 °C. The model, contrary to a typical technique of injecting molten wax, was machined from a wax block, since, the final casting piece to be produced was a cylinder with a 16 mm in diameter and 20 mm in length (Figure 3.2 a). The smooth surface obtained in the model guaranteed the high-quality final surface of the metallic sample. In addition machining the wax block avoided undesirable injection characteristics of the wax such as shrinkage during solidification, dimensional stability, strength, thermal expansion near room temperature, etc. Maintaining the proper wax model properties helped ensure that the final metal shape was an exact replica of the wax pattern.

The finished wax model was encased in a ceramic mold material known as the “investment”. The mold was made by the flask molding method. In this molding method, the wax model was set into the flask and ceramic slurry was poured around the pattern. The ceramic used was hydrostone gypsum and the resulting mold is in the shape of a solid cylinder or block (see Figure 3.2 b). Once the mold is ready and completely dry the pattern must be removed. This operation is referred to as “dewaxing”, which is usually accomplished by inserting the mold into a steam autoclave or a high-temperature furnace (flash firing). The steam autoclave was the more appropriate technique for our particular goal, as is shown in Figure 3.2 c. The dewaxing setting parameters were 120°C and 30 minutes. Shells were normally fired immediately after dewaxing to burn off any residual wax and other organics. After residuals have been burned out, the mold is ready for metal pouring (Figure 3.2.d). As a particular experience, it was found that the removal of a pattern can be done

manually without melting the wax if the model surface was so much smooth and the model geometry was very simple. It helped to save time but implied additional changes in the model to hold it when the model was removed.

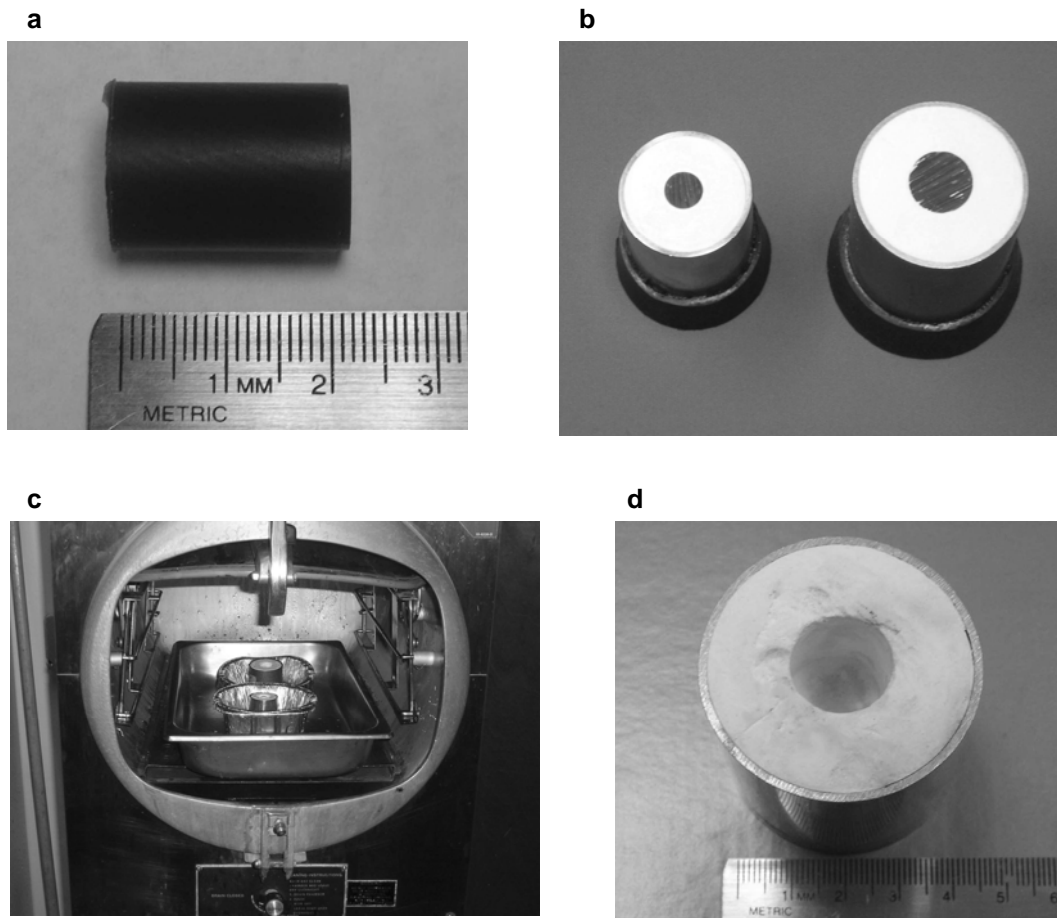


Figure 3.2 Investment Casting Process a) Model b) Investment c) Dewaxing d) Mold

3.2 Centrifugal Casting Process

Centrifugal casting is a technique used to obtain materials with higher density in the outer regions of a casting due to applied centrifugal forces. A Romanoff 79-049-T centrifugal casting machine (see Figure 3.3 a) was employed to cast two composites containing Al-5wt% B, and Al-4wt% B-2wt% Mg. This casting unit is

spring-driven for straightforward operation and uses flask sizes up to 88.9mm diameter x 127mm long. Additionally, a 340g capacity transfer scoop was utilized to pour the molten material, which subject to centrifugal forces, is driven into a mold placed in the flask (Figure 3.3 b). This mold produced by investment casting technique was preheated prior to centrifugal casting in order to facilitate the molten metal into the mold. Normal preheat temperature was 400°C during 1 hour. The centrifugal casting process was carried out with an initial (maximum) rotation speed of 200 rpm while the pouring temperature of the material was 750 °C. The samples finally obtained were cylinders with a 16 mm diameter and 20 mm length. This rotation velocity is normal in centrifugal casting operation [45].

The centrifugal casting technique that was used reached a maximum rotation speed which decreased gradually until it stopped; the rotation time and its speed depended on the strength of the spring. This small scale (50-60 g of charge material) equipment was suitable for laboratory experiments.

a



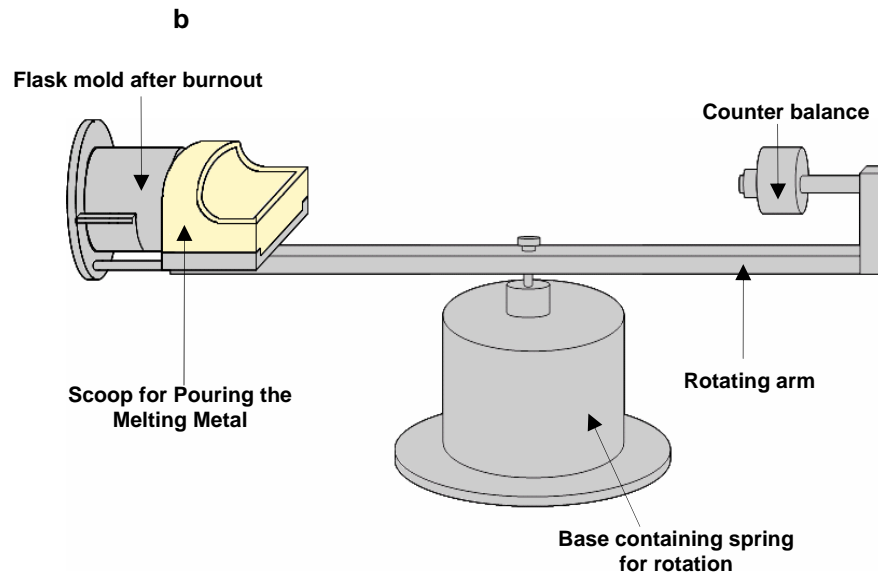


Figure 3.3 Centrifugal Casting Machine. a) Romanoff 79-049-T. b)Schematic drawing.

3.3 Sample Preparation

The cylindrical samples obtained from centrifugal casting process with dimensions of 16mm in diameter and 20mm in length (Figure 3.4 a) were cut to produce external, middle, and internal cross sections along the centrifugal casting direction, as shown in Figure 3.4 b. This longitudinal mapping of the centrifugally cast piece was done to identify the study zones on which the characterization of the FGMs-AMCs would be conducted. The cutting of the samples was done with BUEHLER IsoMet™ Low Speed Saw.

The whole metallographic procedure was carefully documented for reproducibility purposes. Grinding, the first step of the metallographic preparation, was carried out with a series of 320, 400, 600, and 800 grit SiC paper using water as

the coolant/lubricant. Next a first step of polishing was carried out using 3 μm diamond suspension (StruersTM DP), and lubricant (StruersTM DP) on a short felt cloth (Struers MD-MOLTM) followed by final polishing with a SiO_2 emulsion (StruersTM OPS) on short felt cloth (Struers MD-CHEMTM). For the metallographic preparation BUEHLER Alpha & beta grinder-polishers were used.

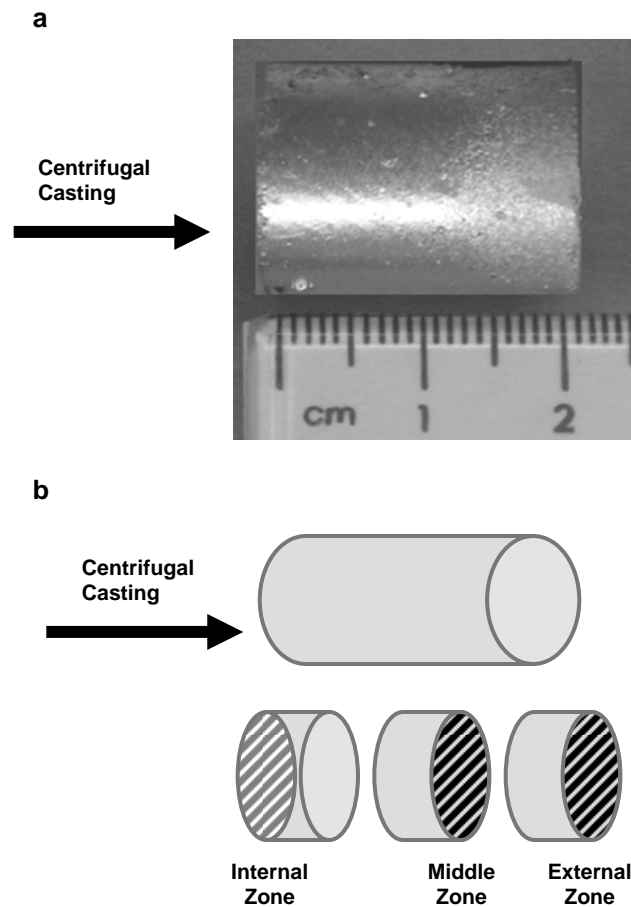


Figure 3.4 Centrifugally Cast Piece a) Final piece. b) Mapped longitudinal zones

The grinding and polishing steps produced smooth and scratch-free surfaces. These surfaces were finally cleaned in a Cole-Parmer[®] 8890 ultrasonic cleaner in ethyl alcohol as solvent.

3.4 Characterization

3.4.1 Microstructure

The microstructure analysis of these two Al-B, and Al-B-Mg composites was performed using a Nikon Epiphot 2 inverted optical microscope. Figure 3.5 presents the resulting microstructure with AlB_2 reinforcements embedded in the aluminum matrix for a binary Al-5wt% B composite.

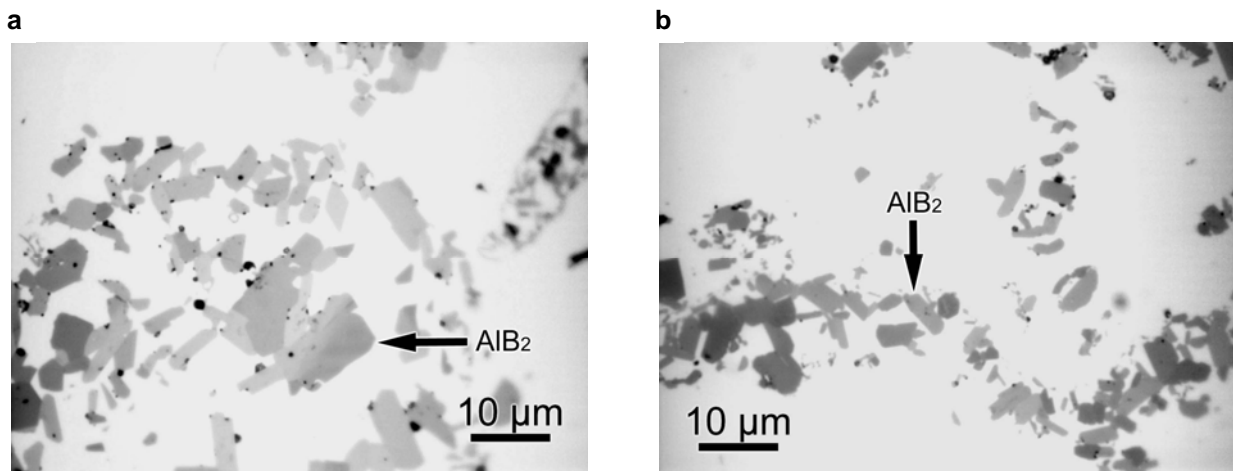


Figure 3.5 Micrograph of the microstructure of a centrifugal cast Al-5wt% B composite. a) Longitudinal section. b) Cross section.

As mentioned before, in the Al-B system the practical insolubility of boron in solid and liquid Al turns the Al-rich alloy into practical AMCs reinforced with AlB_2 particles [46]. This kind of AMC combines the low density of the Al matrix with the high hardness of the aluminum diboride reinforcements. The AlB_2 diboride has a higher density, 3.19 g/cm^3 [47], than liquid Al (approximately 2.4 g/cm^3) [48] at the semisolid composite casting temperatures ($> 700^\circ\text{C}$).

3.4.2 Analysis of the Volume Fraction of Reinforcement

Figure 3.6 presents the distribution of reinforcement (AlB_2) volume fraction based on one measurement of representative part and obtained by quantitative analysis performed manually. Naturally, the as-received and gravity cast AMC's exhibited a uniform distribution of the reinforcement particles. The composite samples produced by centrifugal casting showed higher densities of reinforcement particles in the outer regions compared to the inner regions of the casting. This occurs since the dispersed particles are segregated by centrifugal forces and the thickness of particle-rich region is strongly influenced by the speed of rotation, local solidification time and the density difference between the base alloy and the reinforcement [8].

In addition, Al-Mg-B composite exhibited more significant reinforcement particles segregation than the Al-B composite. As mentioned in chapter 2 this can be attributed to that the lower density of Al-Mg molten alloy (approximately 2.375 g/cm^3) [25], which provides more fluidity to the melt. On the other hand, it has already been established that higher boron levels, i.e. higher diboride volume fractions, increase the viscosity of the semisolid material [4]. This higher viscosity inhibits the movement of the diboride particles, which causes a lesser gradient of diboride volume fraction from the inner to the outer sections of the cast.

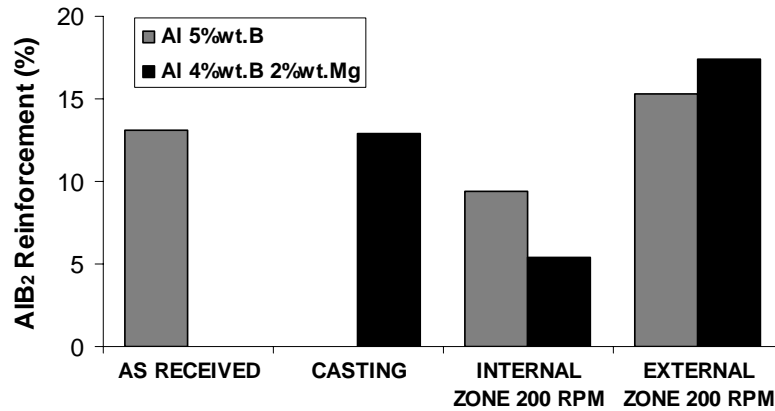


Figure 3. 6 Measured volume fraction of reinforcement particles in the AMC samples investigated in this study.

3.4.3 Superficial Rockwell Hardness and Vickers Microhardness Testing

The ASTM (American Society for Testing and Materials) standard test method for Rockwell superficial hardness of metallic materials is issued under the fixed designation E 18. In the Rockwell superficial hardness test the preliminary test force is 3kgf (29N) and total test force are 15 kgf (147N), 30 kgf (294N), and 45 kgf (441N). The standard indenters are the diamond spheroconical and the steel ball indenters 1/16, 1/8, 1/4, 1/2 inch (1.588, 3.175, 6.350 and 12.70 mm) in diameter. The Rockwell superficial hardness scale used on the Al-5wt% B and Al-4wt% B-2wt% Mg composites was 15 HRW (15 kgf, 1/8 inch. indenter) [49].

Figure 3.7 shows the variation of superficial Rockwell hardness on cross-sections of these AMCs measured for the aforementioned experimental conditions. The results revealed that the value of superficial hardness increases as a function of distance from the internal zone to the external zone in the experimental Al - 4wt.%B

- 2wt.% Mg composite. The Al-5wt.% B alloy did not demonstrate this behavior because the reinforcement particle gradient is not as apparent as the one observed in the Al-Mg-B composite.

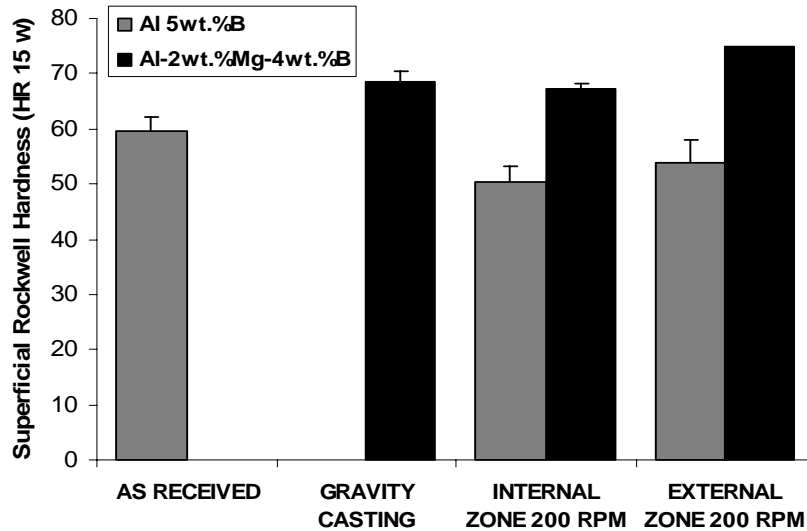


Figure 3.7 Rockwell superficial hardness (HR 15w) measured in the AMC samples investigated in this study.

The ASTM E 384 standard test method is used to determine the microhardness of materials. A Vickers microindentation test uses a calibrated machine to force a pyramidal diamond indenter of specific geometry, under a given load onto the test material surface; then the resulting rhomboid diagonals are measured optically. The Vickers number is then obtained by dividing the applied load in kilograms-force by the projected area of the indentation in square millimeters, computed from the measurement of the mean of the measured diagonals [50].

In the specific Vickers microhardness test conducted on the Al-B and Al-B-Mg composites, 50 gf was the test load: HV₅₀. The microhardness tester employed was a Buehler-Micromet[®] II.

Results of Vickers microhardness analysis selectively done on the Al matrix and reported in Figure 3.8 are in agreement with the superficial Rockwell hardness results. One could assume that the hardness of the matrix was not affected by reinforcement particles. However, this behavior has not often been observed since the values of Young's modulus and the thermal expansion coefficients in ceramic and intermetallic compound particles are different from those of the metal matrix. Hence, the residual strain energy caused by the stress field present in the metal matrix of the FGMs, depends on the composition gradient. The mutual relation among hardness, volume fraction of particles and strain energy can satisfy the supposition that the hardness and strain energy are proportional to the composition gradient [7].

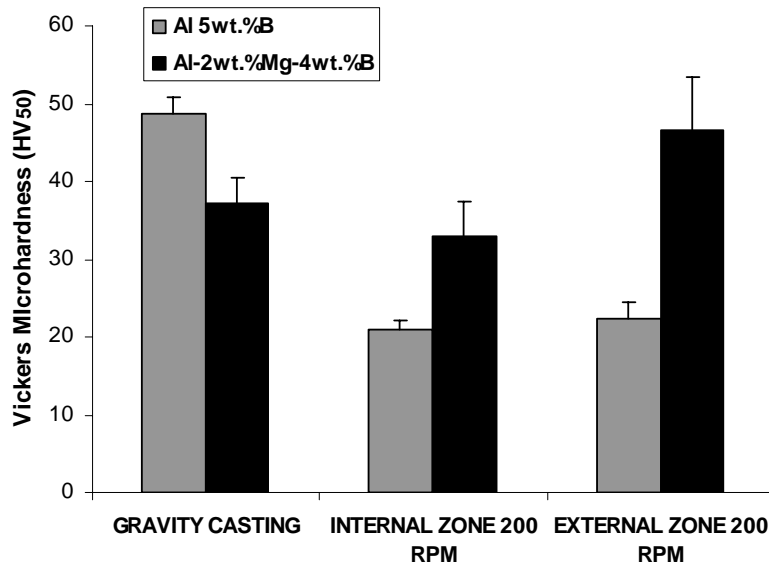


Figure 3. 8 Vickers microhardness (HV₅₀) values measured on the matrices of the different AMCs investigated in this study.

The addition of magnesium to the aluminum matrix had significant effects on their mechanical and microstructural properties compared with Al-B composites [29]. This

occurs because magnesium has a very high solid solubility in aluminum and the rate of precipitation of the supersaturated solid solution is low [25]. Furthermore, the high purity Al-Mg binary alloys show a more rapid rise in tensile strength than in yield strength, indicating that magnesium is promoting work hardening [25]. This explains the higher values of microhardness in the matrix of Al-Mg-B composites with respect to the matrix hardness of Al-B composites. These Vickers microhardness values are in agreement with prior research [51]. The microhardness result of Al-B casting can be attributed to its larger reinforcement particle size regarding Al-B centrifugally cast composites. This particle size can be diminished owing to interaction between particles during centrifugal casting. Even though the effect of reinforcement particle size was not dealt in this study, its influence has already been analyzed in the literature [10].

3.5 Pin - On - Disk Wear Testing

This test method covers a laboratory procedure for determining the wear of materials during sliding using a pin-on-disk apparatus and is issued under the standard ASTM G 99. For the pin-on-disk wear test conducted in this research, the two specimens were a pin with a rounded tip, which is positioned perpendicular to a flat circular disk (the test sample). A ball, rigidly held, is often used as the pin. The test machine causes either the disk specimen or the pin to revolve about the disk center. The sliding path is a circle on the sample surface [52]. The pin is pressed against the disk at a specified load usually by means of an arm or lever and attached

weights, as shown in Figure 3.9 a. A schematic drawing of a typical pin-on-disk wear test system is illustrated in the Figure 3.9 b.

Unlubricated pin-on-disk configuration wear tests were conducted on the external and internal zones of the centrifugally cast AMC's and on stationary (gravity) cast specimens (disks). The wear tests were conducted at a constant sliding speed of 0.0066 ms^{-1} . The counter-surface (pin) used was 3.175mm diameter ball of AISI 410 martensitic stainless steel ball. The duration of the wear test and the applied normal load were maintained at 45 min and 0.15N (15g), respectively, for all tests. The total sliding distance under these conditions was 18.5 m.

The wear volume was calculated from topographical characterization of the wear track. The track perimeters, widths, and depths were determined using a Nikon SMZ 1500 stereoscope, a Nikon Epiphot 2 optical microscope, and a Nanosurf easyScanTM atomic force microscope (AFM) respectively.

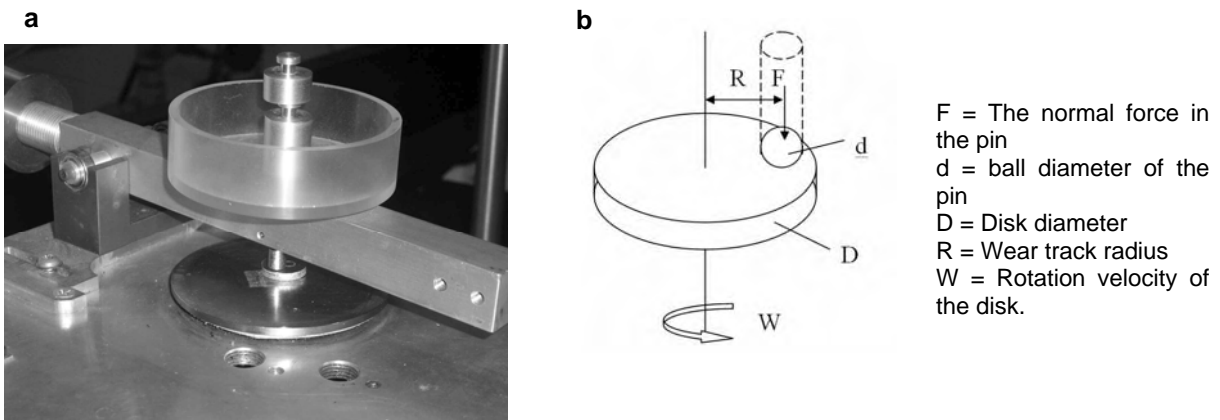


Figure 3.9 Pin-on-disk wear test system a) Unlubricated Pin-on disk tester. B) Schematic drawing [51].

3.5.1 Wear Volume and Wear Coefficient

The topographical aspects as well as the dimensions of the pin-on-disk wear tracks such as perimeter, width and depth are presented in Figure 3.10. These parameters allowed for the calculation of the wear volume on each sample. To calculate the volume of material removed, The profile was assumed to be a triangle based on optical microscope and AFM image data. Thus, the triangle area obtained was multiplied by the track perimeter.

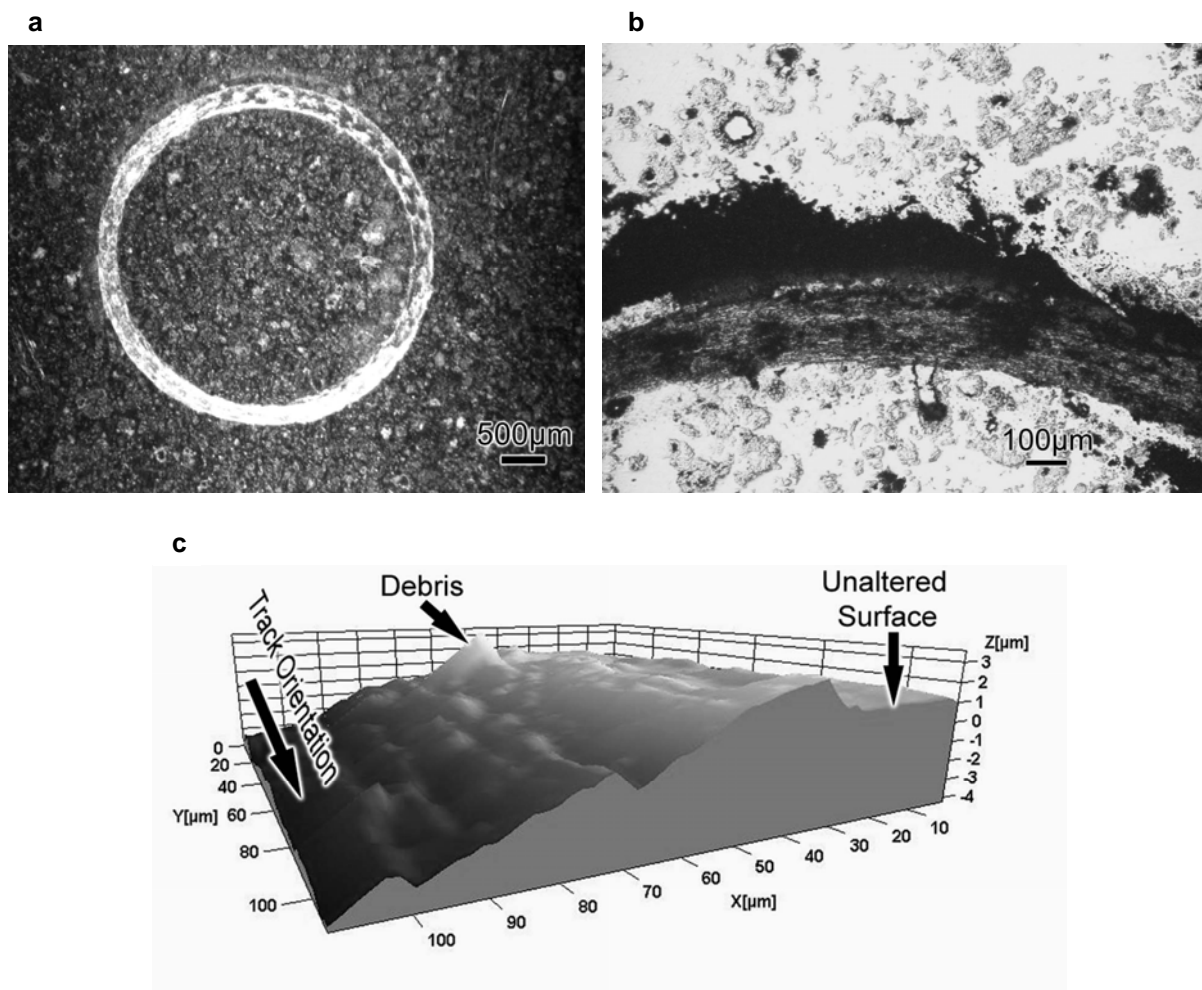


Figure 3.10 Images of wear tracks resulting from pin-on-disk wear tests a) Wear track of Al-4wt.%B-2wt.%Mg external zone of FGM b) Track width of Al-5wt.%B casting c) Track depth of Al-5wt.%B internal zone of FGM

Figure 3.11 shows the volumetric wear results obtained from gravity-cast samples as well as on the internal and external zones of the centrifugally cast samples of the Al-5wt%B and Al 4wt.%B 2wt.%Mg. The smallest wear volume measured was observed on the external zone of the FGMs. This is in agreement with the observed higher volume fraction of boride phases in these outer regions.

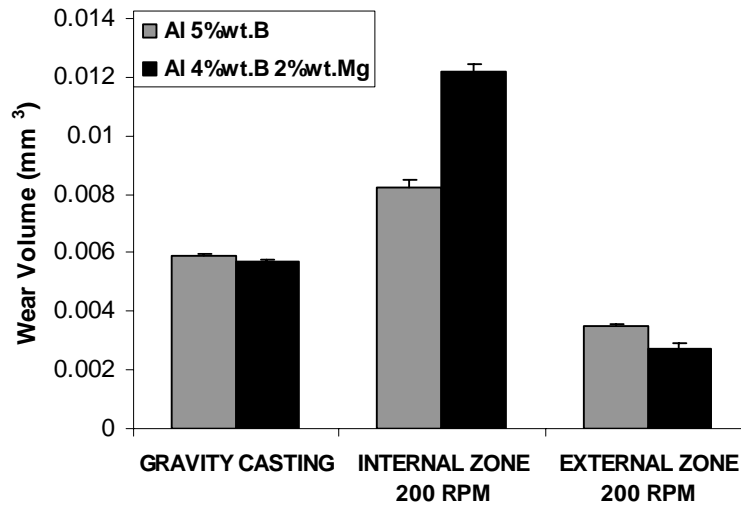


Figure 3. 11 Wear volume for the various AMC samples after undergoing pin-on-disk wear tests under identical conditions.

On the other hand, the internal zone of the FGMs (more depleted of AlB_2 particles) resulted in higher wear volume. The gravity-cast sample displayed a wear volume loss in between those exhibited by the outer and inner regions of the sample. Furthermore, the Al-4 wt.%B-2 wt.%Mg composite exhibited lower wear volume on the external zone than the centrifugally cast Al 5wt% B alloy. This effect is attributed to solid solution strengthening and precipitation hardening of metastable Mg-containing phases. Table 3.11 shows the wear coefficients according to Equation 2.4, calculated for the samples exposed to unlubricated pin-on-disk wear tests.

WEAR COEFFICIENT RESULTS (mm ³ /N·m)		
	Al 5%wt.B	Al 4%wt.B 2%wt.Mg
CASTING	0.001879	0.002342
INTERNAL ZONE 200 RPM	0.002958	0.004612
EXTERNAL ZONE 200 RPM	0.001246	0.000897

Table 3. 1 Calculated wear coefficient for the various AMC samples.

Wear test results, and wear track analysis are consistent with the microstructural gradients observed in these alloys. In effect, the higher volume fraction of reinforcing boride particles in the outer regions (external zones) of the centrifugally cast samples translates into a higher overall wear resistance in those regions. On the other hand, the internal regions (internal zones) are fairly depleted of boride reinforcement particles and, thus, are subject to high wear rates. Finally, as expected, the control sample (gravity-cast composite) displayed an intermediate behavior as the volume fraction of diborides is evenly distributed throughout the composite mass.

In general reinforcing AlB₂ particles (with higher bulk density than liquid aluminum) segregate towards the surface regions as a result of the inertial forces created the centrifugal casting process. Additionally, hardness values, wear test results, and wear track analysis are consistent with the microstructural gradient observed in Al-B-Mg composites. In effect, the higher volume density of reinforcing boride particles in the outer regions of the centrifugally cast samples translates into a higher hardness and higher overall wear resistance on those regions. On the other

hand, the internal regions are fairly depleted of boride reinforcement particles and, thus, are subject to higher wear rates. As expected, the control sample (gravity-cast composite) displayed an intermediate behavior as the volume fraction of diborides is evenly distributed throughout the composite mass. On the other hand Al-B composites did not fully display this behavior. Superficial hardness and microhardness were lower than Al-Mg-B composite and reinforcement particles gradient was not particularly relevant.

4. PROCESSING AND CHARACTERIZATION OF FGM Al-B-Mg COMPOSITES

The previous chapter dealt with the development of a processing and characterization methodology for FGM – Al-B and Al-B-Mg composites, from those results, the beneficial effect of magnesium in the composition gradient and wear resistance of these AMCs becomes apparent. In the present chapter further experimentation on Al-B-Mg composites was performed. In this case centrifugal casting was applied to experimental Al - 2wt%Mg - 1, 2, 3 and 4wt%B alloys. Qualitative and quantitative microstructural characterization methodologies are developed. Quantitative image analysis by Image J software Version 1.34s (see Appendix A) allowed measuring the reinforcers and pores volume fraction for Al-B-Mg composites in two conditions: gravity casting condition and at 0, 5, 10 15 and 20 mm from the internal centrifugally cast samples. In addition, matrix grain size and reinforcement particle size were determined by the Image J software. Superficial Rockwell hardness and Vickers microhardness were also measured on the composites and related to the properties previously measured. Pin-on- disk wear testing was carried out on Al-B-Mg samples (disks) in the two conditions described earlier. Morphological characterization of worn surfaces by scanning electron microscopy (SEM) was done on Al-2wt.%Mg-1wt.%B in both conditions, i.e. centrifugally cast and gravity cast. Figure 4.1 displays the steps of this experimental procedure used to process and characterize the Al-B-Mg composites.

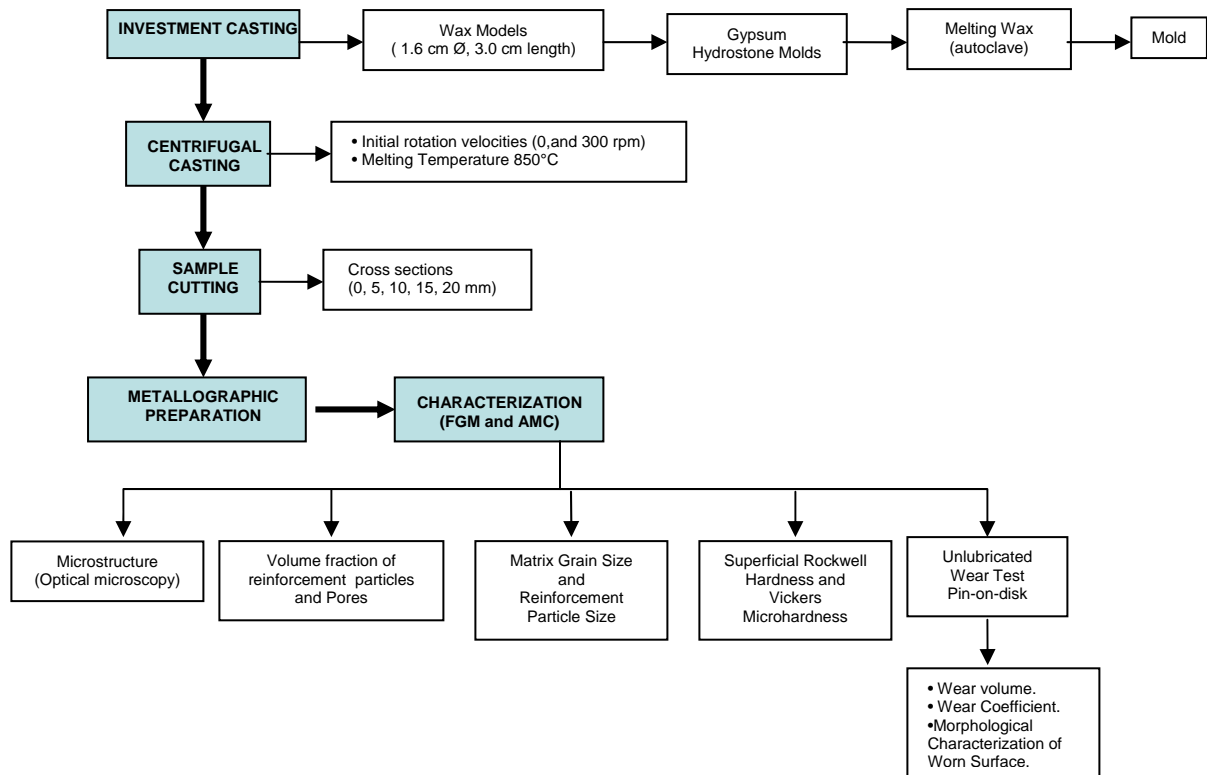


Figure 4. 1 Diagram showing the experimental procedure sequence to Al-B-Mg composite.

4.1 Investment casting

The investment casting process used to obtain a final mold for the semisolid Al-B-Mg composite was the same as the procedure established in the previous chapter. However, for the work presented the cast piece produced had larger dimensions. For this reason, the wax model dimensions (wax pattern) were 16 mm and 30 mm in diameter and length respectively.

4.2 Centrifugal Casting Process

The centrifugal casting technique carried out to obtain Al-B-Mg FGMs was similar to the method described on the section 3.2. Nevertheless, the centrifugal casting process was conducted with an initial (maximum) rotation speed of 300 rpm. This rotation speed is considered a normal operation velocity [45]. Furthermore the pouring temperature of the molten material was 850 °C. This temperature was established because mold filling problems occurred during experimental set up, provoked by very fast cooling of the semiliquid material. In addition, it is important to mention that the dimensions of the final cast pieces were increased. The samples finally obtained were cylinders with a 16 mm diameter and 25 mm length (see Figure 4.2 a).

4.3 Sample Preparation

The cylindrical samples centrifugally cast (Figure 4.2 a) were cut to generate 0, 5, 10, 15, 20 mm cross sections along the centrifugal casting direction, as shown in Figure 4.2 b. This longitudinal mapping of the centrifugally cast piece was made to categorize the study zones on which the characterization of the Al-B-Mg centrifugally cast would be conducted. The cutting of the samples was done with a Buehler IsoMet™ Low Speed Saw. The resulting samples of the cutting process were processed according to metallographic preparation procedure described in chapter 3.

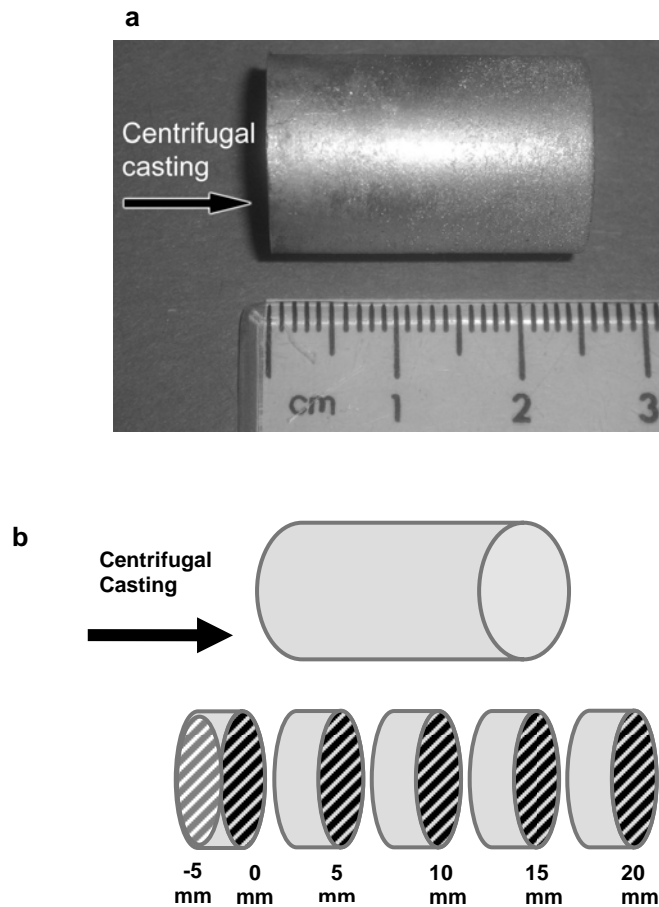


Figure 4. 2 Centrifugally Cast Piece a) Final piece b) Mapped longitudinal zones

4.4 Characterization

4.4.1 Microstructure

The microstructure analysis of the Al-B-Mg composite was performed using a Nikon Epiphot 2 inverted optical microscope. Figure 4.3 presents the resulting microstructure with AlB_2 reinforcements embedded in the aluminum matrix for a Al-2wt.%Mg – 1wt.%B composite. It can be observed that equilibrium precipitate $Al_3Mg_2(\beta)$ is present as well. This is one of stable phases in the Al-Mg system [27]. In addition, magnesium has a very high solid solubility in aluminum; this solubility

decreases to approximately 1.7 wt% at room temperature, but the rate of decomposition of the supersaturated solid solution is very low [25].

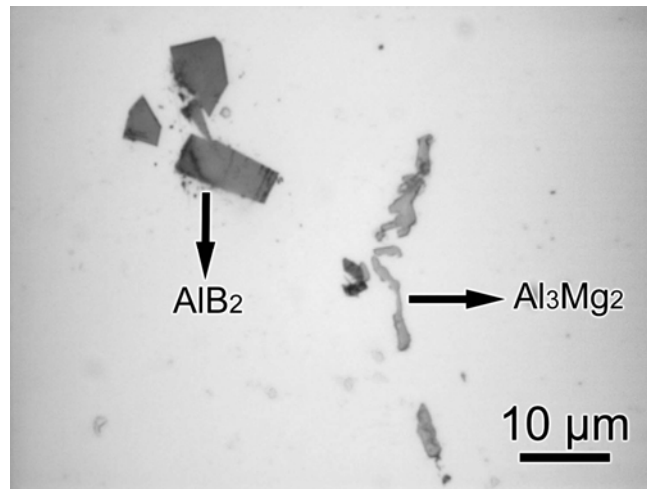


Figure 4.3 Microstructure of a centrifugal cast Al-2wt%Mg-1wt%B composite.

Thermodynamic and physical properties of the Al-Mg system are important for the production of these light, multicomponent alloys. The increasing magnesium content produces an increase in yield strength and ultimate tensile strength while the elongation falls with small Mg additions [25]. Advantages of the Al-B system and the importance of AMCs reinforced with AlB₂ particles were mentioned in prior chapters.

4.4.2 Volume Fraction of Reinforcement and Pores

The micrographs shown in Figure 4.4 present the distribution of AlB₂ particles along Al-2wt.%Mg-2wt.%B alloy centrifugally cast at 300 rpm. Figure 4.5 illustrates the results of reinforcement volume fraction obtained by Image J quantitative analysis to Al-B-Mg FGMs (see Appendix B). In the composite with 1%B, noticeable

segregation of reinforcers was observed starting at 15 mm, while the diboride volume fraction reaches a maximum in the 20 mm section. Al-B-Mg composites with 2 and 3%B showed AlB_2 particles displacement from 10 mm to 20 mm sections. At 4%B the composite displayed dispersion of reinforcement particles from 5mm to 20mm.

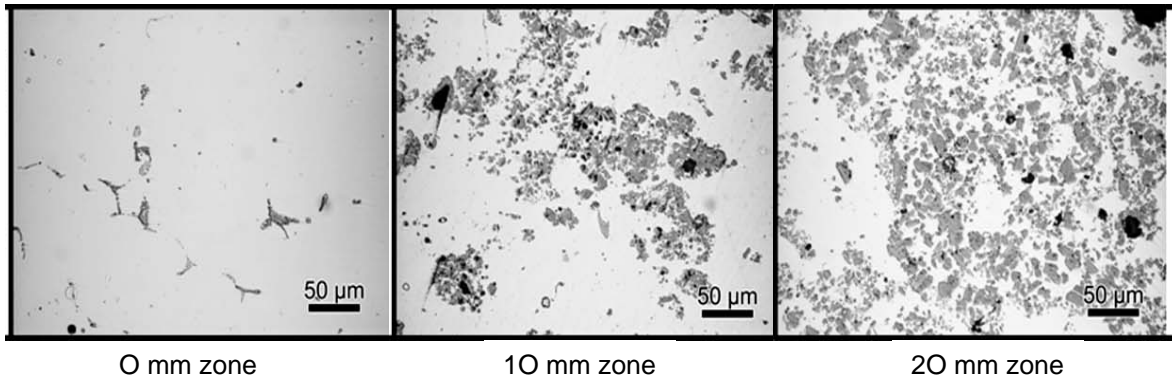


Figure 4. 4 Micrographs of Al-2wt%Mg-2wt%B FGM mapped longitudinal sections

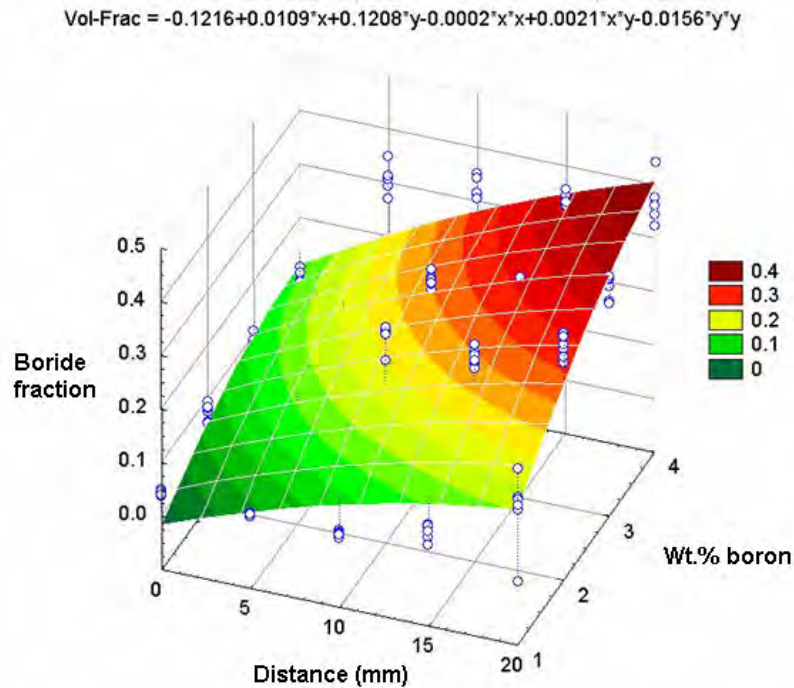


Figure 4.5 Measured volume fraction of reinforcement particles in the FGM samples as a function of distance.

The segregation of AlB_2 particles occurs due to the centrifugal force applied to the semisolid mixture of molten metal and dispersed particles, which leads to the formation of the desired composition gradient. Here, the gradient is controlled mainly by the differences in density between the matrix and the dispersed material [53]. Furthermore, percentage of boron affected the segregation in these FGMs. This can be explained by the composition gradient induced by centrifugal casting. The segregation is affected by the rotational velocity, density and size of the particles, the viscosity of the semisolid material, mean volume fraction of particles, and the local solidification time [53]. In particular the higher boron levels increase the viscosity of the semisolid material by increasing the number of solid AlB_2 particles.

Figure 4.6 shows the reinforcement volume fractions in a Al-2wt.%Mg -B gravity casting alloys when its boron percentage varies from 1 to 4wt%. These gravity casting composite values are identified as intermediate values in relation to reinforcers volume fraction of the FGMs. Furthermore these results confirmed quantitatively the influence of boron in the formation of aluminum diborides into Al-Mg-B alloy.

Variation of pore levels in the Al-B-Mg FGMs is illustrated in Figure 4.7. This variation determined by Image J (Appendix C) helped to identify that in the centrifugally cast composite Al-2wt.%Mg-1wt%B a lower number of pores are present. However, the porosity increases when the volume fraction of reinforcement increases in the 10 mm section. A similar tendency was revealed in the 2 and

3wt%B composites. Furthermore, these composites exhibited more porosity than the 1wt.%B. The 4wt.%B composite exhibited the maximum pore percentage with respect to the other three conditions.

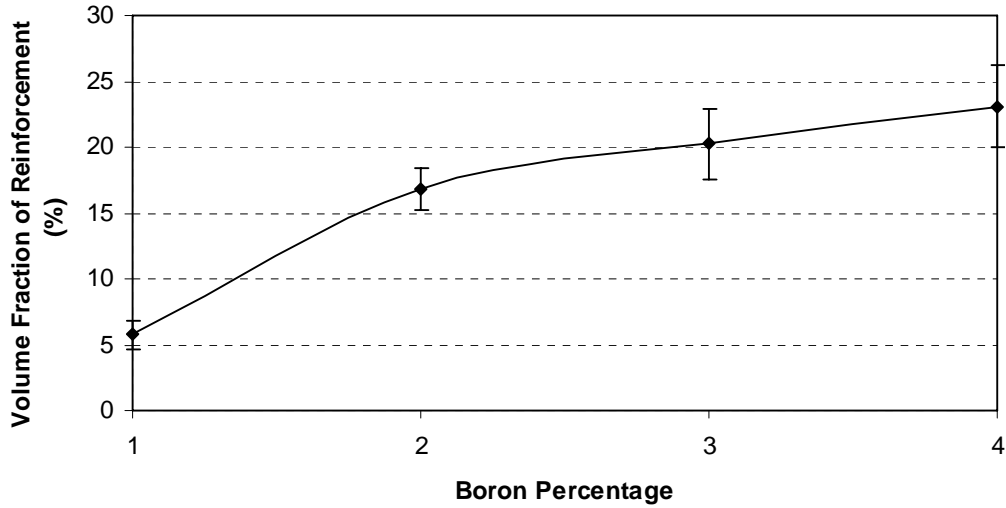


Figure 4.6 Measured volume fraction of reinforcement particles in the gravity cast samples as a function of %wt.B.

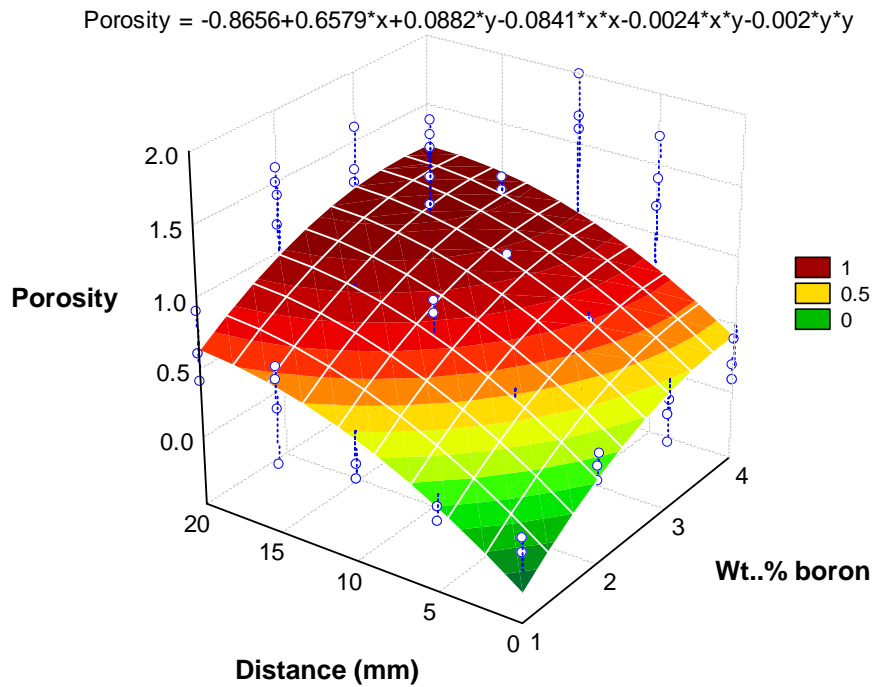


Figure 4.7 Measured volume fraction of pores in the FGM samples as a function of distance.

The measurements of porosity shown in Figure 4.8 did not reveal a large variation in the Al-B-Mg gravity cast composites when the boron percentage increased. In addition gravity cast alloys exhibited lesser porosity than centrifugally cast composite. This might be essentially due to the lower quantity of trapped air in slow pouring condition adopted during gravity casting compared with the stirring experienced in centrifugal casting.

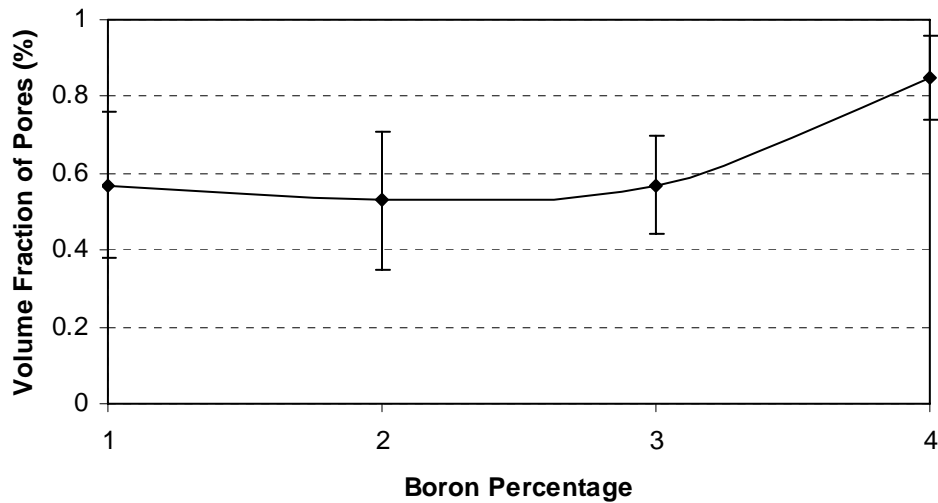


Figure 4. 8 Measured volume fraction of pores in the gravity casting samples as a function of %wt.B.

In agreement with the results one can observe some influence of reinforcement particles upon porosity. The increase in porosity with the increasing amount of particulates could be due to the increase in the apparent viscosity of the semisolid composite, limiting its ability to discharge trapped air, and the inability of the disintegrated molten melt to infiltrate the micrometer sized crevices in the inefficiently packed ceramic particles [5].

Porosity in a casting is attributed to both solidification shrinkage and trapped air. In addition, any residual porosity will have a deleterious influence on mechanical properties of FGMs. It has been observed that the magnitude of the modulus of elasticity decreases with volume fraction porosity. It can occur due to porosity reduce the cross-sectional area across which a load is applied and acts as stress concentrators and when the pore reaches the critical value, a crack forms and propagates since there are no large energy-absorbing processes. There are several factors affecting porosity such as pouring rates too slow, low casting temperatures, and filling mold problems among others.

It is therefore important to determine the level of porosity presents in these FGMs. The effect of the centrifugal casting process on porosity distribution is critical to establish its potential influence on final mechanical properties.

4.4.3 Superficial Rockwell Hardness and Vickers Microhardness Testing

The standard method for the determination of superficial Rockwell hardness is ASTM E 18. The superficial Rockwell hardness used on Al 2wt.%Mg-1,2,3 and 4%B composites was 15 HRW (15 kgf, 1/8 inch. indenter).

Figure 4.9 displays the superficial Rockwell hardness results measured on the Al-B-Mg FGMs for the experimental conditions previously established. The results indicate that the value of superficial hardness increases as a function of the distance in the experimental Al-B-Mg alloys. We found a direct relation between the

superficial Rockwell hardness and the volume fraction of reinforcers. Thus, the superficial Rockwell hardness starts increasing from 10 mm to Al-B-Mg composite with 1wt.%B. At 2 wt.%B this hardness increases from 5 mm while 3 and 4wt.%B achieved the maximum hardness value at 5mm, which remains unchanged until the end of the casting.

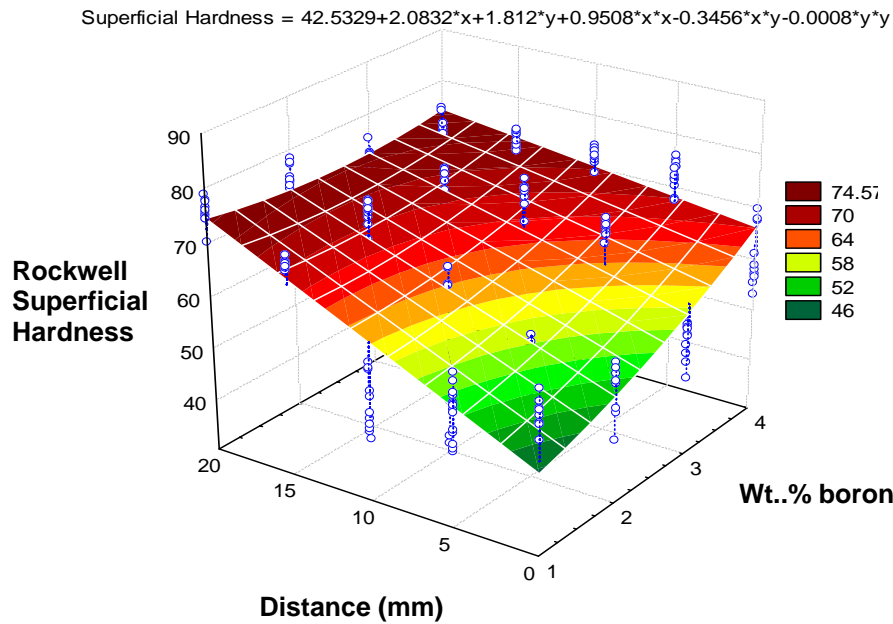


Figure 4.9 Rockwell superficial hardness (HR 15W) measured in the FGM samples as a function of distance.

Figure 4.10 shows evidence of the direct relation between the superficial hardness and boron percentage on Al-B-Mg gravity cast composites. This relation is function of reinforcement volume fraction too, as explained earlier.

The ASTM E 384 standard test method was employed to determine the microhardness in the FGMs and gravity casting composites. In the Vickers

microhardness tests a 50 gf load was applied (HV_{50}). The microhardness tester employed was a Buehler-Micromet[®] II.

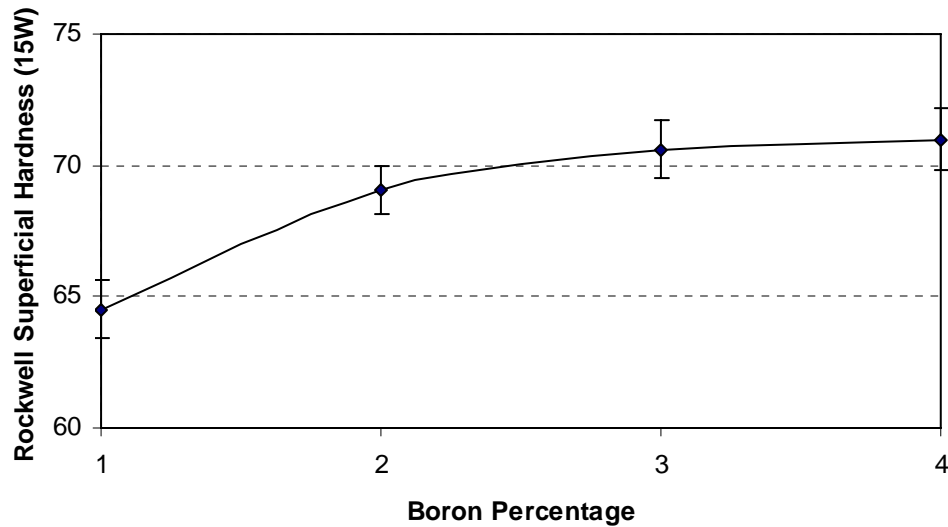


Figure 4.10 Rockwell superficial hardness (HR 15W) measured in the gravity casting samples as a function of %wt.B

Results of Vickers microhardness analysis made on the Al matrix of Al-B-Mg FGMs and depicted in Figure 4.11 confirm the mutual relation among volume fraction of particles, superficial Rockwell hardness, and Vickers microhardness measurements. Furthermore, although superficial hardness and microhardness increase toward the end of the casting this trend is less noticeable in H_V microhardness values. This can be explained because of a larger influence of the particle hardness than matrix hardness in mechanical properties of these composites since diborides are harder than aluminum matrix.

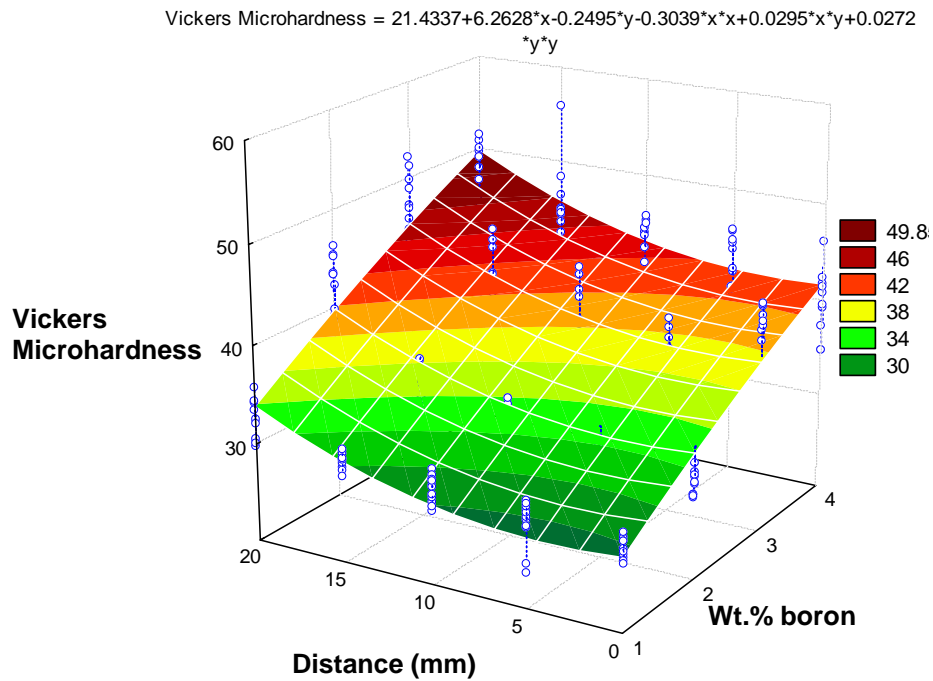


Figure 4.11 Vickers microhardness (HV₅₀) values measured on the matrices of the different FGMs as a function of distance.

The Vickers hardness results presented in Figure 4.12 indicate the direct influence of percentage of boron upon microhardness values of Al-B-Mg gravity casting alloys specially, at 1 and 2wt.%B. That is, the greater the boron quantity, larger is the microhardness value. This relation can be explained by the large difference in coefficient of thermal expansion between Al and the particles which leads to an increase in the dislocation density in the matrix, thus resulting in hardening of the matrix; this effect has been shown to increase with the increasing presence of ceramic particles [5].

Superficial Rockwell hardness and Vickers microhardness values determined the influence of matrix and reinforcing particles and how the interaction of these phases affected the overall mechanical properties of AMCs. Even though, initially the aluminum matrix hardness was not considered as a factor into material composite hardness, Vickers microhardness measurements enabled to demonstrate a direct relation between matrix and reinforcer phases. On the other hand, the superficial Rockwell hardness measures showed the major effect of solid particles respect with the matrix on mechanical properties of FGMs.

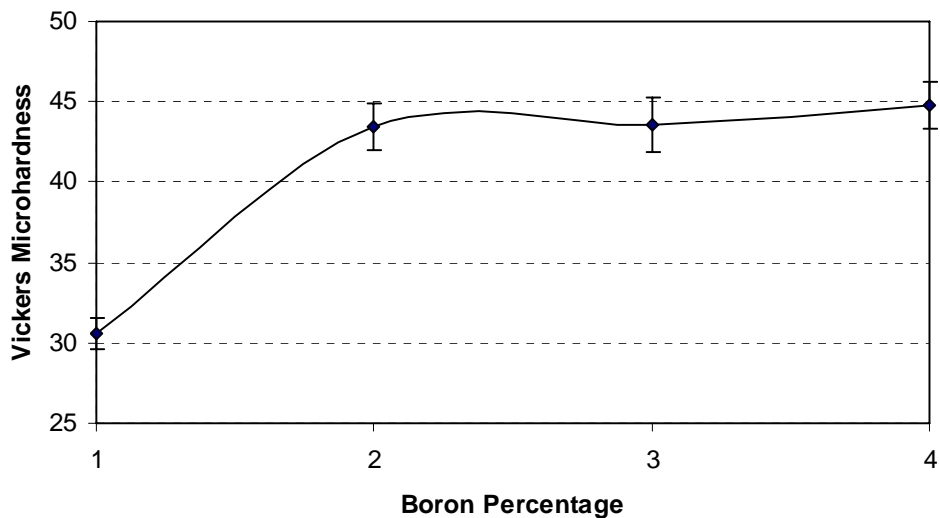


Figure 4.12 Vickers microhardness (HV50) values measured on the matrices of the different gravity casting samples as a function of %wt.B.

4.4.4 Reinforcement Particle Size and Matrix Grain Size

The micrograph showed in Figure 4.13 demonstrates a typical AlB_2 particle, in Al-B-Mg composites. Nevertheless, additional energy dispersive spectroscopy (EDS) and electron microprobe analysis (EMPA) indicated that, when Mg is present in the composite, it diffuses in the AlB_2 particles to substitute Al atoms and form an Al_xMg_{1-x} .

$x\text{B}_2$ compound. Additionally, it is believed that this $\text{Al}_x\text{Mg}_{1-x}\text{B}_2$ compound is harder than AlB_2 . These assumptions have to be corroborated by means of nanoindentation studies currently under way.

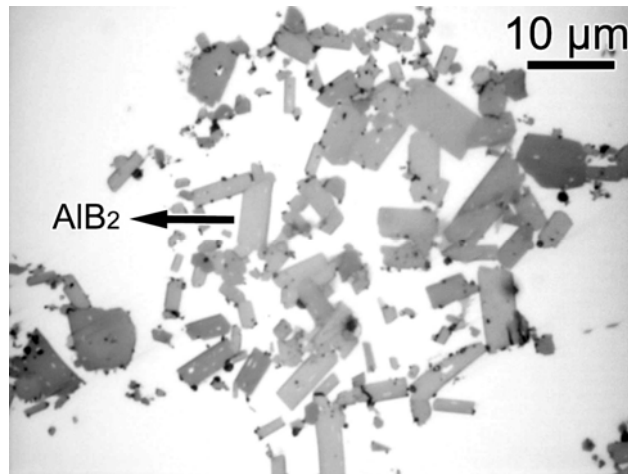


Figure 4.13 Micrograph of the reinforcement particle size of a centrifugal cast Al-2wt%Mg-4wt%B composite.

Quantitative analysis made with J (Appendix D), determined distribution of reinforcement particles size in Al-B-Mg FGMs and gravity cast composites, as shown in Figures 4.14 and 4.15. The results of centrifugally cast composites do not demonstrate a specific variation in the particle size of the reinforcers in spite of the interaction of the particles under the centrifugal force action. The small particle size (aprox. 5 μm) found in this study can be the reason for these results because the particle size was not affected, since the potential interaction volume per particle with matrix and other particles is lower in small particles than for large particles. Additionally, gravity cast composites showed no remarkable changes in the reinforcement particle sizes, when the boron percentage is increased. The effect of centrifugal casting on particle size provoked by higher centrifugal velocities, lead to

decreased mean particle size [10]. However, further considerations are necessary in order to understand the reduction in particle area fraction and in mean particle size, particularly for less severe casting conditions.

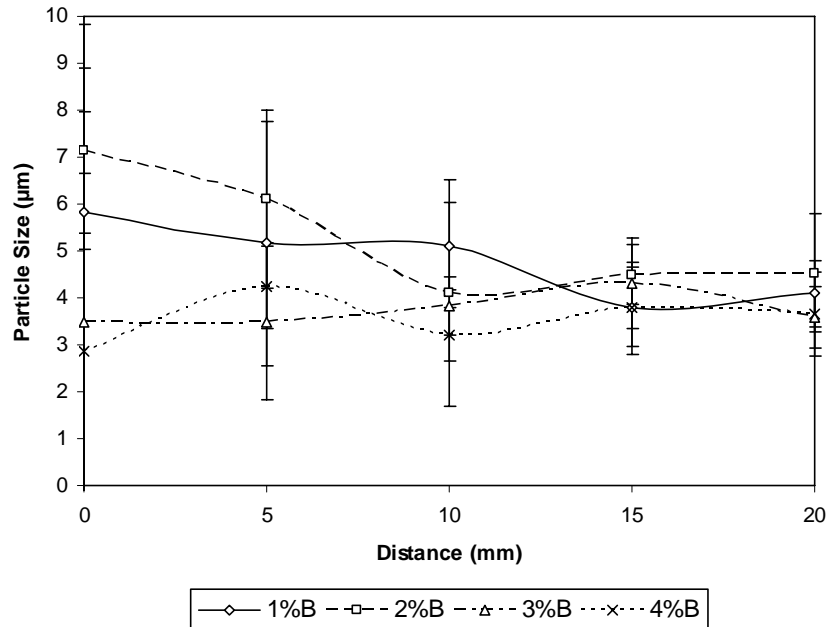


Figure 4. 14 Reinforcement particle size values measured on the FGM samples as a function of distance.

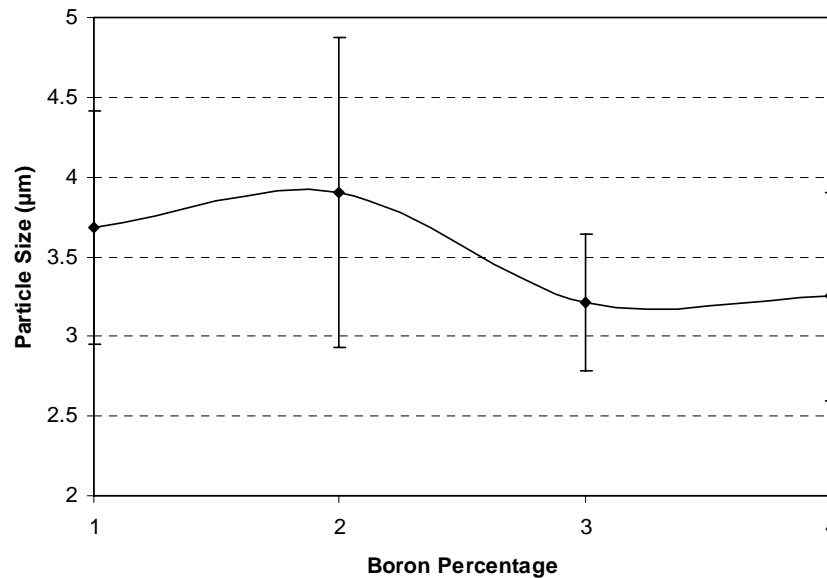


Figure 4. 15 Reinforcement particle size values measured on the gravity casting samples as a function of %wt.B.

Figure 4.16 shows a micrograph of grains in the matrix of a Al-B-Mg gravity cast composite. The matrix grain size results obtained by quantitative image analysis (Appendix E) done on both the FGMs and gravity cast composites did not reveal any considerable difference. The uniform distribution of the matrix grain size of Al-B-Mg centrifugally cast alloys is shown in Figure 4.17. Similar behavior was found in the gravity cast composite, as illustrated in Figure 4.18. The small difference in grain size detected between FGMs and gravity cast alloys (measure of dispersion is large) may be due to the slower solidification rate in gravity cast composites than in centrifugally cast alloys [8].

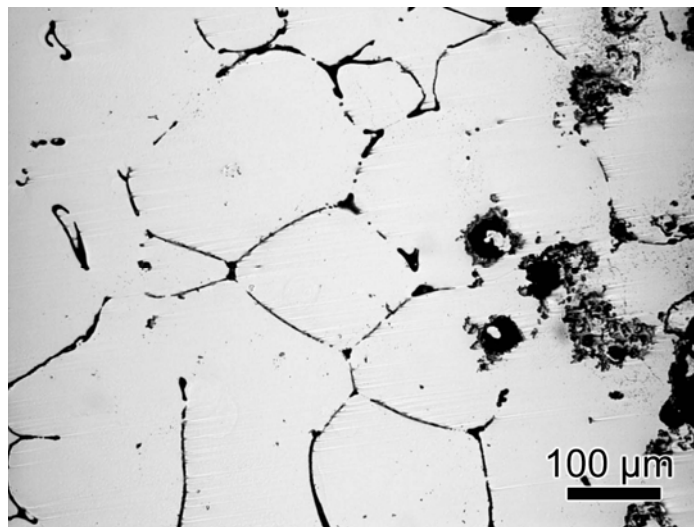


Figure 4.16 Micrograph of the matrix grain size of a gravity casting Al-2wt%Mg-4wt%B composite.

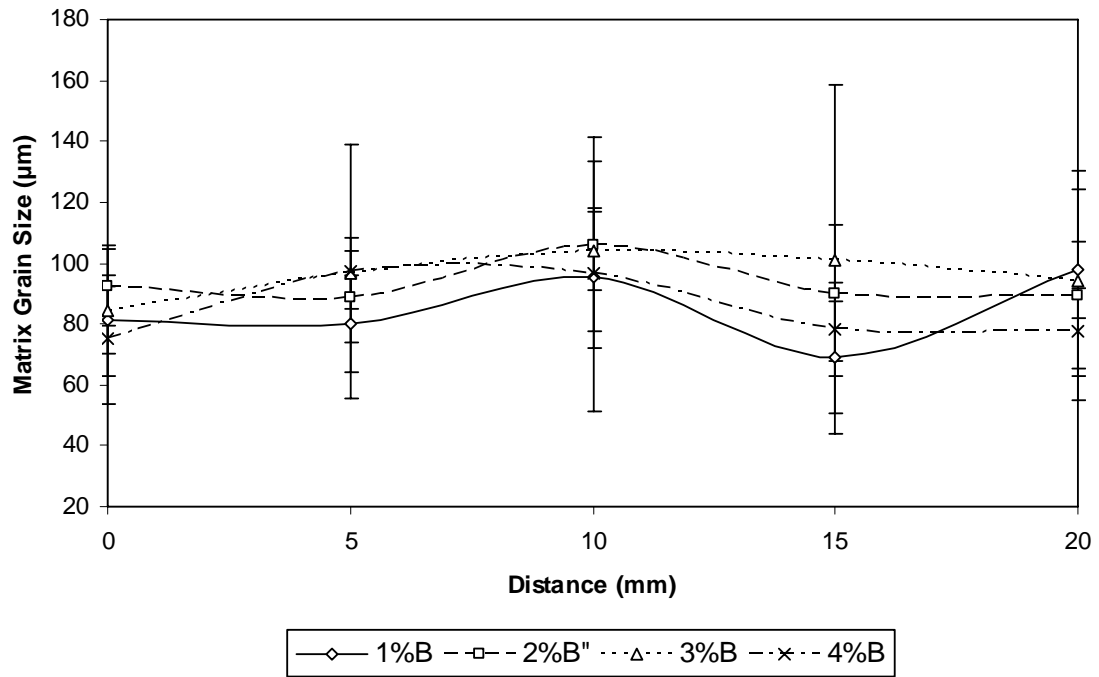


Figure 4.17 Matrix grain size values measured on the FGM samples as a function of distance

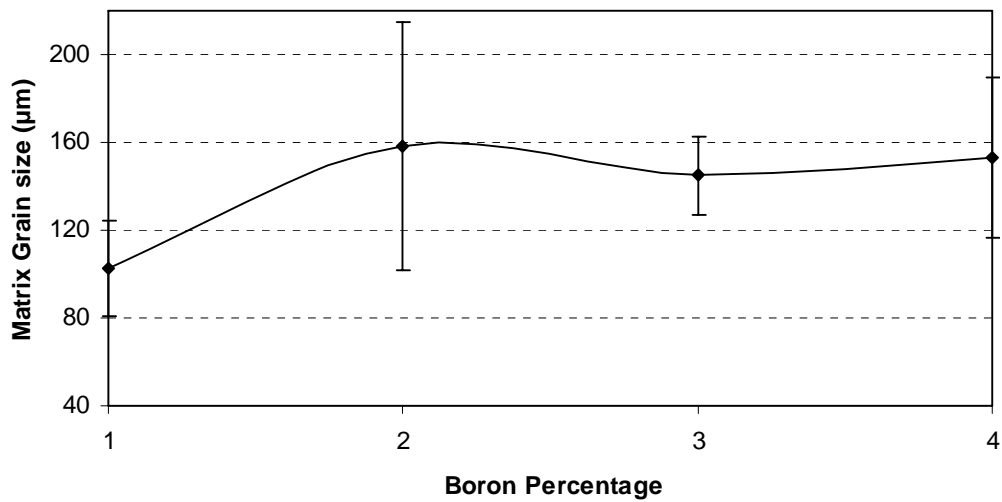


Figure 4.18 Matrix grain size values measured on the gravity casting samples as a function of %wt.B.

4.4.5 Possible Scenario of Liquid-Particle Flow and Microstructure Formation of Al-B-Mg Composites Centrifugally Cast

The transport phenomena occurring in solidification processes of FGMs are complex due to different factors such as the transport of fluid, heat and solute (which governs the migration of particles in a liquid matrix), and the interactions of particles with the solidifying matrix [54].

Various processing parameters, such as crucible furnace temperature, mold heating furnace temperature and velocity of mold rotation can significantly influence the composition gradient in the FGM. Because of the high rotational speed of the mold experimental estimation of the solidification time and temperature distribution during solidification through heat-and mass-transfer analysis is a complex problem under realistic condition for this centrifugal method [55].

The above statement indicate that any further conjecture about solidification mechanism involving liquid-particle flow and microstructure formation of Al/AlB₂ matrix composites can be speculative in nature for this centrifugally casting process. Figure 4.19 illustrates the liquid-particle laminar flow filling the mold (due to the initial rotational velocity) through centrifugal casting method. Additionally it is assumed that the motion of the particles is stopped by the liquid front; the particles do not move in the mushy zone of the casting and they are not rejected by the solidification front. The first assumption is reasonable due to the rapid increase of the viscosity of the semisolid composite due to the forming solid phase fraction. It is to be noted also

that the viscosity of the liquid varies with temperature which will affect the segregation velocity of the particles.

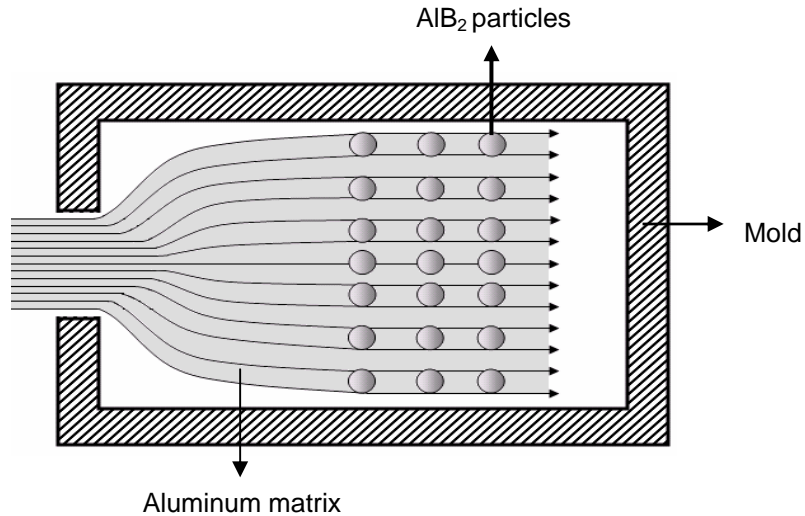


Figure 4. 19 Liquid-particle laminar flow filling the mold.

Three interlacing phenomena have to be considered when a liquid containing suspended particles solidifies in a mold rotating at high velocity: a) interaction between the solidification front and the moving particles, b) variation of the viscosity of the liquid before complete solidification and c) possible interaction among particles in the liquid. For the sake of simplicity, only the first one will be considered in the following discussion.

As mentioned previously, the Al/AlB₂ matrix composite system offers the advantage that the reinforcements are appropriately incorporated in to the molten alloy due to excellent wettability between the borides (acting as reinforcing particles) and the aluminum melt. Al-rich alloys of this system are used as master alloys for grain refining of aluminum alloys [12]. Since AlB₂ phase present in these alloys is a catalytic substrates for the early crystallization of the aluminum phase [13].

The production of an equiaxed zone requires the existence of small crystallites, or nuclei, in the bulk during freezing. Constitutional supercooling driven heterogeneous nucleation is one mechanism for the provision of these nuclei. However, constitutional supercooling does not drive the nucleation of equiaxed grains except in the presence of a grain refiner or other efficient substrate [56]. As mentioned, AlB_2 particles promote heterogeneous nucleation.

Figure 4.20 a. shows the growth of equiaxed grains in a preferential zone of a casting piece as a result of the segregation of AlB_2 particles by centrifugal forces. This particle-rich region promotes the formation of an equiaxed region produced by heterogeneous nucleation due to the reinforcement particles. Moreover, additional AlB_2 particles away from the particle-rich region could also be promoting the formation of equiaxed grains. As the liquid metal becomes in contact with mold walls, solid nuclei form, creating a chilled zone [56]. On the other hand, high undercooling and high solidification rates generated through the centrifugal casting process will tend to form dendrites at the liquid-solid interface, as shown in Figure 4.20 b.

Figure 4.20 c. shows a schematic of the resulting structure of equiaxed solidification where the reinforcement particle is much smaller than the grain size. Furthermore, there is good wetting between particles and liquid, which implies particle engulfment, resulting in a uniform distribution of particles within the grains. As it was mentioned earlier the nucleation of aluminum matrix grain is favored by AlB_2 particles; for this

reason this phenomenon is observed preferentially where most particles were segregated.

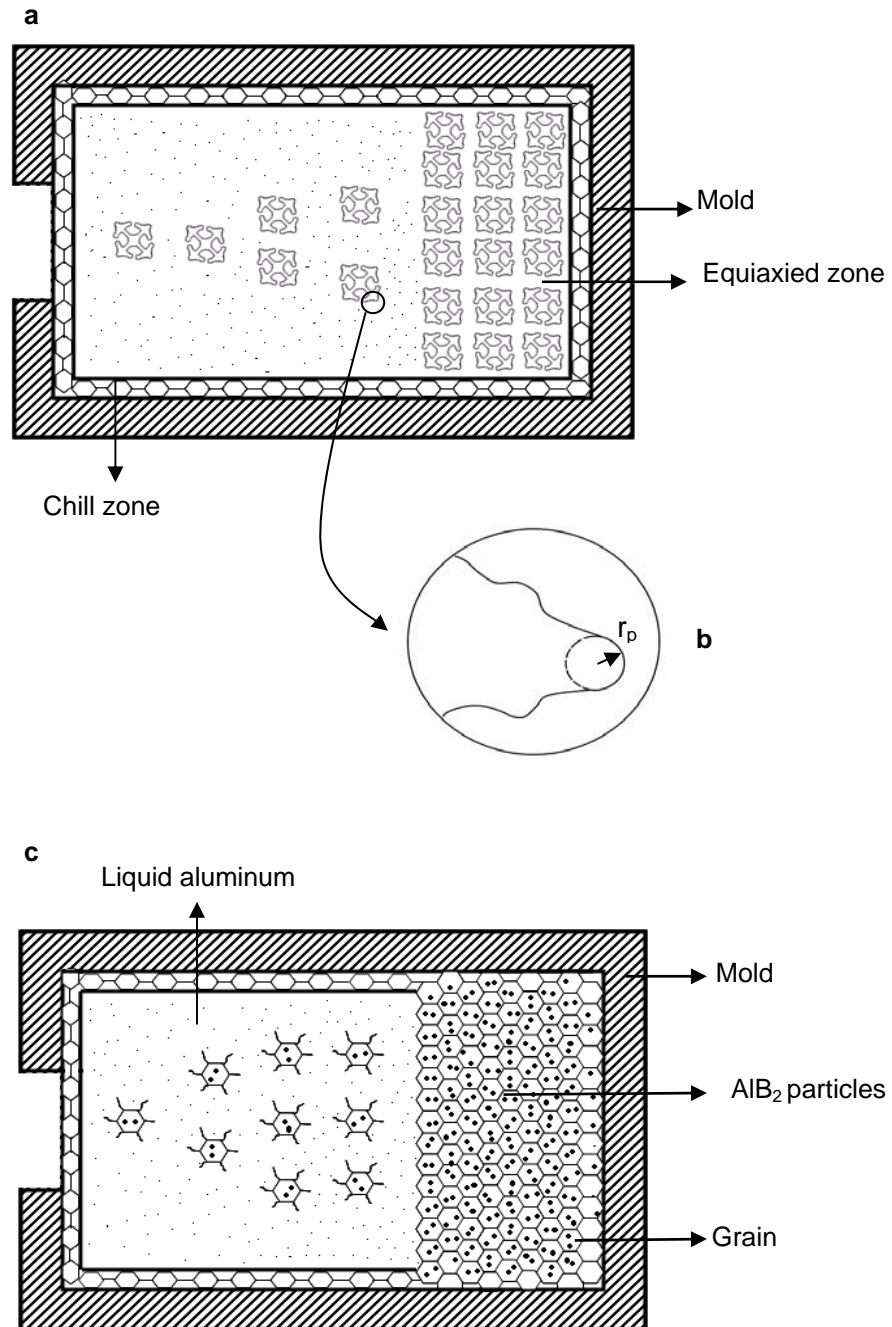


Figure 4.20 Schematic of microstructure zone formation in centrifugally cast piece. a) Equiaxed zone preferentially formed in the outer zone by effect of AlB₂ particles. b) Growth of a dendrite. c) Resulting structure of crystal growth in equiaxial solidification.

4.5 Pin - On - Disk Wear Testing

The test method used for determining the wear of Al-B-Mg composites is based on standard ASTM G 99. The procedure to carry out this test was explained in the previous chapter.

Unlubricated pin-on-disk configuration wear tests were performed at 0, 5, 10, 15, and 20 mm from the edge of the centrifugally cast AMC's and on gravity cast samples (disks). The wear tests parameters were: constant sliding speed, 0.0060 ms^{-1} ; counter-surface (pin) 3.175mm diameter ball made of AISI 410 martensitic stainless steel ball; time 45 min, applied normal load 0.15N (15g). The total sliding distance under these conditions was 16.5 m.

4.5.1 Wear Volume and Wear Coefficient

Topographical images of the pin-on-disk tracks obtained by AFM and presented in Figure 4.21 revealed qualitatively and quantitatively the wear response of centrifugally cast Al-B-Mg composite.

The assessment of the volume of removed material as determined by the topographical dimensions of the wear track was developed in agreement with the procedure established in the section 3.5.1.

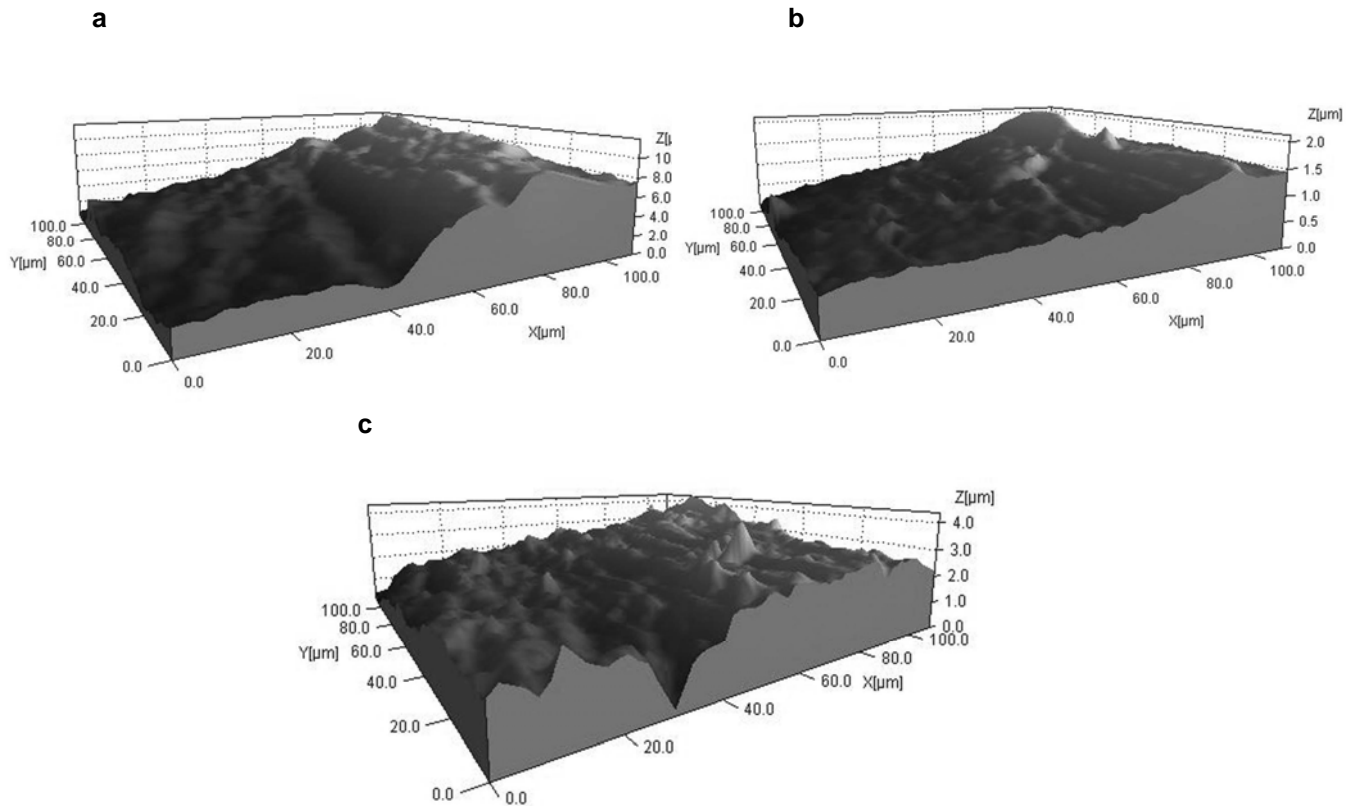


Figure 4. 21 AFM images of tracks depth resulting from pin-on-disk wear tests on Al-2wt%Mg-1wt%B FGM a) 0 mm zone. b) 10 mm zone. c) 20 mm zone.

Figure 4.22 shows the wear volume results measured in the Al 2wt.%Mg 1, 2, 3, and 4wt.%B centrifugally cast samples. The highest wear volume was observed on the 0 mm section of the FGMs. The wear rate decreases as a function of the distance, where the 20 mm section has the smallest wear volume. These results are compatible with the higher volume fraction of boride phases found in the 15 and 20 mm sections. This corroborates that the wear resistance of the FGMs is controlled by the boron percentage, (as the diboride volume fraction) since, the results displayed larger wear in Al-B-Mg composites with 1wt.%B than those with 3 and 4wt%B. The results of wear volume in gravity cast composites shown in Figure 4.23

support the previous statement. Besides, these results exhibited an intermediate range of wear volume values regarding those in the opposite zones of FGMs.

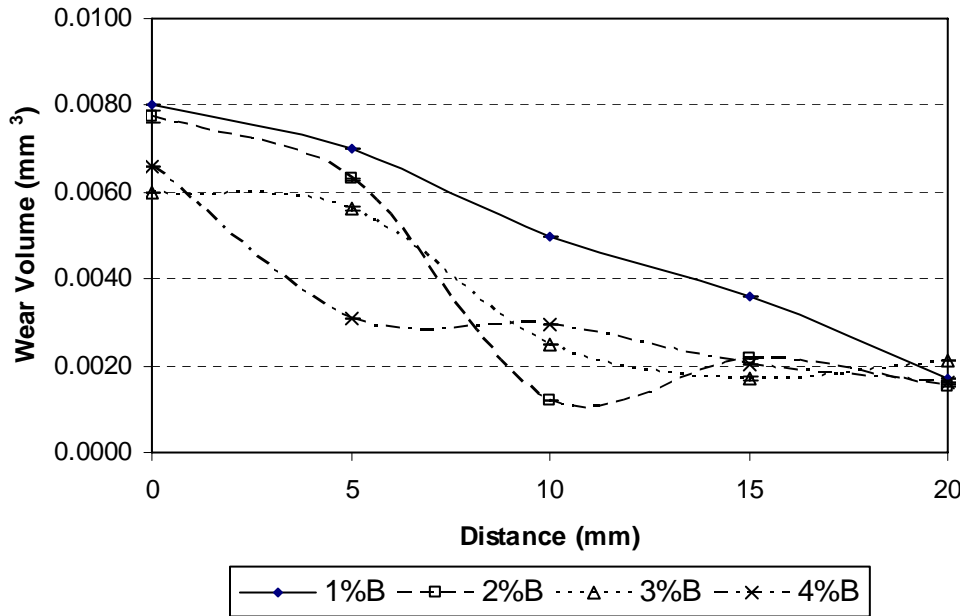


Figure 4.22 Wear volume for the various FGMs-AMCs samples after pin-on-disk wear tests under identical conditions.

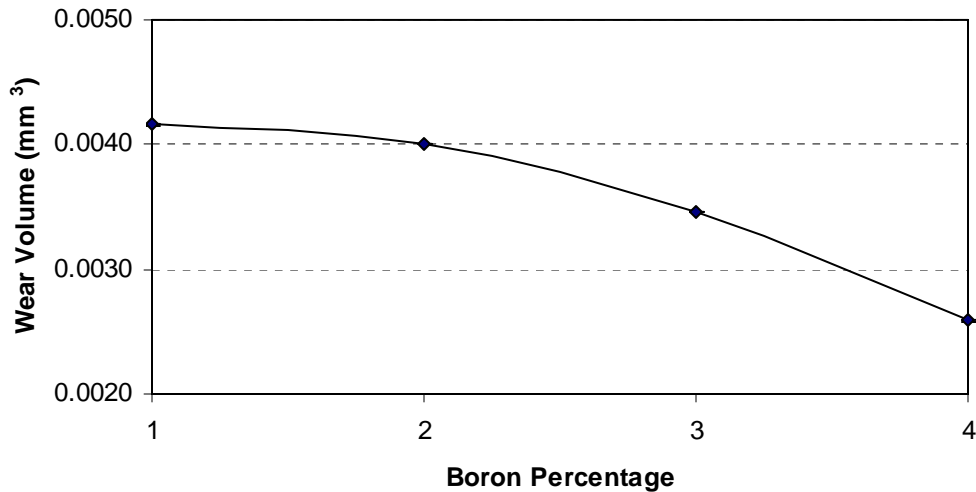


Figure 4.23 Wear volume for the various Gravity Casting - AMCs samples after pin-on-disk wear tests under identical conditions.

Wear coefficient results provided in Table 4.1 were calculated using equation 2.4. These results exhibited a similar tendency as the data reported previously: low values of wear coefficient obtained for the 20mm sections of FGMs indicated better wear resistance compared to the gravity cast composites. This result is rather obvious since the wear coefficient depends directly on the wear volume.

WEAR COEFFICIENT RESULTS (mm ³ /N·m)				
Sample	Al-2wt%Mg-1wt%B	Al-2wt%Mg-2wt%B	Al-2wt%Mg-3wt%B	Al-2wt%Mg-4wt%B
FGMs - 0 mm zone	0.0030	0.0034	0.0022	0.0029
FGMs - 5 mm zone	0.0026	0.0029	0.0021	0.0014
FGMs - 10 mm zone	0.0019	0.0005	0.0011	0.0013
FGMs - 15 mm zone	0.0014	0.0007	0.0007	0.0007
FGMs - 20 mm zone	0.0007	0.0006	0.0009	0.0007
Gravity Casting	0.0016	0.0016	0.0015	0.0012

Table 4.1 Calculated wear coefficient for the various AMC samples.

Wear test results of the FGMs and gravity cast composites demonstrated a great dependence on the composition gradient. Conversely, higher volume fraction of reinforcing boride particles translates into a lower overall wear rate. A similar relation was found between wear rate and hardness.

4.5.2 Morphological Characterization of Worn Surface

Morphological characterization of worn surfaces samples was performed by scanning electron microscopy (SEM) using a JEOL-JSM 5410 LV. Backscattered electron image (BEI) was the technique used to analyze the morphology of the wear track in the Al-2wt%Mg-1wt.%B centrifugally cast and gravity cast composites. This

technique was useful for our particular application since backscattered electron detector may be used as an additional source of topographic contrast information [57]. In addition at low magnification, backscattered electron micrographs can give a better impression of the surface topography than secondary electron micrographs [58].

The worn surface morphology of the 10mm cross section FGM shown in Figure 4.24 a is characterized by uniform wear track with large cavities caused by matrix detachment. Furthermore, wide plastic deformation with plowing grooves are aligned with the sliding movement and flat smooth regions. This morphology occurs due to the low presence of aluminum diboride particles in the sample, which caused a high deterioration in the aluminum matrix.

Figure 4.24 b presents the BEI of the track on the 20mm section of centrifugally cast composite. The uneven wear track surface displayed AlB_2 particles fragments detached on the matrix surface; at the same time it evidenced some matrix detachment and the presence of dispersed adherent tribolayers with smooth appearance. Both, the protruding aluminum diboride particles and the adherent tribolayers explain the high wear resistance of the FGM [9].

Morphological analysis on worn surface of the Al-B-Mg gravity casting shown in Figure 4.24 c demonstrated a combination of the wear modes present in FGMs. Large cavities caused by matrix detachment and reinforcing particles as load

bearing elements are the prevalent mechanisms. Fragments lost from the mating surface can be picked up and observed at the end of the groove at which they have formed (see “A” in Figure 4.24 c) [43].

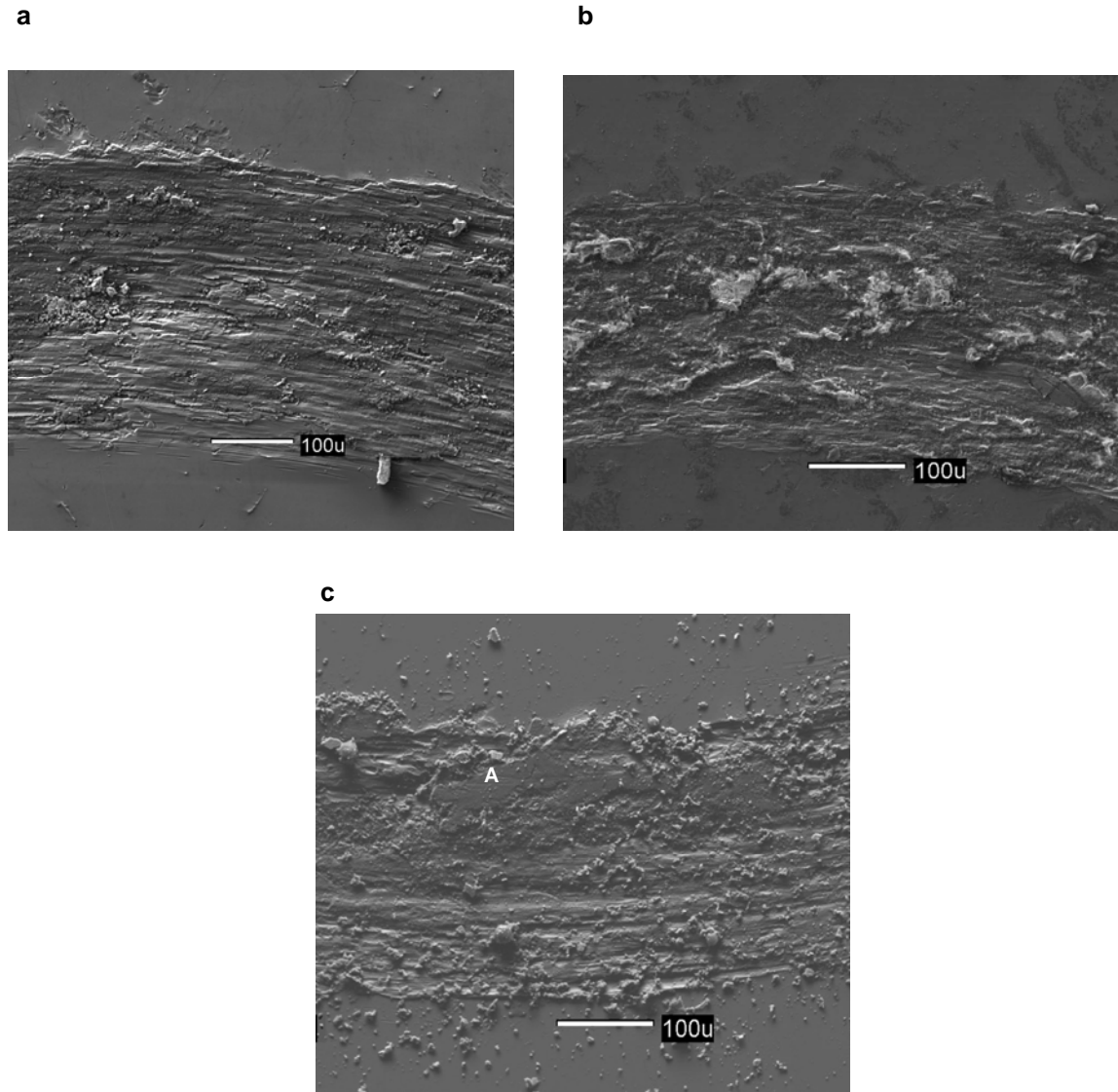


Figure 4. 24 Wear Track backscatter electron image of Al- 2wt %Mg- 1wt.% B alloy, a) FGM 10mm zone, b) FGM 20mm zone, c) Gravity casting.

According to the SEM images it can be concluded that the 10 mm section in FGM showed a larger wear rate compared with the 20mm section of centrifugally

cast sample and gravity casting composite. It corroborates the observation that wear resistance can be improved by increasing the volume fraction of hard particles [43].

Characterization of worn surfaces indicated that the combined effect of reinforcing particles as load bearing elements and the formation of protective adherent tribolayers plays a decisive role on the friction and wear properties of aluminum matrix composites [9]. In addition, the reinforcer fragments detached from the composite surface can be transferred to the mating surface due to adhesion. Further sliding causes more fragments to be formed by either of the two mechanisms. After certain time this attached fragment became loose and separate from the surface [44]. It can be concluded that Al-B-Mg composites exhibited two dominant types of wear; abrasive and adhesive. The oxidational wear requires additional analysis to be detected but it frequently takes place when the humidity in the environment is high or when high temperatures are reached during the wear process.

In closing, composition gradient was observed in Al-B-Mg composites when they are subjected to centrifugal forces upon casting. Aluminum diborides particles (denser than liquid Al) are displaced towards the outer regions as a result of the inertial forces. In addition, superficial hardness and Vickers microhardness values showed a direct linear relation with respect to the volume fraction distribution of reinforcement. Wear test results revealed a dependence of these composites on both microstructural gradient and hardness. In effect, the higher volume density of

reinforcing boride particles in the 20 mm sections of the centrifugally cast samples caused a higher overall wear resistance on those regions, while the 0 mm sections experienced the highest wear rates. Gravity cast composites demonstrated an intermediate wear volume values with respect to opposite zones of FGMs, while volume fraction of diborides is uniformly dispersed along the composite mass. Results of reinforcement particle size and matrix grain size did not reveal a significant difference in both centrifugally cast composites and gravity cast alloys. Morphological analysis of worn surface by SEM displayed two wear modes: abrasive and adhesive. These types of wear lead to matrix detachment with plowing grooves, AlB_2 particles detached and sitting on the matrix and the formation of adherent tribolayers, which contribute to improve the wear resistance of Al-B-Mg composites.

5. CONCLUSIONS

1. A centrifugal casting technique was developed to manufacture functionally graded aluminum matrix composites.
2. Centrifugal casting process permitted to obtain functionally graded aluminum matrix composites reinforced with aluminum diboride particles from experimental Al-B-Mg composites.
3. Higher composition gradient was observed in external zone (20mm) of Al-B-Mg composites compared with Al-B composites, which corroborated the beneficial effect of Mg in the FGMs-AMCs.
4. Superficial Rockwell hardness and Vickers microhardness results of Al-B-Mg centrifugally cast composites demonstrated to be influenced by the microstructure gradient where higher volumen fraction of AlB_2 particles involves larger hardness.
5. Reinforcement particle size and matrix grain size results of FGMs were not significantly affected by centrifugal forces as compared with gravity casting composites.

6. Wear test and wear coefficient results were consistent with the composition gradient observed in centrifugally cast composites where higher volume of reinforces translated in smaller wear rate.

7. Morphological analysis of worn surface by SEM exhibited two wear modes: abrasive and adhesive. These types of wear lead to the detachment of aluminum matrix and AlB_2 particles and the presence of adherent tribolayers, which contributed to improve the wear strength of Al-B-Mg composites.

6. RECOMMENDATIONS

Other materials phenomena found during this research not fully reported in this thesis took place, would require both extensive and in-depth study to provide complementary information. In addition, other topics around of this subject will assist to a better comprehension for this new functionally graded material. Therefore, I recommend emphasizing the following themes:

- ✓ Fabrication of the new FGMs with appropriate dimensions for mechanical testing and full characterization of the mechanical properties of these composites.
- ✓ Development of numerical model to predict the redistribution of the boride particles in the molten aluminum matrix for different rotational speeds.
- ✓ Production a new FGMs doing use of other metal diborides particles (Nb, Hf, Zr, Ti, Cr).
- ✓ Full study of the effect of magnesium on Al-B alloys and possible formation of $(Al,Mg)B_2$ as reinforcement particle.
- ✓ General corrosion behavior of the Al-B-Mg FGMs.
- ✓ Experimental determination of the temperature gradient during centrifugal casting and validation with theoretical model.

7. REFERENCES

- [1] Gomes, J.R. A.S. Miranda, D. Soares, A. E. Días, L. A. Rocha, S. J. Crnkovic., "Tribological Characterization of Al-Si/SiCp Composites: MMC's vs FGM's," Ceramic Transactions 114.2000, 579 – 586.
- [2] Korkut, M.H., "Effect of Particulate Reinforcement on Wear Behaviour of Aluminum Matrix Composites," Materials Science and Technology 20. 2004, 73-81.
- [3] Paulino, G.H., and J.H. Kim, "A New Approach to Compute T-stress in Functionally Graded Materials by means of Interaction Integral Method," J. Engineering Fracture Mechanics 71. 2004, 1907-1950.
- [4] Duque, N.B., Z.H. Melgarejo, and O.M. Suárez, "Functionally Graded Aluminum Matrix Composites Produced by Centrifugal Casting," J. Materials Characterization 55. 2005, 167-171.
- [5] Nai, S., M. Gupta, and C. LIM, "Synthesis and Wear of Al based, Free Standing Functionally Gradient Materials: Effects of Different Reinforcements," Material Science and Technology 20. 2004, 57-67.
- [6] Asthana, R. "*Solidification Processing of Reinforced Metals*," Trans Tech Publications, Enfield. New Hampshire, 1998, 254-257.
- [7] Watanabe, Y. and Y. Fukui., "Microstructures and Mechanical properties of Functionally Graded Material Fabricated by Centrifugal Casting Method," Metallurg.& Materials Sci 4. 2000, 51-93.
- [8] Kang, C.G., and P.K. Rohatgi, "Transient Thermal Analysis of Solidification in a Centrifugal Casting for Composite Materials Containing Particle Segregation. Metallurgical and Materials Transactions 27B. 1996, 277-285.
- [9] Gomes, J.R., L.A. Rocha, S.J. Crnkovic, R.F. Silva, and A.s. Miranda, "Friction and Wear properties of Functionally graded Aluminum matrix Composites," Materials Science Forum, 423-425, 2003, 91-96.

[10] Velhinho, A., P.D. Sequeira, and F. B. Fernandes, "Al/SiC_p Functionally Graded Metal-matrix Composites Produced by Centrifugal Casting: effect of Particle Grain Size on Reinforcement Distribution", *Materials Science Forum* 423-425. 2003, 257-262.

[11] Calderón, H., "Effects of Mechanical Deformation on Aluminum Matrix Composites Treated Heating," M.S Thesis University of Puerto Rico, Mayagüez. 2004.

[12] Wang, Q., Y. X. Li, and X. C. Li, "Grain Refinement of Al-7Si Alloys and the Efficiency Assessment by Recognition of Cooling Curves," *Metallurgical and Materials Transactions A* 34A. 2003, 1175-1182.

[13] Suárez, O. M., and J. H. Perepezko, "*Microstructural Observation of Nucleants in Al-Ti-B Master Alloys,*" in "*Light Metals 1992,*" E.R. Cutshall, ASM International, Materials Park. OH, 1992, 851-859.

[14] Hirai, T., "Processing of Ceramics," vol. 17B, Weinheim, New York. NY, 1996, 293.

[15] Jeong, H., G.H., Paulino, "The Interaction Integral for Fracture of Orthotropic Functionally Graded Materials: Evaluation of Stress Intensity Factors," *International Journal of Solid and Structures* 40. 2003, 3967-4001.

[16] Wenzhou C., W. Qudong, Z. Chunquan, M. Chunjiang, Z. Yanping , and H.Wei, "Functionally Graded Zn-Al-Si in-situ Composites Fabricated by Centrifugal Casting," *Journal of Materials Science Letters* 20. 2001, 823-826.

[17] Watanabe, Y., R. Sato, I. Kim, S. Miura and H. Miura. "Functionally Graded Material Fabricated by Centrifugal Casting Method from ZK60A Magnesium Alloy," *Materials Transactions* 46. 2005. 944-949.

[18] Lajoie, L., and M. Suery, "*Cast Reinforced Metal Composites,*" S.G. Fishman and A.K. Dhingra, ASM INTERNATIONAL, metals Park. OH, 1998, 15-20.

[19] http://www.efunda.com/processes/metal_processing/invest_casting.cfm

[20] <http://www.hitchiner.com/home.html>

[21] Callister W. D., “*Material Science and Engineering an Introduction*,” Sixth Edition John Wiley & Sons. Inc.,. River Street. Hoboken. NJ, 2003, 783.

[22] Smith, W. F., “*Foundation of Materials Science and Engineering*,” Second edition, Mcgrawhill. Inc, New York. 1993, 636.

[23] Composite Material Handbook. “*Metal Matrix Composites*,” Vol 4, Department of Defense Handbook, 2002. 32-37.

[24] Harris, B., “*Engineering Composite Materials*,” Second edition. IOM Communications Ltd, London 1999, 27-29.

[25] Handbook of aluminum, “*Phisycal Metallurgy and Processes*,” Vol 1. G.E Totten, D. S. Mackenzie, and M. Denkker, Inc, New York, 2003, 339.

[26] Gasior, W., Z. Moser, and J. Pstrús, “Densities of Solid Aluminum-Magnesium (Al-Mg) Alloys,” *Journal of Phase Equilibria* 21. No. 2, 2000, 167-171.

[27] Bhargava N.R.M.R., I. Samajdar, S. Ranganathan, and M.K Surapa. “ Role of Cold Work and SiC Reinforcements on the β' / β precipitation in Al-10 pct Mg Alloy,” *Metallurgical and Materials Transactions A* 29A. 1998, 2835-2842.

[28] Sabatino, M.D., and L.Arnberg, “A review on the Fluidity of Al based Alloys,” *Metallurgical Science and Technology* 22. No. 1, 2004, 9-15.

[29] Gubicza, J., N.Q. Chinh, Z. Horita, and T.G. Langdon. “Effect of Mg Addition on Microstructure and Mechanical Properties of Aluminum,” *Materials Science & Engineering A* 387 -389. 2004, 55-59.

[30] Duschanek H., and P. Rogl, “The Al-B System,” *Journal of “Phase Equilibria* 15. No 5, 1994, 543-552.

[31] Fjellstedt, J., E. Anders, W. Jarfors, T. El-Benawy, "Experimental Investigation and Thermodynamic Assessment of the Al-rich side of the Al-B system," *Materials and Design* 22. 2001, 443-449.

[32] Loa, I., K. Kunc, K. Syassen, and P. Bouvier, "Crystal Structure and Lattice Dynamics of AlB_2 Under Pressure and Implications for MgB_2 ," *Physical Review B*, 66. No 13, 2002. 1-8.

[33] Raman, A., "On the AlB_2 Type Phases," *Zeitschrift für Metallkunde*, 58. No 3, 1967, 179-184.

[34] Vajeeston, P., P. Ravindran, C. Ravi, and R. Asokamani, "Electronic Structure, Bonding, and Ground-State Properties of AlB_2 -Type Transition-Metal Diborides," *Physical Review B*. 63. 2001, 45115-1-12.

[35] Nakano, N., and I. Higashi, "The Hardness of NbB_2 Single Crystals," *J. Less-Common Metals* 67. No 2, 485-492.

[36] Rogl, P. "*Phase Diagrams of Ternary Metal-Boron-Carbon Systems*," ASM International. Materials Park. OH, 1998.

[37] Okamoto, H., "*Phase Diagrams for Binary Alloys*," ASM International. Materials Park. OH, 2000.

[38] Post, B., "*Boron, Metallo-Boron Compounds and Boranes*," Chapter 5, R. M. Adams. Interscience Publ., New York. NY, 1964, 301-371.

[39] "*Practical Guide to Image Analysis*," ASM international, Materials Park. OH. 2000, 4.

[40] Russ, J. C., and R.T. Dehoff, "*Practical Stereology*," Second edition, Kluwer Academic/Plenum Publishers, New York, 2000, 1-19.

[41] Ohser, J., and F. Mücklich, "*Statistical Analysis of Microstructures in Materials Science*," John Wiley & Sons. Ltda, West Sussex. England, 2000, 4.

[42] Rabinowicz, E., "*Friction and Wear of Materials*," Second Edition, John Wiley & Sons. Inc, New York, 1995.

[43] ASM Handbook, "*Friction, Lubrication, and Wear Technology*," Vol 18, USA, 2004.

[44] Bhushan, B., "*Introduction to Tribology*," John Wiley & Sons. Inc, New York, 2002.

[45] Romanoff, P., "*The Complete Handbook of Centrifugal Casting*," TAC BOOKS. Inc, USA, 1981.

[46] Suárez, O.M., "Mechanical Properties of a Novel Aluminum Matrix Composite Containing Boron," *Journal of the Mechanical Behavior of Materials* 11, 2001, 225.

[47] David, R., "*Handbook of chemistry and physics*," CRC Press, Boca Raton. FL, 1998.

[48] Rai, A., D. Lee, K. Park, and M.R. Zachariah, "Importance of Phase Change of Aluminum in Oxidation of Aluminum," *Journal of Physical Chemistry B* 108. 2004, 14793-95.

[49] Annual Book of ASTM Standard, "*Designation. E 18. Standard Test Methods for Rockwell Hardness and Rockwell Superficial hardness of Metallic Materials*," ASTM International, Philadelphia. PA. USA, 1992.

[50] Annual Book of ASTM Standard, "*Designation. E 384. Standard Test Method for Microhardness of Materials*," ASTM International, Philadelphia. PA. USA, 1992.

[51] Suárez, O.M., J. Yupa luna, and H. E. Calderon, "Precipitation Hardening in Novel Cast Aluminum matrix Composite", *American Foundry Society Trans* 111, 2003, 159-66.

[52] Annual Book of ASTM Standard, "*Designation. G 99. Standard Test Method for Wear Testing with a Pin-on-Disk Apparatus*," ASTM International, Philadelphia. PA. USA, 2004.

[53] Watanabe, Y., N. Yamanaka, and Y. Fukui, "Wear behavior of Al-Al₃Ti Composite Manufactured by a Centrifugal Method," *Metallurgical and Materials Transactions A*, 30A, December 1999, 3253-3261.

[54] Gao, J.W., C.Y. Wang, "Transport Phenomena During Solidification Processing of Functionally Graded Composites by Sedimentation," *Journal of Heat Transfer* 123, April 2001, 1-8.

[55] Watanabe, Y., N. Yamanaka and Y. Fukui, "Control of Composition gradient in a Metal-Ceramic Functionally Graded Material Manufactured by The Centrifugal Method," *Composites Part A*, 29A, 1998, 595-601.

[56] ASM Handbook, "Casting," Vol 15, 9th edition, USA, 1998.

[57] Goldstein J. I. et al. "Scanning Electron Microscopy and X-ray Microanalysis", Third edition, Kluwer Academic/Plenum Publisher, New York, N. Y. 2003.

[58] Reimer, L., "Scanning Electron Microscopy," Second Edition, Springer-Verlag Berlin Heidelberg, New York. 1998.

APPENDIX

APPENDIX A. Image J Application Version 1.34s for Microstructure Quantitative Analysis

The open source nature of Image J (Figure A.1) makes it a prime choice for any researcher working with cost restrictions. Also it is very versatile software with many capabilities that are not explained in this manual. It has a website (<http://rsb.info.nih.gov/ij/>) dedicated to the program and forums that help keep the researchers connected. The web site maintains a database of plug-ins that helps the analysis process. The program also has a record option that creates macros of different processes that the user produces. This becomes very handy when the user needs to complete a series of commands repeatedly for a large number of images.

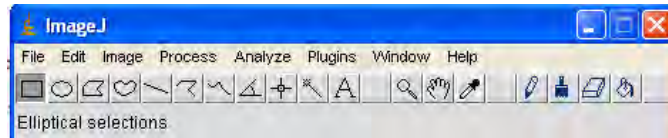


Figure A.1

Drop Down Menus

Figure A.2 presents a series of print-screen shots of the program's main drop down menu. It has *File*, *Edit*, *Image*,

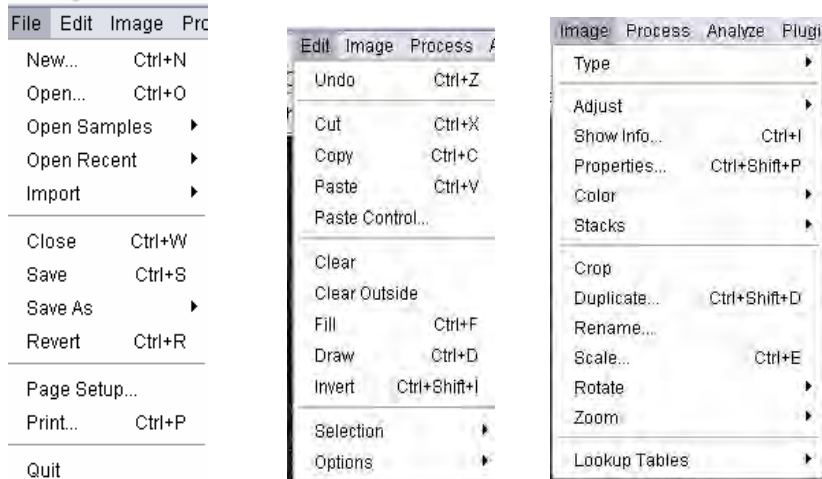


Figure A.2

Also as part of the drop downs menus Figure A.3 presents the options *Process*, *Analyze*, *Plug-in*, *Window* and *Help*.

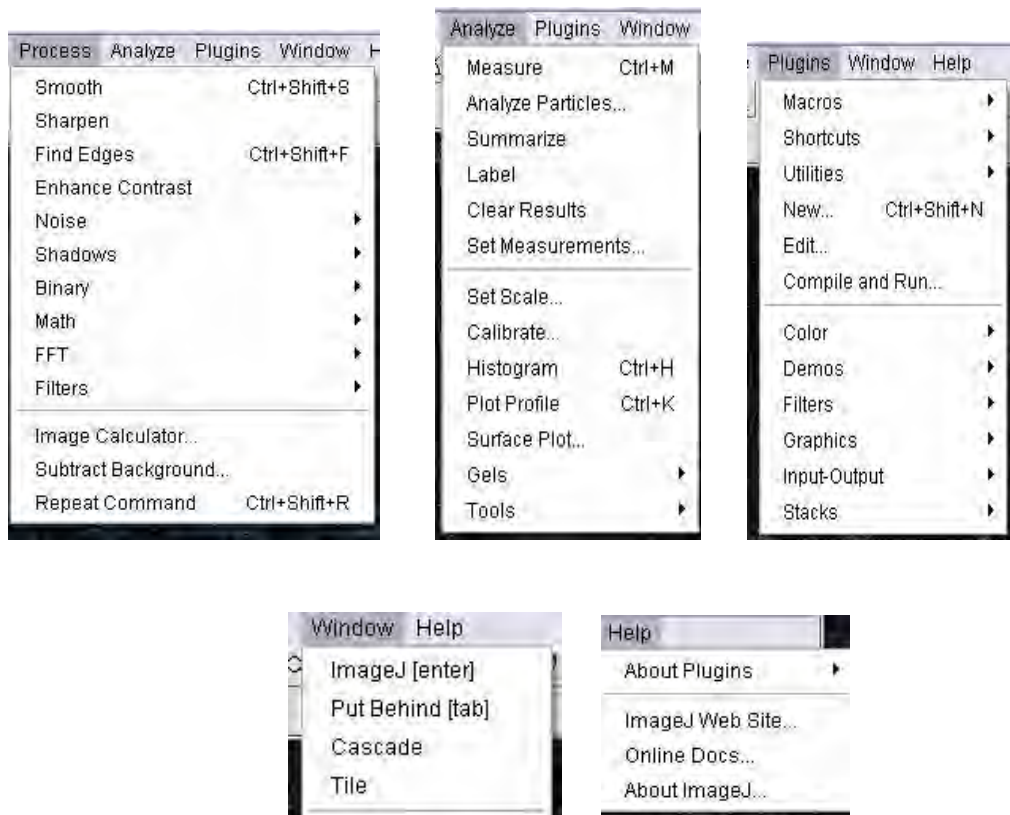


Figure A.3

APPENDIX B: Quantitative Analysis of Volume Fraction Procedure

1. General Procedures for one type of Reinforcements:

1.1. Processing the Image for Analysis:

Even if the user creates an image of pristine quality, the image still needs some level of processing so that some of the analysis commands can work properly. There is a need to create a level of quality that improves the results even more than when the researcher took the time and effort to meticulously capture the best images under the circumstances (type and properties of the material and the equipment at hand). For images taken in an optical microscope with a magnification of 50X, the following are a series of procedures that the user can complete to process the photographs. *Note: It is assumed in this procedure that the user already opened the software and the image of interest to do the following processing procedures.*

1.1.1. Eight Bit Images

First, it is necessary to transition the image into an 8 bit one (a grayscale photograph) instead of a color RGB image, which is the image format that the microscope produces. Go to the drop-down menu *Image>Type>8 bit* (Figure B.1)

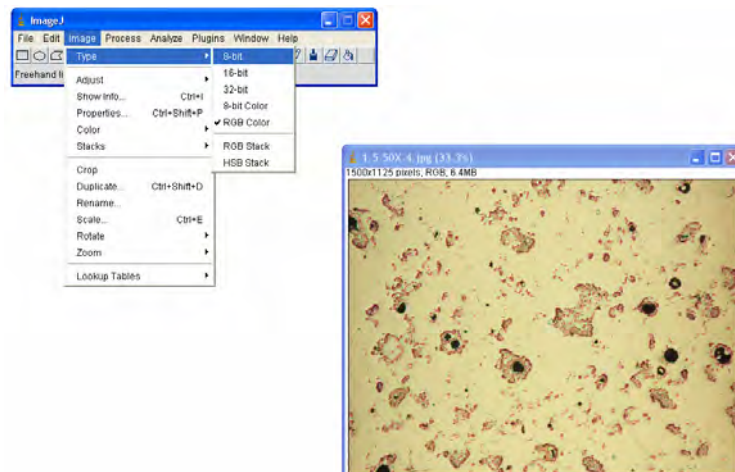


Figure B.1

1.1.2. Enhance contrast (Figure B.2)

This option essentially enhances the contrast (hence the name). When you press the command button a pop up menu will appear. The researcher will need to enter a saturated pixel value. The *Saturated Pixels* is the number that determines the pixels in the image that are allowed to become saturated. If the researcher increases this value, it will increase the contrast. The saturated pixel value is set at a standard value of 0.5 and the researcher should use this value. To use the command go to *Process>Enhance Contrast* and select “ok”.



Figure B.2

1.1.3. Normalize Image (Figure B.3)

Normalizing the image will recalculate the pixel values of an image so the range of the image is equal to the maximum range. The maximum range is 0-255 for 8-bit images. This normalization process can not be done for RGB images. To use the command go to *Process>Enhanced Contrast* and select the “Normalize” check box and then “ok”.

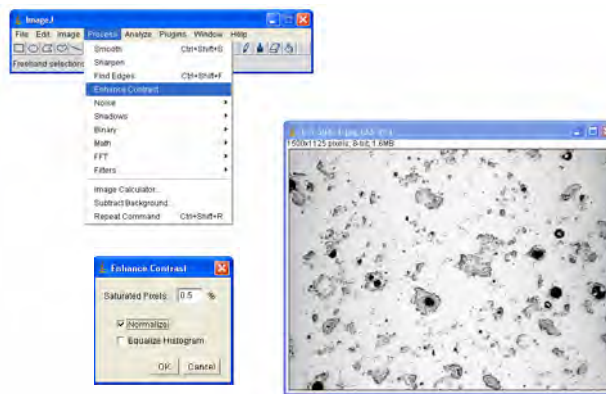


Figure B.3

1.1.4. Find Edges (Figure B.4)

It performs a 2-D spatial gradient measurement on the image and highlights regions of high spatial frequency that correspond to edges. It is used to find the approximate absolute gradient magnitude at each point in a grayscale image. Spurious noise will appear afterward on the resulting image, but they can be removed by thresholding. To use the command go to *Process> Find Edges*.

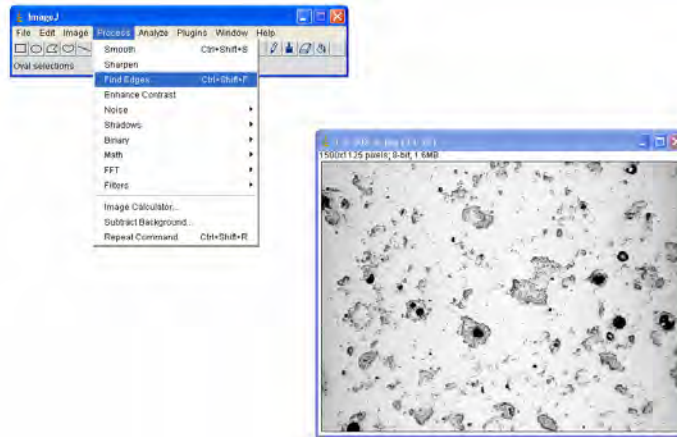


Figure B.4

1.1.5. Threshold (Figure B.5)

This command converts a grayscale image to black and white. The threshold level is determined by the histogram of the entire image. To use the command go to *Process> Binary> Threshold*.

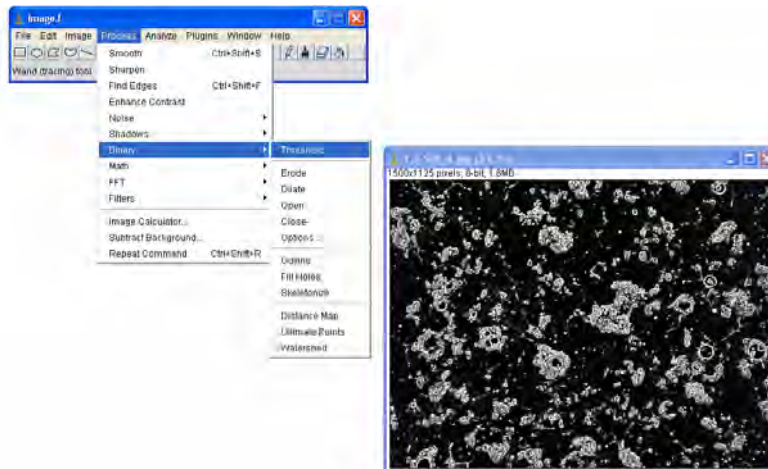


Figure B.5

1.1.6. Watershed (Figure B.6)

This segmentation command separates apart particles that touch in an image. It requires a binary image containing black particles on a white background. To use the command go to *Process> Binary> Watershed*.

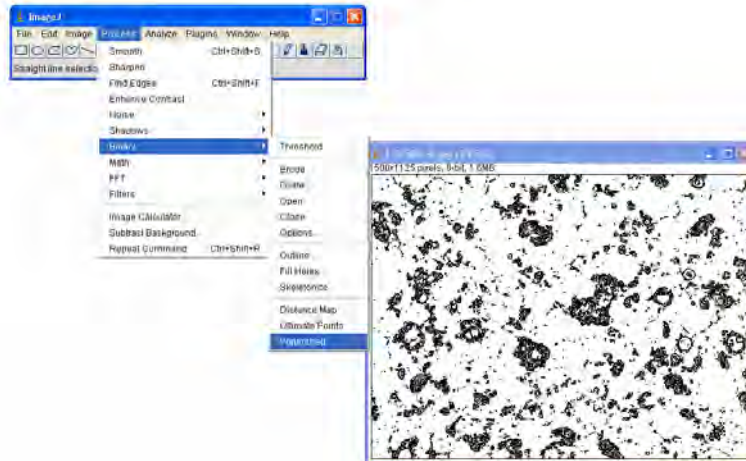


Figure B.6

1.2. Image Analysis

The “analyze particles” command counts and measures objects in binary or thresholded images. To use it go to *Analyze>Analyze Particles*. The user can press the esc key to abort this process, and to restart the process the user must close the pop-up windows of results and summaries that shows (these are now useless and incomplete) and initiate the same process again. (Figure B.7)

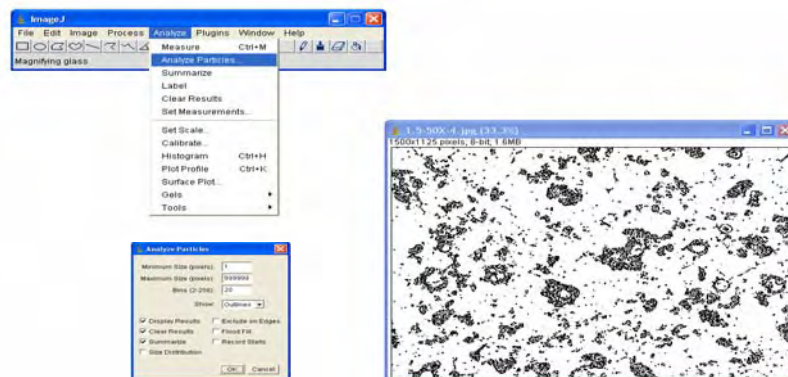


Figure B.7

The final result of reinforcement volume fraction that displays the analysis of particles is shown in Figure B.8.

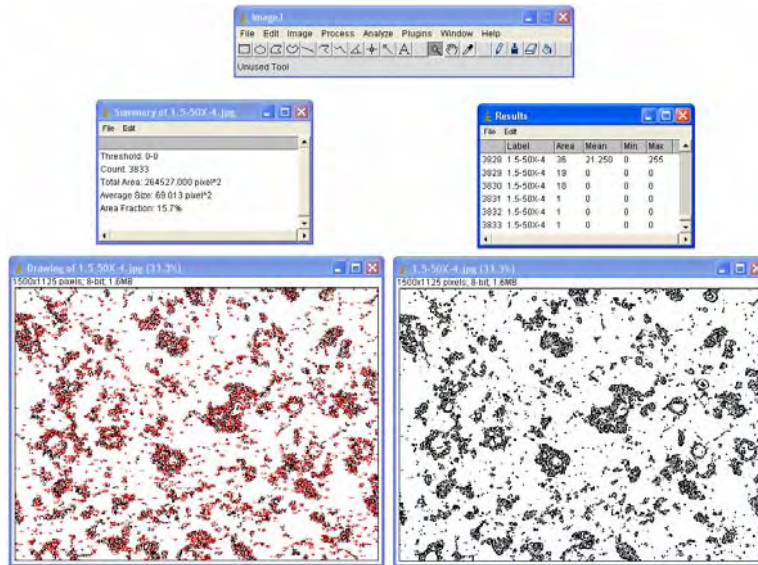


Figure B.8

2. Differentiate between two or more types of reinforcements

To differentiate two or more reinforcement and find their Volume Fraction the researcher should use the “Threshold color” plug-in. This process should be done on images of 200X and 500X. The researcher can follow these steps:

1. Open the Threshold Plug-in (Figure B.9)

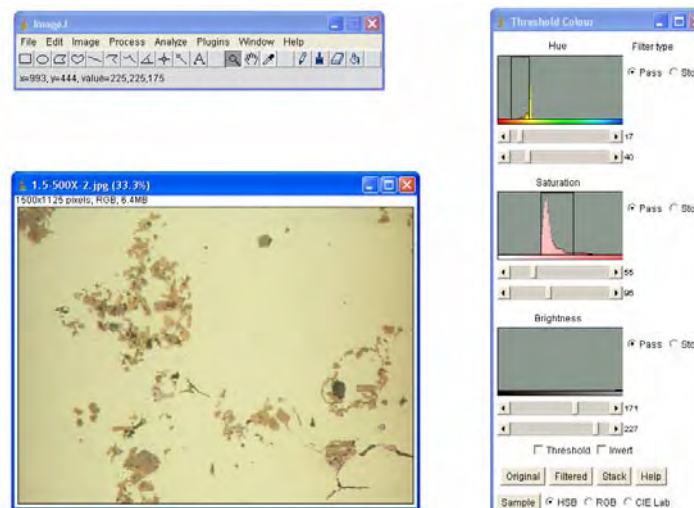


Figure B.9

2. First select the region of interest (ROI) with the freehand line selection tool (Figure B.10)

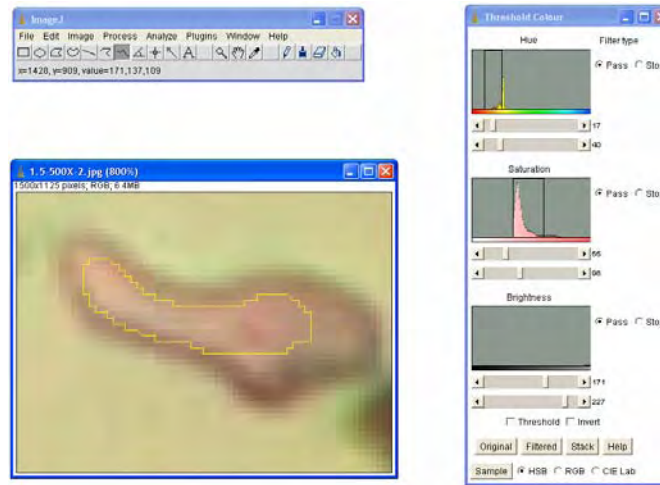


Figure B.10

3. Select the “sample” button . The Threshold color process will be completely done. It is important to take note of the threshold numbers for each process for future purposes (Figure B.11).

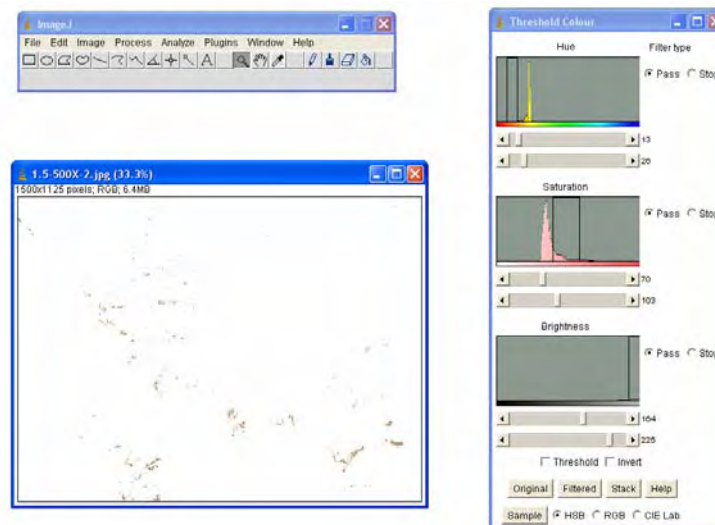


Figure B.11

4. Then follow the steps of the processing and analyze procedures of 50X images learned in item 1. The proceeding image shows the result (Figure B.12).

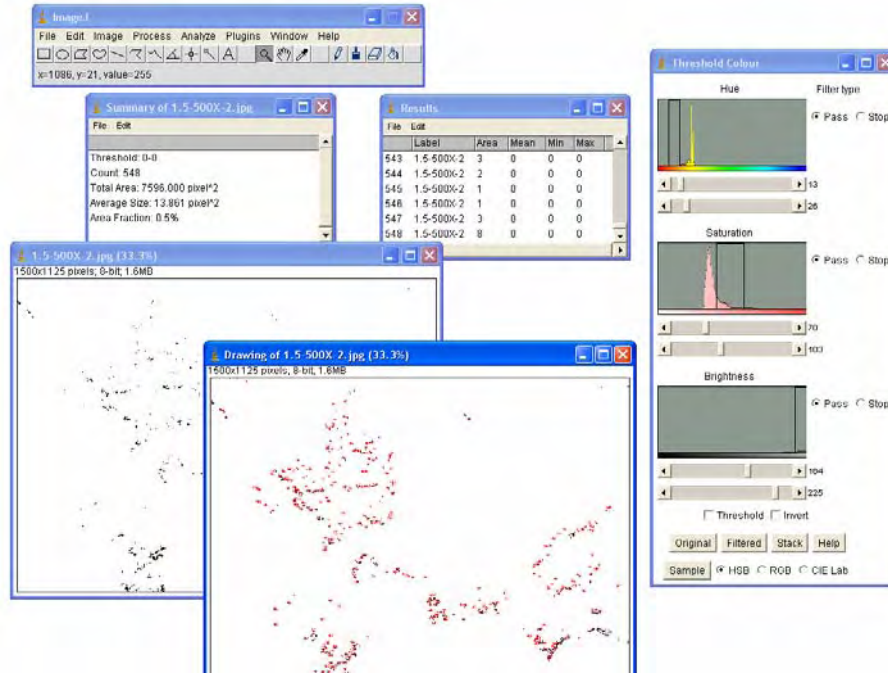


Figure B.12

APPENDIX C: Quantitative Analysis of Volume Fraction of Pores

To find Volume Fraction of pores the researcher should use the “Threshold color” plug-in. For this procedure the researcher should use 50X images (Figure C.1):

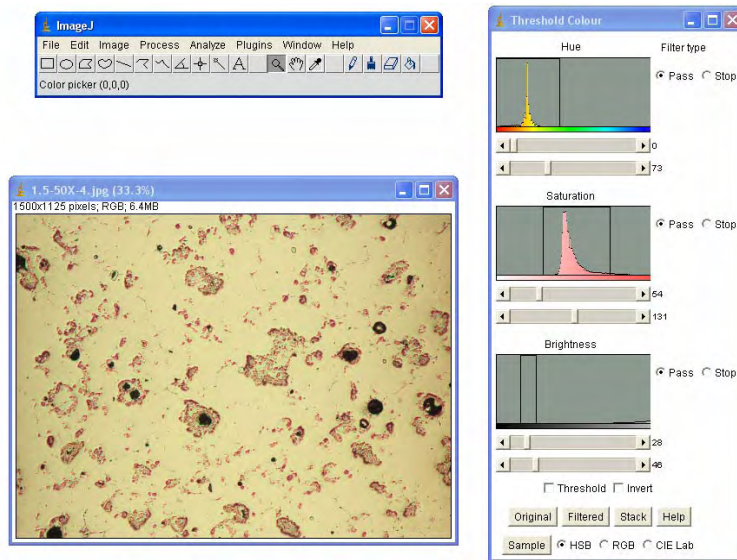


Figure C.1

1. Use a ROI to select the black color region of a pore and then from the

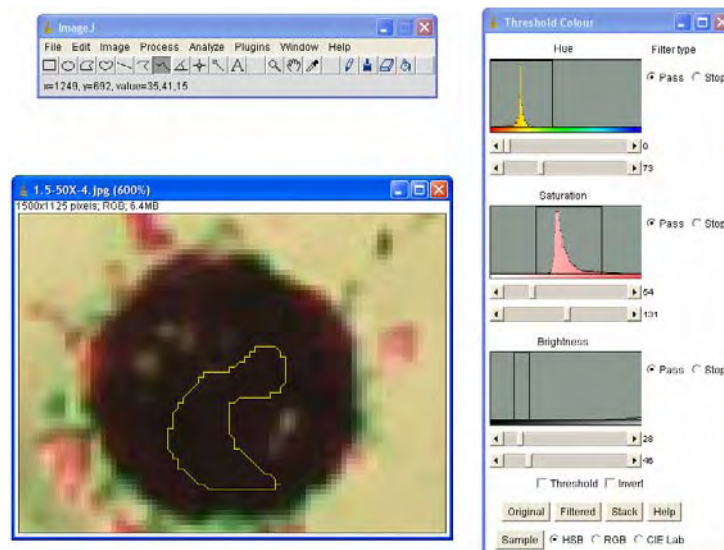


Figure C.2

2. Select in the Threshold color plug-in pop-up menu the “Sample” button Sample. (Figure C.3)

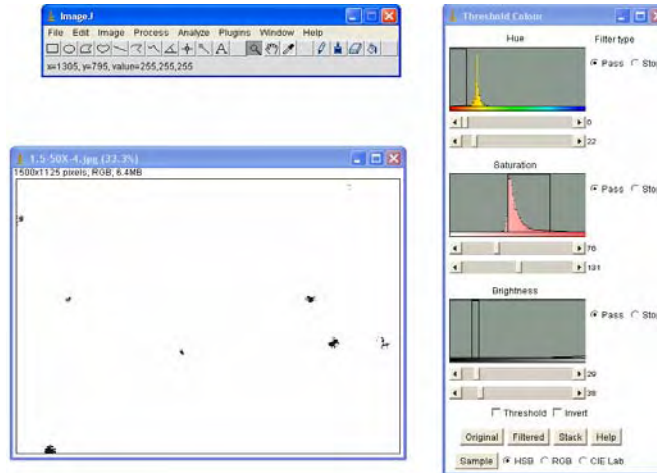


Figure C.3

3. At this point the difference respect with reinforcement procedure begins. Before the traditional processing, do a “smooth” command and then do the same processing and analysis procedure as if the researcher was looking for the Volume Fraction of the reinforcements. The “smooth” command is *Process>Smooth* (Figure C.4).

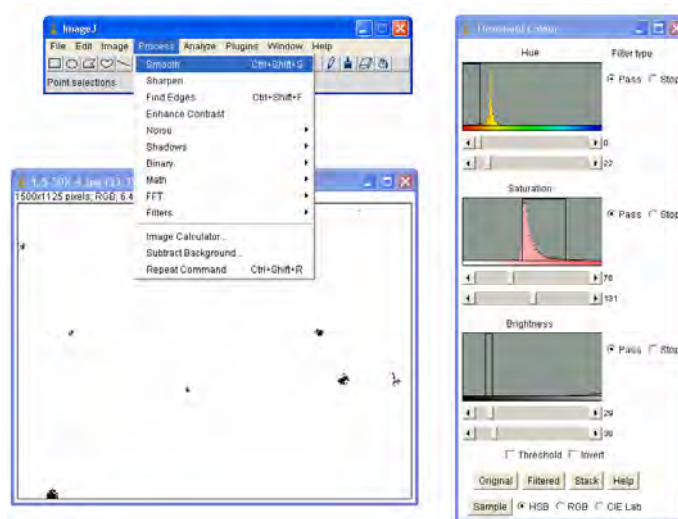


Figure C.4

4. Then follow the steps of the processing and analyze procedures of 50X images learned in item 1. The proceeding image shows the result (Figure C.5).

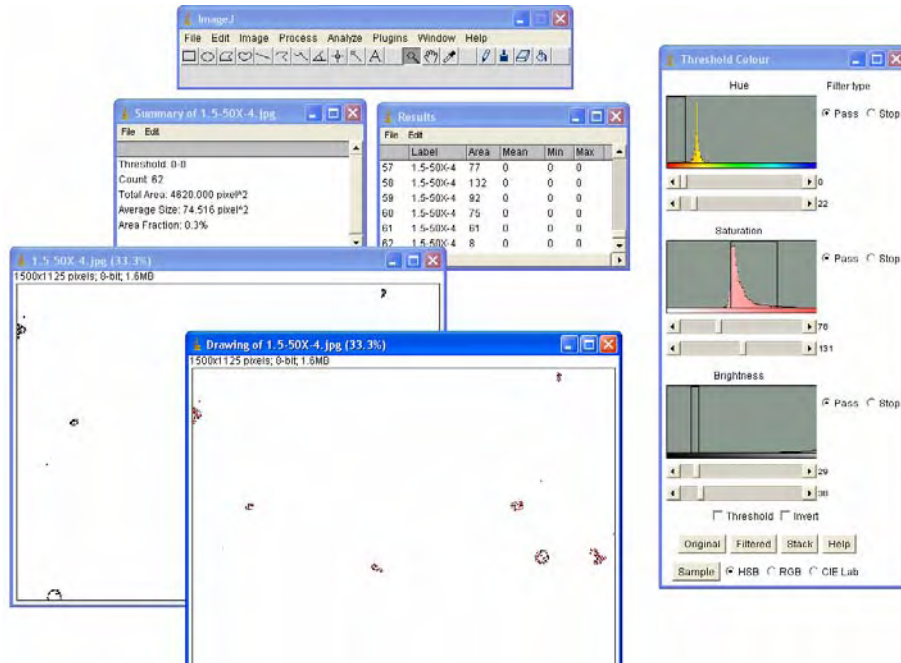


Figure C.5

APPENDIX D: Quantitative Analysis of Matrix Grain Size

The user should use images at 100X magnification (Figure D.1) and follow these steps:

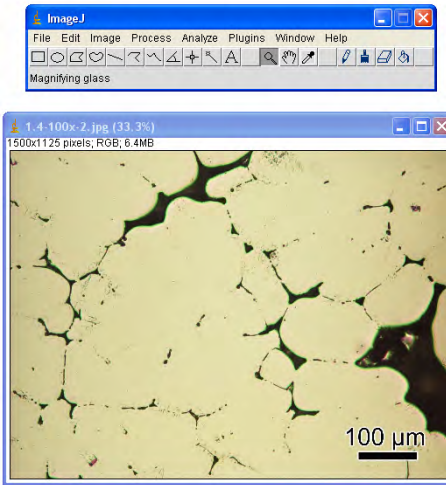


Figure D.1

1. With the magnification tool magnify to 100% 
2. With the line tool  make a horizontal line over the Micro-scale in the image from one border to the other (Figure D.2)

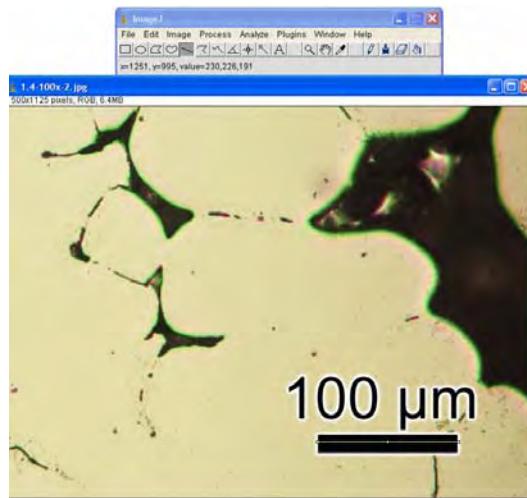


Figure D.2

3. Go to *Analyze>Set Scale...* and a pop-up window will appear. Set the known distance to the distance of the micro-scale and then check the “Global” Checkbox, essentially setting the scale to all the images after this to the micro-scale (Figure D.3).

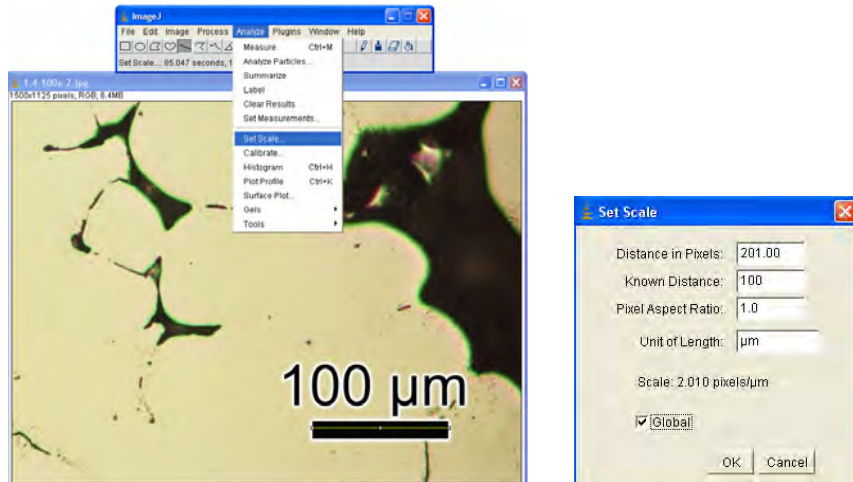


Figure D.3

4. Now select which grain size to study (Figure D.4)

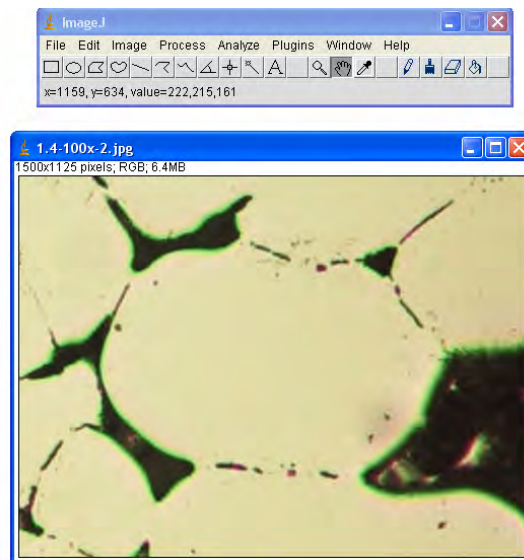


Figure D.4

5. Horizontally select the edges of the grain boundary (Figure D.5).

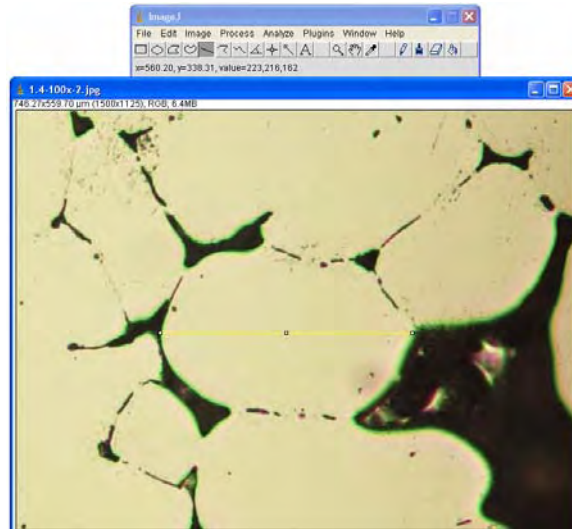


Figure D.5

6. Measure the length using the measure command. Go to *Analyze> Measure* (Figure D.6).

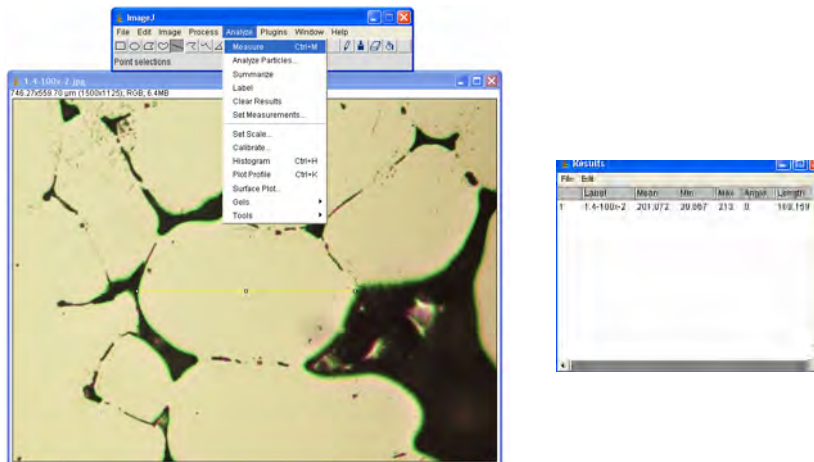


Figure D.6

*Note: A result table will appear. After measuring a sufficient amount of grains, save the table and name it "Results **name of photo**". Then move on to the next photograph and repeat the procedure. The text file will not be found with the file extension; so after the researcher puts the file name, add the file extension **.txt**. This so that the file can be opened with the notepad or excel software programs.*

APPENDIX E: Quantitative Analysis of Reinforcement Particle Size

The user should use images at 1000x magnification (Figure E.1) and then should follow these steps:

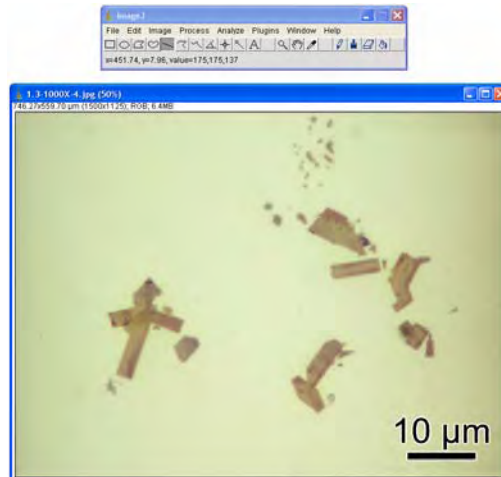


Figure E.1

1. With the magnification tool magnify to 100%  through 3
2. Use the steps made in Appendix D from 1 through 3
3. Now select which reinforcement particle size to study (Figure E.2)

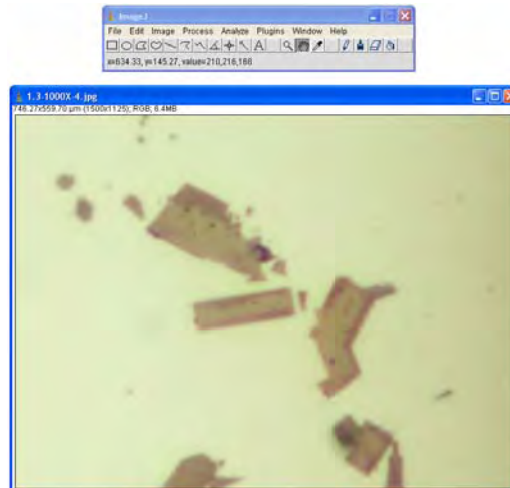


Figure E.2

4. Horizontally select (relative to the particle) the edges of the particle boundary (Figure E.3)

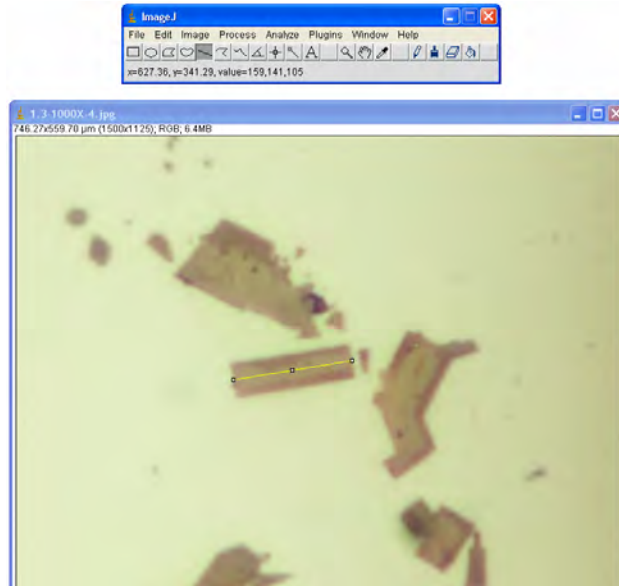


Figure E.3

5. Measure the length using the measure command. Go to *Analyze> Measure* (Figure E.4)

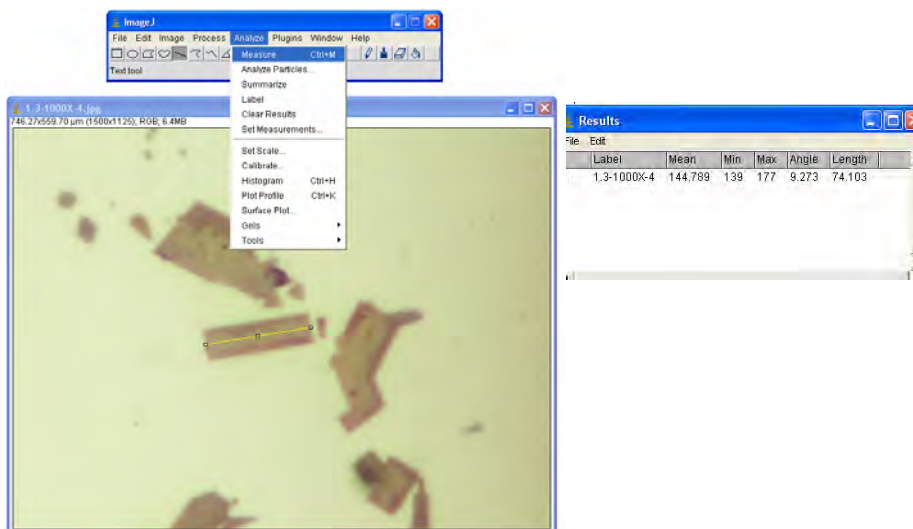


Figure E.4

- Vertically (relative to the particle) select the edges of the particle boundary (Figure E.5)



Figure E.5

- Repeat Step 5.

*Note: A result table will appear. After measuring a sufficient amount of reinforcements save the table and name it "Results **name of photo**". Then move on to the next photograph and do the same procedure.*